In silico screening of zeolites for application in high pressure hydrogen dehydration

Daan Ferdinand Geerdink

Fictitious reservoirs

Simulation box

- Hydrogen
- Water
- Extra-framework cation
- Zeolite framework
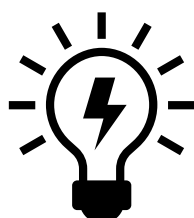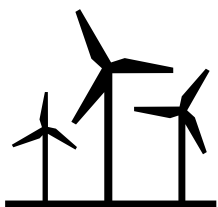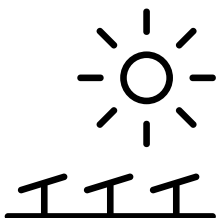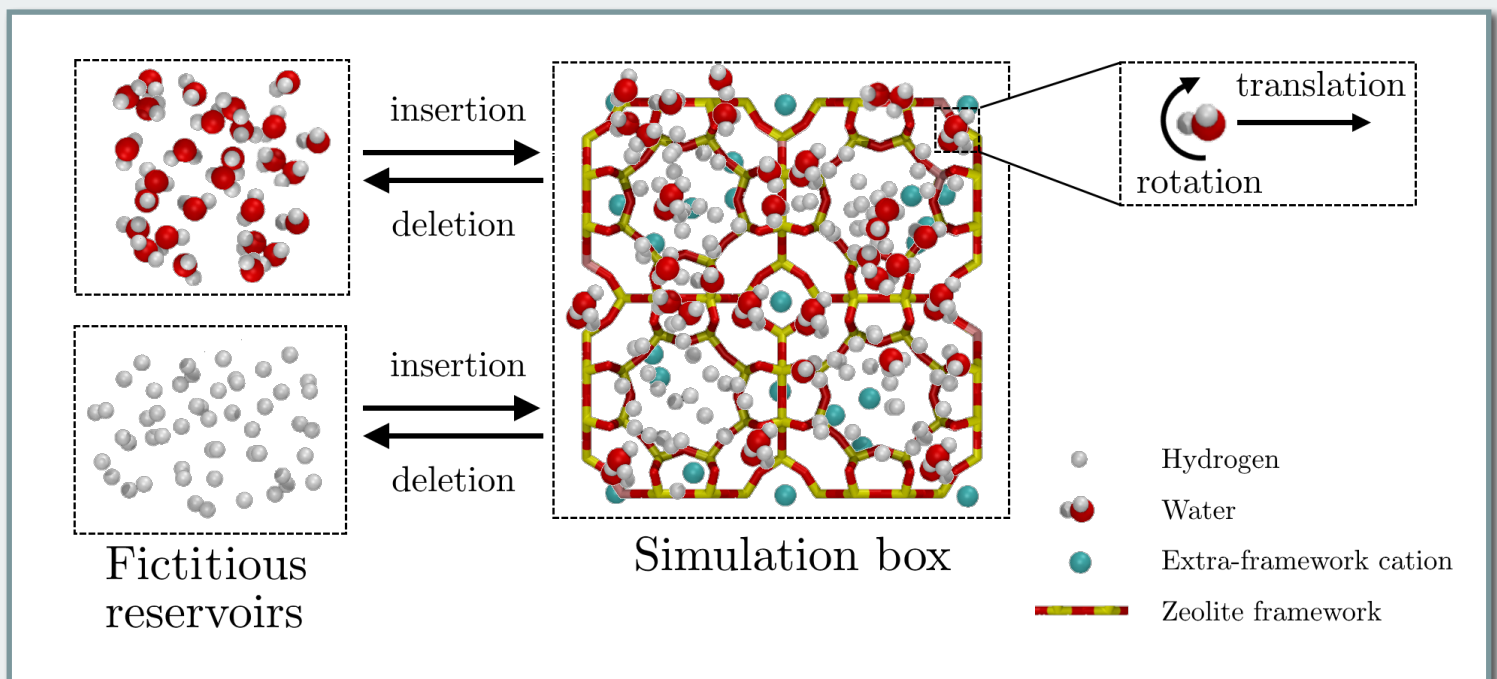
In silico screening of zeolites for application in high pressure hydrogen dehydration

by

Daan Ferdinand Geerdink

in partial fulfillment of the requirements for the degree of

Master of Science

in Chemical Engineering

at the Delft University of Technology,

to be defended publicly on Friday April 17, 2020 at 14:00.

An electronic version of this thesis is available at `http://repository.tudelft.nl/`.

TUDelft

Abstract

The energy mix of the future is likely to feature hydrogen due to its versatility. For effective use in energy storage, hydrogen has to be compressed. Conventional electrolysis of water and subsequent mechanical compression of hydrogen is an energy intensive process. A one-step conversion and compression can take place in a Electrochemical Hydrogen Compressor (EHC). This has the disadvantage that the resulting stream of high pressure hydrogen contains water. In order to assess the capability of hydrophilic zeolites as a means of selectively adsorbing this water, a in silico screening study of 6 zeolites was performed. To this end, a force field was constructed to allow for the simulation of high pressure hydrogen dehydration using Monte Carlo methods. The validity of this force field was evaluated by replicating simulation studies of adsorption of water/ hydrogen on zeolite frameworks with the presence of extra-framework cations. At the system pressure of 875 bar, prediction of the fugacity coefficient by means of the Peng-Robinson Equation of State (PR-EOS) yields inaccurate results. Therefore, these are calculated in the CFCNPT ensemble. It is demonstrated that the Ideal Adsorbed Solution Theory (IAST) is not suited to predict binary adsorption isotherms in this system. As a result of the screening study, it is found that the selectivity of water over hydrogen is almost linearly correlated to the amount of Al atoms in the zeolite framework. Furthermore, it is observed that topologies which feature a low amount of void space outperform those where significant void spaces are present. This can be attributed to the fact that the interactions of the zeolite with water are stronger than those with hydrogen in the limit of a low Si/Al ratio (Si/Al=1). It is theorised that water adsorbs preferentially at the surface of the zeolite, and competitive adsorption by hydrogen can only take place in sufficiently large void spaces.

Contents

1. Introduction

As the worldwide energy demand is expected to increase by 23%–40% by 2040 [1], the focus will shift from fossil fuels towards renewable energy sources. Hydrogen is often put forward as a versatile and potentially sustainable constituent of the future energy mix, that might strengthen energy security [2]. So-called green hydrogen is produced by electrolysis of water with temporary electricity surpluses that are inherent to renewable energy sources. This method is benefiting from significant scientific, political and business momentum.

Hydrogen for usage in proton-exchange membrane (PEM) fuel cells
For effective use in energy storage, hydrogen has to be compressed due to its low volumetric energy density. The compressed hydrogen is conventionally obtained by electrolysis and subsequent mechanical compression, which is an energy- and capital intensive process. Instead, recently developed electrochemical hydrogen compressors (EHC's) turn this into a one-step process which reduces overall cost. The downside of this method is that hydrogen compressed by EHC's is saturated with water due to the use of hydrated membranes. As a guideline, companies that produce green hydrogen aim to comply with the ISO 14687—2:2019 standard [3]. This standard dictates that hydrogen for use in PEM fuel cells, such as in hydrogen powered electric vehicles, may contain at maximum 5 parts per million (ppm) of water as an impurity. This limit ensures that water remains gaseous at high pressures close to ambient temperatures, and thus, prevents corrosion of metallic components and the formation of ice upon expansion. Recently, Ligen et al. proposed an industrial-scale method to purify hydrogen for use in PEM fuel cells [4], which demonstrates the economic potential of this type of technology.

This work builds upon the efforts of Rahbari et al., who investigated the solubility of water in hydrogen at high pressures close to ambient temperatures [5]. It was concluded that an additional step for removing water (dehydration) is required, since the solubility of water in the gas phase at coexistence is significantly higher than 5 ppm. The Hyet Company BV [6] has attempted to achieve this dehydration by condensation as the result of cooling, lowering the amount of water in the gaseous stream to 12.3 ppm. Reducing the water content even further requires alternative dehydration methods such as the use of ionic liquids [7] or porous materials. Among nanoporous materials, hydrophilic zeolites are promising candidates to selectively adsorb the water. The latter will be the focus of this work. The next section will introduce zeolites, and their possible role in high pressure hydrogen dehydration. Finally, the scope and objectives of this work are outlined.

Zeolites
Zeolites are a class of nanoporous materials with pores that have a characteristic size of a few Ångstroms. The overall chemical composition of silicious zeolites is SiO_2. The structures are made up of sets of interlinked SiO_4 tetrahedra, of which the metal atoms are referred to as T-sites. The tetrahedral building blocks are linked via O atoms and form nanoporous channels and pores varying in size and layout. The success of zeolites in industrial applications such as heterogeneous catalysis, ion-exchange and gas storage, as adsorbents for separations and for use in membranes [8] is linked to the extent of tunability of these materials. The tunability is achieved by three factors:

1. The ability to produce zeolites with a wide variety of pore sizes
2. The ability to produce zeolites with substituted T-sites
3. The ability to produce zeolites with specific extra-framework cations

Precisely sized pores allow for control of surface area and void space, and give rise to most of zeolites' most interesting properties. The substitution of T-sites from Si atoms by Al atoms results in aluminosilicate zeolites. This introduces negative charge defects in the framework that surround the Al atom. These are compensated by extra-framework cations. It is these charge defects that allow for control of the degree of hydrophilicity of the zeolite. The ease of exchanging, and nature of the extra-framework cations (Na^+, H^+, Li^+, …) is the final parameter which can be used to design materials for maximum performance at a specific application. Optimization of these parameters can contribute to cheaper, cleaner and more energy efficient technologies [9].

High throughput screening studies

The goal of high throughput screening (HTS) studies is to generate quantitative structure-property relationships (QSPR) that can predict materials that are best suited for a specific task. That is, to link the performance of a material at the task to its chemical and topological properties. The high throughput aspect comes into play due to the abundance of possible structures to calculate properties for [10–12]. Performing experiments with many or even all of these materials quickly becomes intractable, therefore the purpose of a HTS study can be seen as reducing the amount of candidate structures for a specific application as a precursor to further experimental work. This is illustrated in figure 1.1.
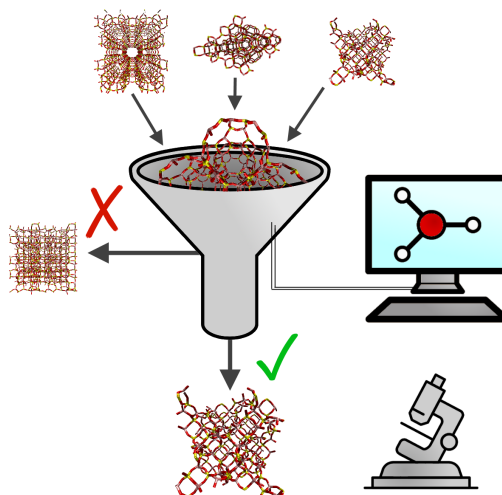
Figure 1.1: Schematic representation of the high throughput screening (HTS) process and its role in the field of materials discovery. Only the structures that are marked as suitable candidates by HTS are investigated experimentally.

In the case of zeolites, there are approximately 200 experimental zeolite frameworks and more than 10^9 hypothetical structures [13], of which 300.000—500.000 are energetically accessible [14]. Often, to avoid computation of all possible structures, a subset with maximal topological dissimilarity is created [15]. HTS has found many applications in nanoporous materials science, and has led to the Materials Genome Initiative [16]. Examples HTS studies include, but are not limited to:

- Zeolites as catalysts for CO_2 reduction [15]
- Materials selection for CO_2 storage [17]
- Materials selection for hydrogen storage [18]
- Separation of xenon/krypton [19]
- Separation of CO_2/H_2 [20]

In all cases, the performance of a materials at the task at hand is linked to so-called descriptors. This entails encoding relevant information about physical, chemical, and topological properties as vectors that can be interpreted by various statistical methods. These include, but are not limited to, random forests, genetic algorithms and various flavours of machine learning models to make the predictions [21]. These type of learning models require three steps:

1. Generation of a training set of the properties of interest as predicted for a set of materials
2. Generation of chemical and topological descriptors corresponding to these materials
3. Constructing models to predict the properties of interest based on the descriptors of novel materials

In many cases, the first step is the most time-consuming. In the field of nanoporous materials, the calculation of material properties using Grand Canonical Monte Carlo (GCMC) simulations can become prohibitively time-consuming. Attempts are therefore often made to eliminate the need for explicit calculation of these properties using GCMC simulations. The best example is the use of the Ideal Adsorbed Solution Theory (IAST)[22] for predicting multi-component adsorption from (idealized) single-component adsorption data. Furthermore, machine learning models are often trained on a small subset of the entire database. The model is then used to predict the property of interest for the remainder of the database [20].

Descriptors

The simplest descriptors for zeolites are one-dimensional. These include the accessible volume (AV), accessible surface area (ASA), diameter of the largest free sphere (MFS) and largest included sphere (MIS) of the pore space [23]. Two-dimensional or even three-dimensional descriptors are preferable, since they have the ability to capture the chemical confinement behaviour that zeolites are known for [24]. These include Voronoi based representations [25], Atomic Property Weighted Radial Distribution Functions (AP-RDF) [26], Topological Data Analysis (TDA) [27] and Pore Geometry Barcodes [28].

Descriptors are often highly correlated to each other. Therefore, it is often necessary to perform feature selection or dimensionality reduction techniques before using the statistical methods. This requires careful evaluation by a domain expert that can mark features as important for the task at hand. This is a major drawback which only recently has been fully appreciated. Krishnapriyan et al. recently proposed a novel method that performs feature selection and property prediction simultaneously with the use of persistent homology [29]. This is a promising development which could in term also be applied to the screening study presented in this work.

After a screening study is completed, often inverse design is performed to find new materials with desired properties. The most promising candidates are synthesized and their real-life performance is verified experimentally. As such, high throughput screening studies can metaphorically been seen as a funnel, and much effort is devoted to narrow down the number of target structures in an efficient way.

Scope and research objectives

Force field based molecular simulation is considered a natural tool to study adsorption and diffusion behaviour on zeolites [30]. The single component adsorption of hydrogen and water on nanoporous materials has been a subject of many experimental-, as well as simulation studies. The binary adsorption of hydrogen and water on zeolites, at high pressures and close to ambient temperatures has, to the best of the authors knowledge, not yet been investigated. The goal of this work is to develop a scientific workflow for identifying high-performing zeolites for application in high pressure hydrogen dehydration. To this end the following research objectives are formulated:

1. Modelling the chemical environment
2. Identifying a screening criterion for determining zeolite performance
3. Identifying key parameters for designing the optimal zeolite
4. Identifying feasible routes to avoid computation of adsorption isotherms

The structure of this report is as follows: In chapter 2 a brief but relevant overview of the theoretical background regarding simulation of adsorption on zeolites will be presented. In chapter 3, a detailed description of the simulation details elaborating on the constructed DEH_2YDR force field, and simulation methods. Then, in chapter 4, the DEH_2YDR force field will be validated. Subsequently, in chapter 5, a screening study of six industrially relevant zeolites will be introduced. Chapter 6 presents and discusses the results of this screening study. Lastly, in chapter 7, a conclusion will be presented as well as an outlook towards possible extensions of this research.

2. Theory

This chapter will focus on the theoretical background regarding the molecular simulation of zeolites, starting off with an overview of zeolite representation and modelling. This is followed by the theory of Monte Carlo simulations, the force fields involved in these simulations and the various statistical ensembles used in this work. Next, the ideal adsorbed solution theory (IAST) is introduced. Finally, topological descriptors of zeolites are introduced.

2.1. Zeolites

The molecular simulation of zeolites requires the formulation of a host structure, guest molecule structures and their interactions. With regards to the zeolite host structure, referred to as the framework, the following design parameters can be identified:

1. Atom position
2. Atom type
3. Atom charge
4. Framework flexibility

Atom position

Zeolites and their atomic positions are commonly described by their asymmetric unit cell and its space symmetry group. The symmetric unit cell can be constructed from this, including all atomic positions in 3D space. The symmetric unit cell is a representation of the perfect zeolite crystal, which does not exist in reality [31] but forms a solid basis for material studies.

Atom type

A choice can be made to distinguish individual atom types such as Si and Al or to create so-called T-atoms which can effectively act as either. An explicit model is beneficial to gain understanding the mechanisms involved in adsorption and diffusion [9]. In the case of explicit atom types the limit of T-site substitution (introduction of Al in the framework) is described by Löwensteins rule, which states that Al—O—Al atom connections are energetically unfavourable. The degree of hydrophilicity of a framework is often expressed as the ratio of the number of Si-, and Al atoms in the framework [32]. Löwensteins rule thus imposes a minimum Si/Al ratio of 1.0, corresponding to a framework with maximum hydrophilicity.

Atom charge

The charge distribution through the framework oxygen atoms can either be considered static, by using (partial) point charges, or dynamic. This determines whether or not polarization of the framework oxygen atoms by nearby guest molecules, charged molecules or extra-framework cations, is taken into account. In this work, point charges were used and as such polarization effects are not accounted for.

Framework flexibility

Following the early works of Kiselev [33], most molecular simulations of nanoporous materials assume that the zeolite framework is rigid. This is a reasonable assumption for materials such as zeolites [22, 34], and has the benefit that the computation cost is lower with respect to including flexibility.

Furthermore, it is often assumed that no bond breaking takes place. The effect of hydrolysis of the framework is therefore effectively omitted. The next section will focus on the use of Monte Carlo methods for use in molecular simulations, it will elaborate on the formulation of guest-host interactions in the form of force fields.

2.2. Monte Carlo

Monte Carlo (MC) methods belong to a domain computational of algorithms that leverage random number generation. They are used in combination with statistical mechanics to generate configurations of particles and predict macroscopic thermodynamic properties from these configurations. A large set of configurations that lead to an identical macrostate is called an ensemble [35]. By imposing constraints on the system by specifying whether or not energy or particle exchange is allowed, different types of ensembles can be constructed which mimic the equilibrium conditions of macroscopic systems. In the context of simulating zeolite systems MC is used to predict equilibrium quantities such as density and adsorption capacity. [36] In the basis, Monte Carlo uses a stochastic process where series of configurations are generated by random moves which are accepted or rejected according to the configuration's Boltzmann probability. These moves typically involve, but are not limited to:

- Translation of a molecule
- Rotation of a molecule
- Intramolecular displacement
- The exchange of molecules between the zeolite interior and a fictitious reservoir

If the exchange of molecules move is included, this allows for the direct simulation of an open thermodynamic ensemble, with thermodynamic equilibrium, without explicit definition of an interface [24]. This is referred to as Monte Carlo in the Grand Canonical Ensemble (GCMC).

In Monte Carlo simulations, the energy of each molecule is calculated as a sum of energies representing the interactions with all of the surrounding molecules. These are known as classical interaction potentials and can consist of the following contributions:

1. Intramolecular potentials
2. Intermolecular potentials
3. Coulombic potentials
4. Polarization potentials

A wide variety of functional forms is available to describe these interactions. The ones that were applied in this work will be highlighted.

Intramolecular potentials

These terms need to be considered for large molecules that can't afford to be approximated by a single interaction site effective model, or when assuming rigidity of molecules with multiple interaction sites leads to unacceptable errors. Since hydrogen and water are both small molecules this type of forces is not included in this work.

Intermolecular potentials

The most common intermolecular potential used in simulations of zeolites is the 12-6 Lennard–Jones (LJ) potential, given by equation 2.1.

$$U_{ij}^{\text{VDW}}\left(r_{ij}\right) = 4p_0 \left[\left(\frac{p_1}{r_{ij}} \right)^{12} - \left(\frac{p_1}{r_{ij}} \right)^{6} \right] \tag{2.1}$$

In this equation p_0/k_B specifies the well depth [K] and is a measure of the energy minimum of the attraction—repulsion potential. p_1 specifies the distance [Å] at which the intermolecular potential between the two particles is zero. This potential is a function of the distance r_{ij} between particles i and j, in Ångstrom.

In molecular simulation it is common to truncate these interactions beyond a certain distance. This length is called the cut-off length r_c. The contribution to the potential beyond the cut-off can be taken into account by means of shifting the potential to zero at the cut-off, by means of analytical tail corrections, or can be entirely neglected, as illustrated in equation 2.2. Analytical tail corrections formally may not be applied to zeolites since the assumption of homogeneity does not hold [37, 38].

$$U_{ij}^{\text{VDW}} = \begin{cases} U_{ij}\left(r_{ij}\right) & \text{if } r_{ij} \leq r_c \\ 0 & \text{otherwise} \end{cases} \tag{2.2}$$

The Feynman–Hibbs quantum effective potential, given by equation 2.3, is used for including quantum effects in simulations of adsorption of light gases such as hydrogen at low temperatures. It is essentially an expansion of the 12-6 LJ potential. It is used in this work for the validation of simulations of adsorption at low temperature.

$$U_{ij}^{\text{FH}}\left(r_{ij}\right) = 4p_0\left[\left(\frac{p_1}{r_{ij}}\right)^{12} - \left(\frac{p_1}{r_{ij}}\right)^6\right] + \frac{\hbar^2}{24p_2 k_B T} 4p_0\left[132\left(\frac{p_1}{r_{ij}}\right)^{12} - 30\left(\frac{p_1}{r_{ij}}\right)^6\right]\frac{1}{r_{ij}^2} \tag{2.3}$$

In this equation p_0/k_B, p_1 and r_{ij} have the same meaning as in equation 2.1. Here $\hbar$ and k_B are the reduced Planck's constant and Boltzmann's constant, T is temperature [K] and p_2 is the reduced mass [u] of the interaction site in unified atomic mass units.

Mixing rules
Whenever a Lennard–Jones interaction pair is not specified, it can be approximated by applying a set of mixing rules on the respective Van der Waals parameters. The ones applied in this work are the Lorentz-Berthelot mixing rules for particles i and j given by equation 2.4.

$$\text{p}_{0,mix} = \sqrt{\text{p}_{0,i}\text{p}_{0,j}}$$
$$\text{p}_{1,mix} = \tfrac{1}{2}\left(\text{p}_{1,i} + \text{p}_{1,j}\right) \tag{2.4}$$

Coulombic potentials
These refer to charge-charge interactions. The potential energy for a system of point charges is given by equation 2.5:

$$U_{ij}^{\text{CLB}} = \sum_{ij}\frac{q_i q_j}{r_{ij}} \tag{2.5}$$

Here q_i and q_j are the elemental charges of interaction sites i and j [e], and r_{ij} is the distance between them [Å].

Due to the truly periodic nature of zeolites, the Ewald summation technique[39] is the natural choice for computing the charge-charge interactions [40]. In this work, aluminosilicate frameworks are investigated which host extra-framework cations to balance charge. These interact strongly with the zeolite and Ewald summation was found to be the technique best capable of handling these strong interactions [41]. In Ewald summation, point charges are artificially screened. Then, the total potential is calculated separately for close- and far interactions. The artificial screening is corrected for after this calculation. The overall potential of a periodic system of charges is given by equation 2.6.

$$U_{ij}^{\text{Ewald}} = U_{ij}^{\text{Ew,real}} + U_{ij}^{\text{Ew,rec}} \tag{2.6}$$

Where $U^{\text{Ew,real}}$ denotes the close range interaction which is given by equation 2.7 and is computed in real space,

$$U_{ij}^{\text{Ew,real}} = \sum_{i<j} q_i q_j \frac{\text{erfc}\left(\alpha\, r_{ij}\right)}{r_{ij}} \tag{2.7}$$

And U^{rec} denotes the far range interactions which is given by equation 2.8 and is computed in Fourier space [42].

$$U_{ij}^{\text{Ew,rec}} = \frac{2\pi}{V}\sum_{\mathbf{k}\neq 0}\frac{1}{k^2}e^{-\frac{k^2}{4\alpha^2}}\left(\left|\sum_{i=1}^{N} q_i \cos\left(\mathbf{k}\cdot\mathbf{r}_i\right)\right|^2 + \left|\sum_{i=1}^{N} q_i \sin\left(\mathbf{k}\cdot\mathbf{r}_i\right)\right|^2\right) - \sum_i \frac{\alpha}{\sqrt{\pi}}q_i^2 \tag{2.8}$$

Again, q_i and q_j are the charges [e] of particle i and j, respectively. Here, $\mathbf{r}_i$ is the position vector of atom i, V the volume of the simulation box, α a damping factor, k the wavelength, and 'erfc' the error function complement.

Similar to the 12-6 Lennard-Jones potential these interactions are truncated at a cut-off distance r_c, as is shown in equation 2.9. Also here, similar tail correction techniques can be applied.-

$$U_{ij}^{\text{Ewald}} = \begin{cases} \sum_{i<j}\frac{1}{4\pi\epsilon}\frac{q_i q_j}{r_{ij}} & \text{if } r_{ij} \leq r_c \\ 0 & \text{otherwise} \end{cases} \tag{2.9}$$

Polarization potentials

Polarizability determines the dynamic response of the charge distribution of a molecule to external fields. These potentials can be modeled by equation 2.10 [43].

$$U_{\mathrm{pol}} = -\frac{1}{2} \sum_i^N \mu_i \cdot \mathbf{E}_i^\circ \tag{2.10}$$

where μ_i is the induced dipole moment of atom i, and $\mathbf{E}_i^\circ$ is the electrostatic field at the atomic position of i. Several methods are available for the calculation of μ, an example is the Ewald-Kornfeld summation [44, 45].

Molecular simulation

In simulations of zeolite systems a force field defines all interactions between interaction sites. They are constructed by fitting interaction models to experimental or ab initio data. Interaction sites do not necessarily refer to individual atoms. Rather, they can also refer to groups of atoms or can be assigned to so-called pseudo-atom. These are utilized to function as the effective centre of mass of a molecule or act as a charge in a polar molecule.

Nearest image convention

For the small systems that are simulated, the ratio of the area and volume is large compared to macroscopic systems. In order to avoid surface effects periodic boundary conditions are implemented. The simulation box is replicated in each spatial direction and interactions are only calculated for a pair of interaction sites if their distance is the shortest of all periodic images. This is illustrated in figure 2.1
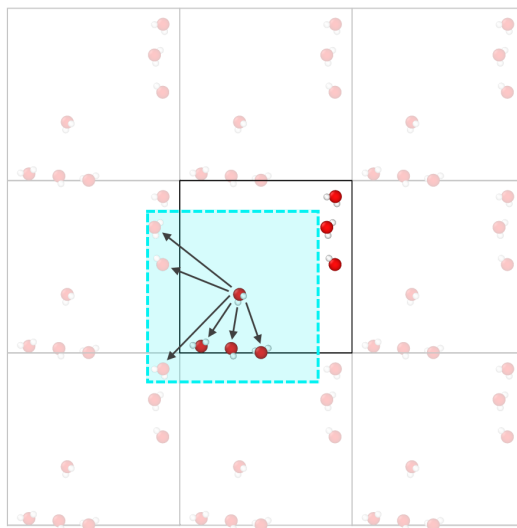
Figure 2.1: Periodic boundary conditions and nearest image convention. Arrows indicate nearest image interaction pairs.

Translation trial move

New system configurations are created during MC simulations using trial moves. The maximum displacement has to be carefully selected. If the translation distance is either too big or too small, the new configuration will not provide proper sampling of the phase space. As a rule of thumb, this distance is chosen such that the trial moves are accepted in 50% of the cases [35].

Widom's test particle insertion method

A special type of trial move is Widom's test particle insertion method [46]. It is used to compute the void fraction of nanoporous materials. Helium is often used as a probe particle due to its application in the experimental determination of the void fraction, therefore also referred to as the Helium void fraction (HeVF) [47]. This method randomly attempts to inserts a probe particle in the simulation box, but never actually

completes the insertion. Rather, the particle samples the potential energy which can be used to calculate the HeVF, as given by equation 2.11

$$\varepsilon = \int d\mathbf{r} \exp\left[-\beta U_{pot}(\mathbf{r})\right] \tag{2.11}$$

Here, ε is the Helium void fraction [-], $\beta = 1/k_B T$.

Henry coefficient
At low pressures, the adsorption of molecules on a nonporous material is governed by Henry's law, given by equation 2.12.

$$q = k_H P \tag{2.12}$$

where P is the pressure of the system, k_H the Henry coefficient and q the amount of adsorbed molecules per unit cell. The Henry coefficient can be calculated using Widom's test particle method [48] using equation 2.13

$$k_H = \beta \cdot \frac{\langle W \rangle}{\langle W_{IG} \rangle} \tag{2.13}$$

where ρ is the density of the zeolite framework, for information on $< W >$ and $< W_{IG} >$ the reader is reffered to [48].

Radial distribution function
The radial distribution function (RDF) describes the average number density $\rho(r)$ at distance r, for a specified pair of interaction sites. It's definition is given in equation 2.14. Figure 2.2 shows a graphical representation. This calculation is performed for all particles that belong to type of the specified pair, summed and then normalized.

$$g(r) = \frac{V}{N} \left\langle \sum_{i=1}^{N} \delta\left(\mathbf{r} - \mathbf{r}_i\right) \times \sum_{j=1}^{N} \delta\left(\mathbf{r} - \mathbf{r}_j\right) \right\rangle \tag{2.14}$$
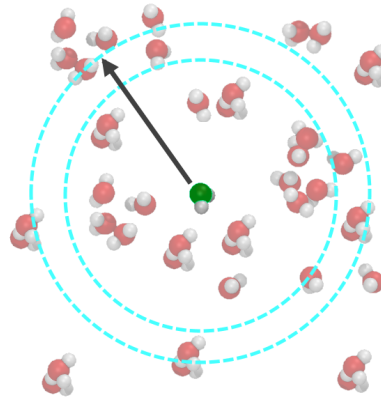
Figure 2.2: The radial distribution function $g(r)$ describes the average number density at a distance r [Å] for a specified pair of interaction sites, in this case Water-Water.

A quantity that can be derived from the RDF is the coordination number n, which is defined by equation 2.15. It is a measure of the local number density of the specified pair particles within a certain radius r'.

$$n\left(r'\right) = 4\pi\rho \int_0^{r'} g(r) r^2 dr \tag{2.15}$$

The next sections will introduce molecular simulation in various statistical ensembles.

2.2.1. Grand Canonical Monte Carlo Ensemble

To study the thermodynamics of adsorption in nanoporous materials, Monte Carlo simulations in the Grand Canonical ensemble (GCMC) are a suitable method. During simulations in this ensemble, the adsorption of guest molecules on the zeolite framework is simulated by fixing the simulation volume (V), average temperature ($< T >$) and average chemical potential ($< \mu >$), whilst allowing particle exchange with fictitious reservoirs. This is illustrated in figure 2.3.
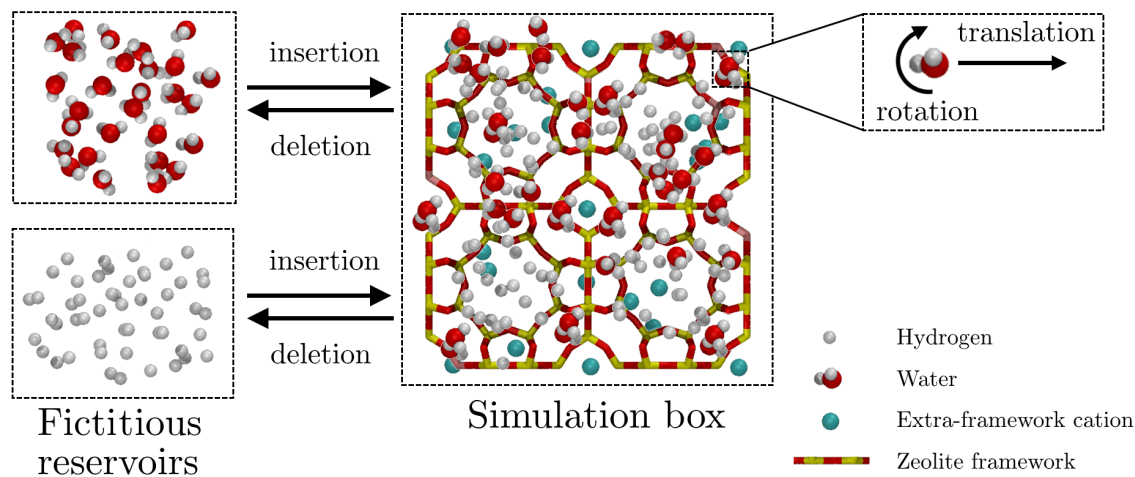
Figure 2.3: Schematic representation of a GCMC simulation of adsorption of hydrogen and water on a zeolite framework.

Every point on a simulated adsorption isotherm is the result of a simulation at fixed (μ, V, T).

Simulation versus Experiment

The greatest merit of GCMC simulations is that their results can be compared to experimental adsorption measurements on nanoporous materials. An advantage that GCMC has over experimental measurement of adsorption on zeolites is the possibility of modelling multi-component adsorption and subsequent separation performance. This can be difficult and time-consuming to conduct experimentally due to the increased number of variables.

During molecular simulations the calculated adsorption quantities are **absolute**, whereas the adsorption loadings measured experimentally are **excess** quantities. These excess quantities are obtained by measuring the *increment* of molecules that adsorb on the zeolite with increased pressure. These values can only be compared if the Helium void fraction is known. Absolute and excess adsorption values are known to deviate at high pressures [49].

Separation of a mixture by selective adsorption can be quantified by the selectivity, defined by equation 2.16.

$$S_{A/B} = \frac{N_{abs,A}}{N_{abs,B}} \tag{2.16}$$

Where $N_{abs,A}$ is the absolute amount of molecule A adsorbed on the zeolite framework and $N_{abs,B}$ is the absolute amount of molecule B adsorbed on the zeolite framework. A value of $S > 1$ thus indicates a preferable adsorption of molecule A.

Relation of chemical potential and pressure

The pressure of the reservoir (P) is specified, which can be converted to chemical potential by means of fugacity, given by equation 2.17. Fugacity is defined as the pressure that an ideal gas system would have, at exactly the same chemical potential [35].

$$f = P° \exp\left[\frac{\mu - \mu°(\text{g})}{RT}\right] \tag{2.17}$$

This is a direct result of the thermodynamic relation that for an non-ideal gas $\mu = \mu°(\text{g}) + RT \ln \frac{f}{P°}$.
In these equations, f is fugacity, $\mu°(g)$ is the standard chemical potential of a gas, $P°$ is the standard pressure,

R is the universal gas constant and T is the absolute temperature. In terms of quantities that are used in molecular simulations the fugacity is given by equation 2.18

$$f = \frac{\exp[\beta\mu]}{\beta\Lambda^3} \tag{2.18}$$

Here f is fugacity, μ is chemical potential, $\beta = 1/k_b T$ and Λ is the thermal wavelength. This is a direct result of the relation that for an ideal gas $\mu = k_B T \ln(\rho\Lambda^3)$ [35].

As such, instead of specifying the chemical potential, often in GCMC simulations the fugacity f or fugacity coefficient ϕ is specified. The fugacity coefficient is defined as the ratio of fugacity and the imposed external pressure $\phi = \frac{f}{P}$. Pressure and fugacity can be related using the thermodynamic relation:

$$\left(\frac{\partial \ln f}{\partial P}\right)_T = \frac{V_{\mathrm{m}}(P,T)}{RT}$$

$$\ln\phi(P) = \ln\frac{f}{P} = \int_0^P \left(\frac{V_{\mathrm{m}}}{RT} - \frac{1}{P'}\right)\mathrm{d}P' \tag{2.19}$$

The integrand $\left(\frac{V_{\mathrm{m}}}{RT} - \frac{1}{P'}\right)$ of equation 2.19 can be calculated with an appropriate Equation of Sate (EOS) such as the Peng-Robinson Equation of State (PR-EOS) [50] which is given by equation 2.20.

$$P = \frac{RT}{V_m - b} - \frac{a\alpha}{V_m^2 + 2bV_m - b^2} \tag{2.20}$$

In this equation P is the pressure, T is the temperature, V_m is the molar volume and R is the universal gas constant. The parameters a, b and α are calculated from the critical constants of the guest molecules: The critical temperature T_c [K], pressure P_c [Pa] and acentric factor ω [-].

An alternative method to calculate fugacity coefficients for adsorption simulations in nanoporous materials is discussed in section 2.2.3.

2.2.2. Isobaric-isothermal (NPT) Ensemble
In the NPT ensemble, also referred to as the isobaric-isothermal ensemble, the number of particles N, the average pressure $< P >$, and the average temperature $< T >$ are fixed, whilst allowing for exchange of volume with a fictitious reservoir. This is illustrated in figure 2.4. The NPT ensemble is used to calculate the macroscopic density of a (mixed) set of molecules.
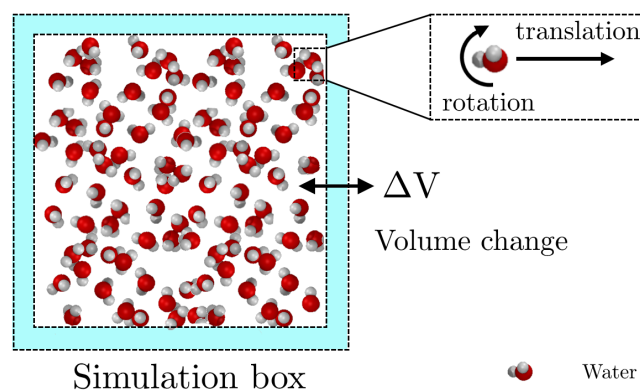
Figure 2.4: Schematic representation of a NPT simulation of water.

Chemical potential
The Widom's test particle insertion method can be used in the NPT ensemble to predict the chemical potentials of a multi-component mixture, as given by equation 2.21 [42, 51]. These can be converted into values of

the fugacity coefficients as demonstrated in section 2.2.1 to be used as the input for a CGMC simulation at a pressure where no Equation of State is available that yields accurate predictions.

$$\mu_A = -\frac{1}{\beta} \ln \left\langle \frac{V/\Lambda_A^3}{N_A + 1} \exp\left[-\beta \Delta U^{A+}\right] \right\rangle_{N_i, P, T} \tag{2.21}$$

Here, $\Delta U^{A}+$ is the interaction potential of the inserted test particle of type A with the system, N_A is the number of molecules of type A in the mixture, P is the imposed pressure, T is the imposed temperature, V is the volume of the system and Λ_A is the thermal wavelength for component A.

The application of equation 2.21 is limited in the case of high density systems due to inefficient sampling [52]. This can be circumvented with the introduction of continuous fractional components (CFC) into the system, which will be discussed in the next section.

2.2.3. Continuous Fractional Component Monte Carlo in the NPT ensmble (CFCNPT)
Fractional molecules are those of which the interaction potential is scaled with a coupling parameter $\lambda \in [0, 1]$ [53]. $\lambda = 0$ corresponds to the situation where the fractional molecule has no interactions with surrounding molecules, and acts as an ideal gas molecule. At $\lambda = 1$, interactions of the fractional molecule maximal, and the fractional molecule acts as a regular molecule. This is illustrated in figure 2.5.
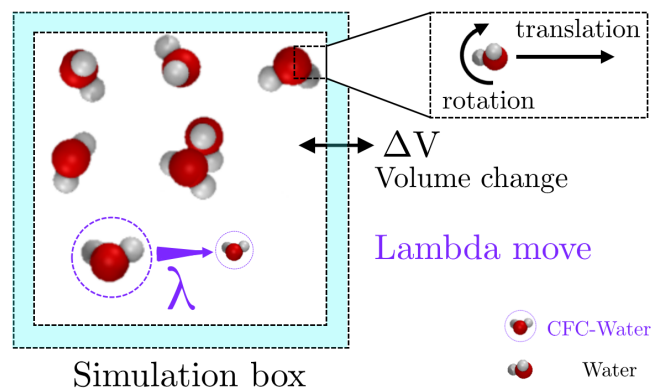
Figure 2.5: Schematic representation of a CFCNPT simulation of water. The Lambda move corresponds to scaling the interaction potentials of a particle with a coupling parameter $\lambda \in [0, 1]$

Rahbari et al. demonstrate that the use of this technique leads to improved sampling and accurate prediction of absolute and excess chemical potentials [52]. These are calculated using the probability distribution of the fractional parameter, $p(\lambda)$, as is shown in equation 2.22.

$$\mu_{NPT}^{CFC} = -k_B T \ln \left\langle \frac{V/\Lambda^3}{N+1} \right\rangle - k_B T \ln \left(\frac{p(\lambda = 1)}{p(\lambda = 0)} \right) \tag{2.22}$$

The supplementary information of [5] displays a proof that this method can be used to predict the fugacity coefficient of component i in a multi-component mixture in the CFCNPT ensemble through equation 2.23.

$$\phi_i = \frac{N_t RT}{P(V)} \exp\left[\mu_{ex}^i/(RT)\right] = \frac{\exp\left[\mu_{ex}^i/(RT)\right]}{Z_m} \tag{2.23}$$

The next section introduces the Ideal Adsorbed solution theory.

2.3. Ideal Adsorbed Solution Theory

Ideal Adsorbed Solution Theory (IAST) [54] is a thermodynamic framework that can be seen as an adsorption analog to Raoult's law for vapor-liquid equilibrium, which describes the equilibrium between a vapor and an adsorbed phase on a surface. It is given by equation 2.24.

$$P_i = y_i P = x_i p_i^0(\pi) \qquad (\text{ Constant } T \text{ and } \pi) \tag{2.24}$$

This approach assumes an ideal solution is formed by the components of the adsorbed phase. To meet this requirement, there may strictly speaking be no interactions between the adsorbate molecules. Assumptions regarding this requirement are discussed later in this section.

In equation 2.24, P_i is to the partial pressure of component i, $p_i^0(\pi)$ is the partial pressure of pure component i calculated at a fixed temperature (T) and spreading pressure (π) of the mixture. The spreading pressure can be calculated for the pure components using equation 2.25.

$$\frac{\pi A}{RT} = \int_0^{p_i^0} \frac{q_i}{P_i} dP_i \tag{2.25}$$

Spreading pressure is a two-dimensional quantity and is analogous to the inverse of surface tension. This is an intensive variable that can be calculated from single component isotherms independent of a physical adsorption model. For adsorption, this term is always positive. The total adsorbed amount, q_T, is calculated using loadings from the pure component isotherms, as can be seen in equation 2.26

$$\frac{1}{q_T} = \sum_{i=1}^{N} \frac{x_i}{q_i^0} \tag{2.26}$$

Evaluating the integral in equation 2.25 is often performed by fitting the single component isotherms to well known physical models of adsorption such as the Langmuir model [22], given by equation 2.27. This requires that adsorption data at low pressure must be known accurately, as inaccurate values translate in a bad prediction of the spreading pressure.

$$q(P) = q_{\max} \frac{K_H P}{1 + K_H P} \tag{2.27}$$

In the case of infinite dilution the interactions between adsorbed molecules are by definition negligible, and therefore the selectivity of species i and j is given by the ratio of their Henry constants: $S_{i,j} = \frac{K_{H,\,i}}{K_{H,j}}$

Assumptions

In order to apply Ideal Adsorbed Solution Theory, three major assumptions are made [54]:

1. Adsorbate molecules in the mixture have equal access to the entire surface area of the adsorbent
2. The adsorbent is homogeneous
3. The adsorbed phase is an ideal solution in which interactions between molecules are equivalent in strength.

One additional assumption that is relevant with fitting adsorption isotherms to physical models of adsorption is: The saturation capacity of the adsorbate molecules is equal [22].

Regarding the validity of these assumptions in applying IAST to adsorption on zeolites, it is well established that the prediction capability is poor when:

- The adsorbate molecules mixtures vary significantly in size, polarity, or adsorption interactions [55]
- The adsorption surface is heterogenous, such as with aluminosilicate zeolites [56]

The next chapter will discuss the details of the simulations performed in this work.

3. Simulation details

This chapter consists of two parts. In the first section, research objective 1 will be addressed: modelling the chemical environment, resulting in the DEH$_2$YDR force field. Then, in the second section, technical specifications of all the simulations performed in the RASPA [57] and BRICK [58] simulation environments are specified.

3.1. System description

Overview

The case study at the heart of this work revolves around the application of zeolites in high pressure dehydration of hydrogen. Therefore operating conditions are specified for which an appropriate type of zeolite is to be identified, these can be found in table 3.1. Furthermore, it is specified that this work considers an unreactive molecular system.

Table 3.1: System conditions

Operating condition	Value in SI Units	Value in operational units
Pressure	$8.75 \cdot 10^7$ Pa	875 bar
Temperature	310 K	310 K
Molar fraction hydrogen	0.9999877	999987.7 ppm
Molar fraction water	0.0000123	12.3 ppm

Next, a list of (pseudo-)atomic species is presented which play a role in the system. Table 3.2 lists the identifiers which are used to refer to these species in the next section. Helium is included because it plays are role in determining the Helium void fraction (HeVF) of zeolite frameworks. For a simplified graphic representation of the system, the reader is referred to figure 2.3.

Force field construction

In order to calculate adsorption properties for the given system, a force field has to be constructed. The binary adsorption of hydrogen and water on zeolites at the specified system conditions has, to the best of the authors knowledge, not yet been investigated. Designing a force field for every individual zeolite material is a very time consuming process. So-called transferable force fields aim to describe many different zeolites using one set of parameters. However, their simplicity comes at the cost of a more approximate description of the system.

Table 3.2: (Pseudo) atomic species

Component	Pseudo atom identifier	Chemical type	Valency	Atomic weight [u]
Zeolite	Si	Si	Si^{4+}	28.0855
Zeolite	Al	Al	Al^{3+}	26.9815
Zeolite	O	O	O^{2-}	15.9996
Zeolite	Oa	O	O^{2-}	15.9996
Extra-framework cation	Na	Na	Na^{+}	22.9898
Hydrogen, H$_2$	H2	H$_2$	H$_2$	2.0016
Water, H2O	wO	O	O^{2-}	15.9996
Water, H$_2$O	wH	H	H^{+}	1.0008
Water, H$_2$O	wL	-	-	-
-	He	He	He	4.0026

13

There thus exists a trade-off which can be considered threefold:

1. The accuracy of the force field
2. The transferability of the force field
3. The availability of parameters that were fitted to experimental data

The last of which has mainly determined the approach taken in this work. The presence of extra-framework cations in the zeolites presents a challenge. Many theoretical-, as well as experimental studies have shown that the parameterization and position of these cations play an essential role in simulations of adsorption on zeolites [9].

Furthermore, the parameterizations of the zeolite framework have to be similar. Though these systems have been extensively studied for the adsorption of hydrogen [59–73] as well as water [9, 40, 74–97], the constraints of similar extra-frame cation types and zeolite parameterisation has limited the availability of force fields in literature to the following:

- For a system involving an aluminosilicate zeolite with Na extra-framework cations where hydrogen is adsorbed: Unpublished work of S. Calero on adsorption of hydrogen on the LTA4A type zeolite is abided. In turn, this is based on earlier work of Deeg et al. on adsorption of hydrogen on the MFI type zeolite [91]. This will be referred to as the *Calero force field*.
- For a system involving an aluminosilicate zeolite with Na extra-framework cations where water is adsorbed, work of Castillo et al. on the adsorption of water on the LTA4A zeolite [98] is abided. This will be referred to as the *Castillo force field*.

The next section focuses on the integration of these two force fields, yielding a single force field that will be used in the remainder of this work, and will be referred to as the DEH_2YDR force field. This is done by evaluating both the original authors' considerations and those of the current work for each of the components: the zeolite, extra-framework cations, hydrogen and finally for the water.

Force field components
Zeolite
Both the *Castillo* and *Calero* force fields have based their description of the zeolite on the work of Garcia-Sanchez et al. The main points that were adapted from this work were the point charges assigned to the framework atoms. Furthermore, the charge distribution was considered static and thus polarization is neglected. The force field explicitly distinguishes Si from Al atoms with a difference of $0.3e^-$ between q_{Si} and q_{Al}.

It was argued that the polarizability as well as the size of the Si atoms are much smaller than those of the O atoms of the zeolite. As such, it is assumed that their contributions are accounted for by using effective 12-6 Lennard–Jones potentials between the oxygen atoms of the framework and the interaction sites of the guest molecules, with the exception of hydrogen, as will be shown in the following sections. Both force fields distinguish framework oxygen atoms that are connected to an Al atom (Oa) from those that are not (O). This differentiation was extended to the point charges for the oxygen atoms. $q_{O,Si}$ was obtained using equation 3.1, making sure the zeolite is neutral in the absence of aluminum, whereas $q_{O,Al}$ was chosen to ensure the total system charge equals zero [76, 77].

$$q_{Si} + (2 \cdot q_{O,Si}) = 0 \tag{3.1}$$

The *Castillo force field* was validated using rigid and flexible frameworks and it was concluded that the inclusion of flexibility did not improve results. As a result, a rigid framework will be implemented in the DEH_2YDR force field.

The Van der Waals parameters and charges for the zeolite structure are given in table 3.3.

Table 3.3: Zeolite point charges

Pseudo atom identifier	Type of interaction	p_0/k_B [K]	p_1 [Å]	Point charge [e]	Source
Si	Coulombic	-	-	0.78598	[91, 98, 99]
Al	Coulombic	-	-	0.48598	[91, 98, 99]
O	Coulombic	-	-	-0.39299	[91, 98, 99]
Oa	Coulombic	-	-	-0.41384	[91, 98, 99]

The guest–host interactions with cations, hydrogen and water will be discussed in the next sections. Possible shortcomings of this approach are discussed in section 6. The following section will discuss the implementation of extra-framework cations in the DEH$_2$YDR force field.

Extra-framework cations

A large body of research has shown that the adsorption calculated by molecular simulation on zeolites with the presence of extra-framework cations may depend on four critical factors

1. The specific position of Al atoms in the framework [84]
2. The chemical nature of the extra-framework cation [74]
3. The specific (preferential) position of the extra-framework cation [100]
4. The mobility of the extra-framework cations during the simulation [41]

Framework Al atom position

The exact position of Al atoms in aluminosilicate zeolites is generally unknown. It has been shown that this is an intrinsic property of zeolites, and that the distribution of Al atoms is kinetically controlled rather than thermodynamically controlled [32, 101]. This property is mimicked in this work using random substitutions of Si atoms whilst obeying Löwensteins rule. The silicious structures were obtained from the IZA structure database [102], and as such these atomic positions were abided.

Extra-framework cation chemistry

The chemical nature of the extra-framework cations has been shown to affect the adsorption mechanisms of various guest molecules in zeolites varying with temperature and pressure [9, 78]. In this work the presence of sodium (Na) cations is investigated.

Extra-framework cation position

As with the position of Al atoms in the framework, the exact position of extra-framework cations in aluminosilicate zeolites is generally unknown. Lots of zeolite frameworks have been investigated with respect to extra-framework cation position [8, 9, 78, 100, 103]. This stresses the importance of a solid equilibration procedure of these positions. In this work, the zeolite frameworks and their extra-framework cations were equilibrated in the absence of other guest molecules at elevated temperatures for $5 \cdot 10^5$ MC cycles.

Extra-framework cation mobility

The fact that cations can act as a preferred adsorption site for guest molecules, specifically water molecules, is well established [104]. Furthermore, it has been demonstrated that they reallocate upon adsorption. Castillo et al. have demonstrated that it is an important consideration for the simulation of water in zeolites [98], even though the mobile cations do not move far from their equilibrium positions. This cation mobility was thus abided in the DEH$_2$YDR force field.

To summarize, the sodium (Na) extra-framework cations are modelled as single-site, charged Lennard–Jones centres that are mobile during the simulations. The Van der Waals parameter and charge for the Na extra-framework cation is given in table 3.4.

Table 3.4: Van der Waals parameter and charge for the extra-framework sodium (Na) cation

Pseudo atom identifier	Type of interaction	p_0/k_B [K]	p_1 [Å]	Point charge [e]
Na	12-6 Lennard-Jones	251.7800	3.1440	0.38340

The guest–host interactions between the cations and the zeolite are discussed next. As can be seen in table 3.5, a difficulty arises at integrating the force field parameters for the Oa–Na guest–host interaction. Both force fields specify different values of p_0 and p_1 for this interaction. This difficulty can be overcome by referring to Castillo et al., who explicitly state that the adsorption of water is not sensitive to this parameter. It is therefore opted to use the parameters put forward by the *Calero force field*, which are signified with a **bold font** in the table. The influence of this choice is evaluated in section 4.

Table 3.5: Van der Waals parameter and charge for the extra-framework sodium (Na) cation

Pseudo atom identifier	Type of interaction	p_0/k_B [K]	p_1 [Å]	Point charge [e]
O - Na	12-6 Lennard-Jones	33.0000	3.2000	[98]
Oa - Na	12-6 Lennard-Jones	33.0000	3.2000	[98]
Oa - Na	12-6 Lennard-Jones	**23.0000**	**3.4000**	S. Calero, [91]

The guest–guest interactions between the cations, hydrogen and water will be discussed in the next sections. Possible shortcomings of this approach are discussed in section 6. The following section will discuss the implementation of hydrogen molecules in the DEH$_2$YDR force field.

Hydrogen

The parameterization of the hydrogen molecule is based on the unpublished work of S. Calero on adsorption of hydrogen on the LTA4A type zeolite. In turn, this is based on earlier work of Deeg et al. on adsorption of hydrogen on the MFI type zeolite [91]. Both S. Calero and Deeg et al. have validated multiple models for hydrogen. The main distinctions between these models is the use of a single-site effective LJ potential versus a multi-site LJ potential. They conclude that adsorption of hydrogen on zeolites is best described with a single-site model.

Similar to these findings, Rahbari et al. conclude that a Marx [105] single-site model is capable of predicting the density and fugacity coefficient of hydrogen at pressures up to P = 1000 bar [5]. These results will be compared to the results obtained in this work. Since the choice of a single-site model is abided in this work, this imposes a point charge of zero. The Van der Waals parameter and charge for the H_2 single-site model is given in table 3.6.

Table 3.6: Van der Waals parameter and charge for hydrogen molecule

Pseudo atom identifier	Type of interaction	p_0/k_B [K]	p_1 [Å]	Reduced mass [u]	Point charge [e]	Source
H2	12-6 Lennard-Jones*	36.7330	2.9580	1.0000	0.00000	S. Calero, [91]

The guest–host interactions between the hydrogen and the zeolite are given in table 3.7.

Table 3.7: Guest–host interactions between the hydrogen and the zeolite

Interaction pair	Type of interaction	p_0/k_B [K]	p_1 [Å]	Reduced mass [u]	Source
H2 - Si	12-6 Lennard-Jones*	28.2560	1.8540	1.8810	S. Calero, [91]
H2 - Al	12-6 Lennard-Jones*	26.5120	1.9870	1.8760	S. Calero, [91]
H2 - O	12-6 Lennard-Jones*	66.0550	2.8900	1.7900	S. Calero, [91]
H2 - Oa	12-6 Lennard-Jones*	66.0550	2.8900	1.7900	S. Calero, [91]

The guest–guest interactions between the extra-framework cations and hydrogen are given in table 3.8.

Table 3.8: guest–guest interactions between the extra-framework cations and hydrogen

Interaction pair	Type of interaction	p_0/k_B [K]	p_1 [Å]	Reduced mass [u]	Source
H2 - Na	12-6 Lennard-Jones*	220.0000	3.0000	1.8530	S. Calero, [91]

As can be seen from the tables, an extra column with reduced mass is included, these values were used by Deeg et al. to implement the Lennard–Jones–Feynmann–Hibbs quantum effective potential (see section 2.2) for incorporating quantum effects at low temperatures (77K). These were applied during the force field validation in section 4. Since the system under investigation in this work operates at close to ambient temperatures, these quantum potentials are omitted.

The following section will discuss the implementation of water molecules in the DEH$_2$YDR force field.

Water

Due to its abundance in nature and crucial role in natural and industrial processes, water might just be the most researched substance that exists. The online repository on water structure and science [106], lists over 50 distinct water force fields [107].

The main differences amongst the force fields that are common for modelling water adsorption on zeolites are:

1. Intramolecular forces, related to the internal motion and flexibility of the molecule
2. Intermolecular forces, related to the amount and magnitude of LJ interaction sites
3. Coulombic forces, related to the amount and magnitude of charged interaction sites
4. Polarization forces, related to the polarizability of the molecule

The amount of effective interaction sites ranges from a single-site model, also referred to as a coarse grained model, to a six-site model. In selecting an appropriate water model a trade-off has to be made. No single force field in use today is able to simultaneously and accurately predict the different properties of water, such as the density and the location of the critical point [40].

From a physical point of view, water is a flexible and polarizable molecule. However, most molecular simulation literature consider rigid water molecules with constant point charges [90, 97, 99]. This can be attributed to the fact that computing intramolecular forces and polarization are computationally disadvantageous for systems involving many water molecules[82]. In general, molecular simulation of water adsorption on zeolites has been shown to be extremely sensitive to the selection of water model, position of the framework atoms, small changes in force field parameters and the partial charges of the zeolite atoms [40].

The *Castillo force field* employs the Tip5p-Ew water model [108]. It was concluded that this water model allows for accurate simulation of water adsorption on zeolites, caused in part because it's parameters have been refitted using Ewald sums [40]. The water–zeolite and water–cation Van der Waals interactions were fitted to the experimental data by Castillo et al.

The Tip5p-Ew water model can be summarized by the following properties:

- Five interaction sites in an almost tetrahedral configuration
  - one 12-6 Lennard-Jones interaction site, placed at the position of the oxygen atom (wO)
  - two point charges, placed at the positions of the hydrogen atoms (wH)
  - two point charges, placed at the positions of the oxygen lone pairs (wL)
- Rigid, no intramolecular forces
- Polarizability neglected, fixed dipole moment of 2.29 D

The specification of 5 interaction sites and the assumption of rigidity requires the specification of bond lengths (L_{wH}, L_{wL}) and bond angles (α, β). Furthermore the point charges on the positions of the hydrogen atoms and oxygen lone pair sites have to be specified. These can be seen in figure 3.1 and in table 3.9.
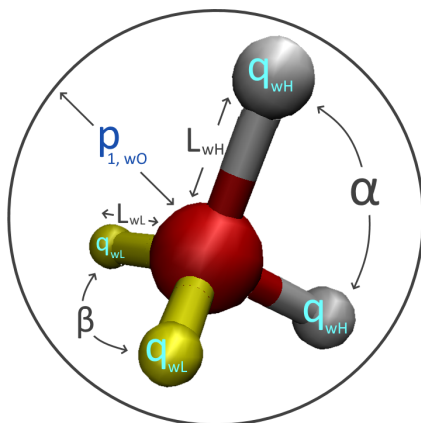
Figure 3.1: Schematic representation of the Tip5p-Ew water model.

Table 3.9: Parameters of the Tip5p-Ew water model

Model	L_{wH} [Å]	L_{wL} [Å]	q_{wH} [e]	q_{wL} [e]	α [deg]	β [deg]
TIP5P-Ew	0.9572	0.7	0.241	-0.241	104.52	109.47

The trade-off that has to be taken in to account is that the Tip5p-Ew water model results in relatively bad predictions of some properties. These include, but are not limited to, the specific heat (141% of experimental value at 298 K) and shear viscosity (91% of experimental values at 298 K) [109]. Rahbari et al. observed that the chemical potential of water at high pressure is overpredicted by -500 K (in units of energy/k_B) by the Tip5p-Ew model.

High pressure & Polarizability
Rahbari et al. conclude that none of the force fields for rigid water with fixed point charges could accurately predict simultaneously the chemical potential and the density of water at high pressures [5]. This might be improved by using polarizable force fields for water [97].

Similarly Castillo et al. warn that at high pressures, the increase in dipole moment of water is a factor that might be disadvantageous to neglect [98]. Including polarizability could improve the accuracy of molecular simulation of adsorption of water on zeolites. They argue that, as the water dipole moment increases, the water–zeolite and water–cation interactions become stronger, and thus the adsorption will increase.

Transferability
As a final remark, Castillo et al. state that their force field is in general not transferable between different zeolite types [98]. This is a significant disadvantage to the efforts of this work, and imposes the need to perform additional experimental- and theoretical validation of water adsorption on various aluminosilicate zeolite framework types.

The Van der Waals parameters and charge for the Tip5p-Ew water model is given in table 3.10.

Table 3.10: Van der Waals parameter and point charges of the Tip5p-Ew water model

Pseudo atom identifier	Type of interaction	p_0/k_B [K]	p_1 [Å]	Point charge [e]	Source
wO	12-6 Lennard-Jones	89.5160	3.0970	0.00000	[98, 108]
wH	Coulombic	-	-	0.24100	[98, 108]
wL	Coulombic	-	-	-0.24100	[98, 108]

The guest–host interactions between the water and the zeolite are given in table 3.11.

Table 3.11: Guest–host interactions between the Tip5p-Ew water and the zeolite

Pseudo atom identifier	Type of interaction	p_0/k_B [K]	p_1 [Å]	Source
wO - O	12-6 Lennard-Jones	13.7100	3.3765	[98]
wO - Oa	12-6 Lennard-Jones	13.7100	3.3765	[98]

The guest–guest interactions between the extra-framework cations and water are given in table 3.12.

Table 3.12: guest–host interactions between the Tip5p-Ew water and the extra-framework cations

Pseudo atom identifier	Type of interaction	p_0/k_B [K]	p_1 [Å]	Source
wO - Na	12-6 Lennard-Jones	75.0000	2.3900	[98]

Possible shortcomings of this approach are further discussed in section 6. The following section will discuss summarize the integrated DEH$_2$YDR force field.

3.2. Integrated DEH$_2$YDR force field

Integration of all force field parameters of the system considered in this work is summarized in tables A.1 and A.2 in appendix A. To summarize, the system is modelled in the following way:

- Zeolite
    - Rigid framework
    - Point charges on all framework atoms
    - 12-6 Lennard–Jones interactions with:
        ◇ Cations, via 12-6 LJ interaction sites on framework oxygen atoms
        ◇ Hydrogen, via 12-6 LJ interaction sites on all framework atoms
        ◇ Water, via 12-6 LJ interaction sites on framework oxygen atoms
- Extra-framework cations (Na)
    - Single-site, point charge and 12-6 LJ interaction site
- Hydrogen
    - Single-site, chargeless, 12-6 LJ interaction site
- Water
    - 5 point multi-site (Tip5p-Ew)
    - 1 12-6 LJ interaction site on oxygen atom
    - 2 point charges on positions of hydrogen atoms
    - 2 Point charges on positions of oxygen lone pairs

In general no tail corrections are applied using this force field, unless otherwise specified. The following section will discuss technical specifications of all the simulations performed in the RASPA and BRICK simulation environments, needed for the validation of the DEH$_2$YDR force field.

3.3. Simulation parameters

In this work molecular simulation of binary adsorption of hydrogen and water on aluminosilicate zeolites is performed with the use of various statistical ensembles. These ensembles, their application in this work and the used software package can be seen in table 3.13.

Table 3.13: Statistical ensembles used in this work.

Ensemble	Application	Software package
NPT	Density calculations	RASPA [57]
CFCNPT	Fugacity calculations	BRICK [58]
GCMC	Adsorption calculations	RASPA [57]

In all Monte Carlo simulations in this work input parameters are specified, which belong to the following classes:

- Handling of intermolecular forces
- Physical conditions
- Zeolite unit cells
- Monte Carlo cycles
- Monte Carlo moves

These will be discussed shortly.

Intermolecular forces

12-6 Lennard–Jones interactions, as well as electrostatics are calculated for all interaction pairs within a certain range. The characteristic size of this range is called the cut-off and is specified to be 12 Å. Furthermore, the electrostatics are calculated with a relative Ewald precision of 10^{-6}.

Physical conditions
Depending on the ensemble, the number of particles, temperature, volume, pressure or fugacity are specified. These are discussed in detail in section 2.2.

As discussed in section 2.2.1, during GCMC simulations the chemical potential can related to the imposed pressure in two ways:

1. Using the Peng–Robinson equation of state (PR-EOS)
2. Using the fugacity as calculated by simulation in the CFCNPT ensemble

At moderate pressures, use of the PR-EOS can be justified. However, at the high pressures discussed in this work the fugacity coefficients are specified through calculation in the CFCNPT ensemble.

Unit cells
All simulations are performed using periodic boundary conditions, with an appropriate amount of unit cells such that all edges are at least twice the cut-off radius. Thus a minimum unit cell edge length of 24 Å is imposed.

Since Monte Carlo simulations do not take free energy barriers of the zeolite frameworks into account, it is necessary to exclude non-accessible regions, so-called block pockets (BP). These are calculated using the Zeo++ [110] software package. Here, the kinetic radius of a guest molecule is used to probe the zeolite framework and a list of excluded regions is generated which can be implemented in adsorption simulations in RASPA.

Monte Carlo cycles
A Monte Carlo simulation usually consists of two parts: Equilibration and production. In the equilibration phase, the energy of the system is minimized. In the production phase, representative equilibrium configurations are sampled and target properties are calculated. The duration of these phases is specified by a number of Monte Carlo cycles. In this work $5 \cdot 10^4$ equilibration cycles and $5 \cdot 10^5$ production cycles are used, unless mentioned otherwise.

Extra care has to be taken in simulations where extra-framework cations are involved. Here, an extra equilibration phase is added where the cations and the zeolite framework are simulated in the absence of other guest molecules. Running this equilibration phase at elevated temperatures ensures that the extra-framework cations can overcome local energy minima and for a large number of cycles ($5 \cdot 10^5$) is a measure that the positions of the cations are close to their equilibrium values. In this work, this type of equilibration is performed at 1000 K.

Monte Carlo Moves
Each MC cycle consist of a number of moves. The number of moves is imposed to be larger or equal to the number of molecules, with a minimum of 20. Furthermore, the maximum distances for translation and rotation are adjusted in the equilibration phase to achieve an acceptance rate of 50%. The the trial moves and corresponding probabilities used in this work can be found in the input files in appendix B.

Quality of results
After having performed a MC simulation, the quality of the results can be interpreted in multiple ways. Independent of the ensemble that is used, the most important factor is the standard deviation of the target property. If this is too high, there can be two reasons:

1. The equilibration phase was not long enough for the system to reach equilibrium

2. The production phase was not long enough to get reasonable statistics

Furthermore in the specific ensembles there are some factors that determine the success of a simulation. In the CFCNPT ensemble, the distribution of the scaling factor of the fractional molecule $p(\lambda)$ has to be flat. In the GCMC ensemble, the number of molecules that are inside the zeolite framework has to stabilize within the equilibration phase. Furthermore, as a rule of thumb, the total number of successful molecule exchanges has to exceed a thousand.

With the DEH$_2$YDR force field and the simulation settings in place, the next chapter discusses the validation of the force field.

4. Force field validation

This chapter aims to validate the correct implementation of the DEH$_2$HYDR force field. Intrinsic properties of the guest molecules at low- and high pressures will be evaluated. These include density of the pure components and fugacities of the mixture at system conditions. Furthermore, molecular simulation experiments performed by S. Calero and Deeg et al. for adsorption of hydrogen on zeolites will be replicated. Since these were performed at low pressures, extra literature is reviewed of adsorption of hydrogen on zeolites at high pressures. Finally, experiments performed by Castillo et al. for adsorption of water on hydrophilic zeolites are replicated [98]. The aim of this section is to gain understanding on the performance of the DEH$_2$HYDR force field in the limits of hydrophobic versus hydrophilic zeolites and low versus high pressures.

4.1. Hydrogen

In order to address the quality of the hydrogen model in the DEH$_2$HYDR force field, multiple experiments are conducted. First, the densities at atmospheric and at the elevated system pressure are calculated with Monte Carlo simulation in the NPT ensemble. Then, a GCMC simulation by Deeg et al. of low pressure adsorption of hydrogen on silicious zeolite MFI at 77 K is replicated. Followed by replication of unpublished work of S. Calero on low pressure adsorption of hydrogen on aluminosilicate zeolite LTA4A at 77 K. Finally, a comparison will be made for adsorption at higher pressures. The adsorption of hydrogen as predicted by the DEH$_2$YDR force field will be compared to the adsorption as calculated by Akten et al., on the aluminosilicate zeolite LTA4A at 298 K.

NPT density

Results of NPT simulations of 512 hydrogen molecules at 310 K and pressures of 1 bar and 875 bar, using the DEH$_2$HYDR force field, are shown in table 4.1. As can be seen in appendix B under simulation inputs, changes in the volume of the system were attempted with a probability of 5%.

Table 4.1: Density calculations for hydrogen with the DEH$_2$YDR force field in the NPT ensemble

Number of molecules [#]	Pressure [bar]	Temperature [K]	Density ρ [kg/m^3]	St. dev. σ_ρ
512	1	310	0.0814	0.003
512	875	310	44.644	0.005

These values are in good agreement with the values obtained in the simulation study at elevated pressure by Rahbari et al. The experimental values from REFPROP and values from simulations with the Buch [60] force field are included. The latter has the closest resemblance to the DEH$_2$HYDR force field since it also uses a single-site uncharged Lennard–Jones interaction site. This can be seen in table 4.2.

Table 4.2: Hydrogen density calculations from Rahbari et al.

ρ [kg/m^3]			
Pressure [bar]	Temperature [K]	REFPROP	Buch [60]
800	323	40.63	40.78
1000	323	47.01	47.22

Next, adsorption of hydrogen on zeolites at low pressures is investigated.

Low pressure adsorption of hydrogen on aluminosilicate zeolite LTA4A at 77 K

Simulations were performed in the GCMC ensemble. The zeolite framework and extra-framework cations were equilibrated without the presence of hydrogen for $5 \cdot 10^5$ cycles. The adsorption was simulated in the pressure range of $0.50 \cdot 10^{-3} - 1.25 \cdot 10^2$ kPa. The inclusion of the Feynmann–Hibbs effective quantum potential was also tested, it can be seen in figure 4.1b that at 77 K, the inclusion of this potential is necessary to yield accurate results. Overall, the results are in good agreement.
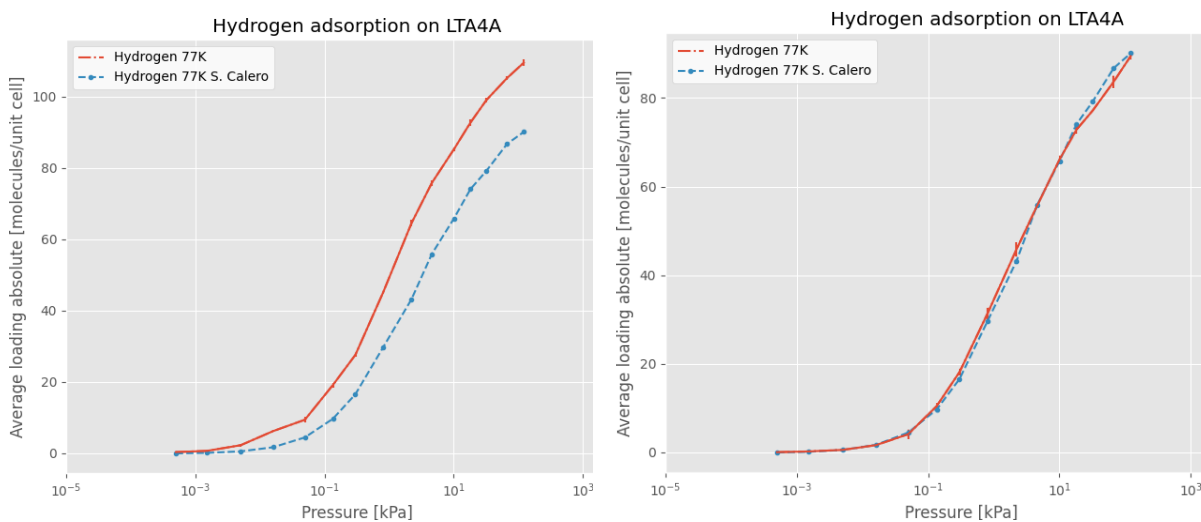
(a) **Absolute loading.** GCMC simulations of adsorption of hydrogen on LTA4A at 77K, using the DEH$_2$YDR force field **excluding FH potentials**, compared to simulations by S. Calero. Lines are guides to the eye.

(b) **Absolute loading.** GCMC simulations of adsorption of hydrogen on LTA4A at 77K, using the DEH$_2$YDR force field **including FH potentials**, compared to simulations by S. Calero. Lines are guides to the eye.

Low pressure adsorption of hydrogen on silicious zeolite MFI at 77 K

Simulations were performed in the GCMC ensemble. The adsorption was simulated in the pressure range of $0.50 \cdot 10^{-3} - 1.25 \cdot 10^2$ kPa. Again, the Feynmann–Hibbs effective quantum potential was included. It can be seen in figure 4.2 that at 77 K, the results are in good agreement.
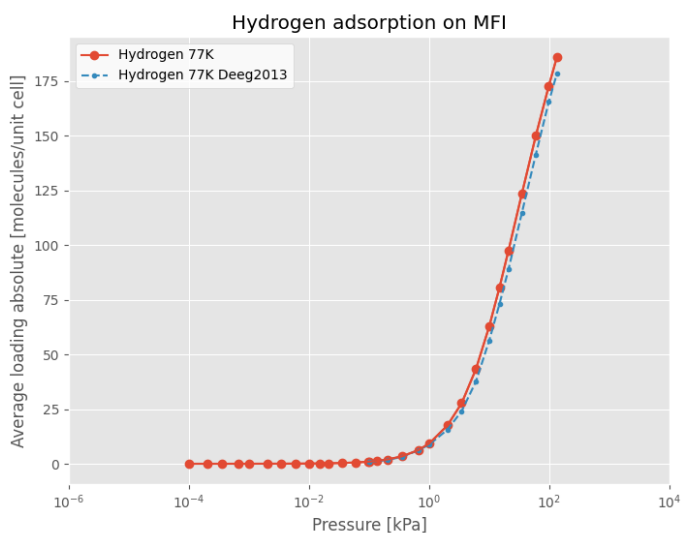
Figure 4.2: **Absolute loading.** GCMC simulations of adsorption of hydrogen on MFI at 77K, using the DEH$_2$YDR force field including FH potentials, compared to simulations by Deeg et al. Lines are guides to the eye. Error bars within symbol size.

Next, adsorption of hydrogen on zeolites at high pressures is investigated.

High pressure adsorption of hydrogen on aluminosilicate zeolite LTA4A at 298 K

The aim of this section is to investigate the performance of the DEH_2YDR force field at predicting adsorption of hydrogen on aluminosilicate zeolites at high pressure. Akten et al. fitted a multi-site hydrogen model to experimental data. A comparison between the predicted adsorption of the Akten et al. force field and the DEH_2YDR force field is made. To this end, simulations were performed in the GCMC ensemble. The zeolite framework and extra-framework cations were equilibrated without the presence of hydrogen for $5 \cdot 10^5$ cycles. The adsorption was simulated in the pressure range of $0.50 \cdot 10^{-3} - 1.25 \cdot 10^2$ kPa.

The approach taken by Akten et al. differs from the DEH_2YDR force field in the following aspects:

1. Use of a multi-site atom model [111]
   (a) Two 6-12 Lennard-Jones interaction sites at the atomic positions of the hydrogen atoms
   (b) Three point charges
        i. Two negative charges at the atomic positions of the hydrogen atoms
        ii. One positive charge at the center of mass of the molecule, chosen to match the quadrupole moments
2. Fixing Na(I) type cations in place whilst leaving Na(II) and Na(III) cations mobile
3. A Lennard–Jones cut-off distance of 11.5 Å
4. Chemical potentials as calculated by Darkrim et al., as opposed to calculation by means of the PR-EOS in this work.

The magnitude of these potentials is given in compared to the DEH_2YDR force field in tables 4.3 and 4.4.

Table 4.3: Van der Waals parameters and point charges for H_2 model by Akten et al.

Pseudo atom identifier	Type of interaction	p_0/k_B [K]	% diff	p_1 [Å]	% diff	point charge [e]	% diff	Source
Si	Coulombic	-	-	-	-	0.80000	2%	[63, 65]
Al	Coulombic	-	-	-	-	1.42000	192%	[63, 65]
O	Coulombic	72.0000	-	2.7080	-	-0.74000	88%	[63, 65]
Na	Coulombic & LJ	251.7800	0%	2.8050	-11%	0.74000	-86%	[63, 65]
$H2_H$	Coulombic	36.7000	0%	2.9580	0%	-0.48290	-	[65]
$H2_L$	Coulombic	-	-	-	-	0.96580	-	[65]

As can be seen from the table, especially the values of the point charges deviate a lot from those of the DEH_2YDR force field. The guest–host interactions between the negatively charged hydrogen atoms and the Aluminum atoms of the framework will therefore contribute to a significant increase in adsorption. Furthermore, it can be seen that the Lennard–Jones potentials used in this force field are weaker than those of the DEH_2YDR.

Table 4.4: Pairwise interaction potentials for H_2 model by Akten et al.

Interaction pair	Type of interaction	p_0/k_B [K]	% diff	p_1 [Å]	% diff	Mixing rule	Source
H2 - Si	12-6 Lennard-Jones	-	-	-	-	-	[65]
H2 - Al	12-6 Lennard-Jones	-	-	-	-	-	[65]
H2 - O	12-6 Lennard-Jones	51.4043	-22%	2.8330	-2%	Lorentz-Berthelot	[65]
H2 - Oa	12-6 Lennard-Jones	51.4043	-22%	2.8330	-2%	Lorentz-Berthelot	[65]
H2 - Na	12-6 Lennard-Jones	96.1266	-56%	2.8815	-4%	Lorentz-Berthelot	[65]
O - Na	12-6 Lennard-Jones	134.6409	308%	2.7565	-14%	Lorentz-Berthelot	[65]
Oa - Na	12-6 Lennard-Jones	134.6409	485%	2.7565	-19%	Lorentz-Berthelot	[65]

These differences lead to a bad agreement in the moderate pressure regime, as can be seen in figure 4.3.
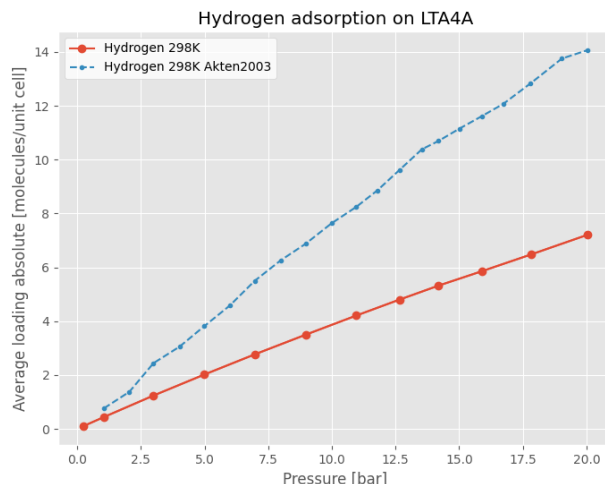
Figure 4.3: **Absolute loading.** GCMC simulations of adsorption of hydrogen on LTA4A at 298K, using the DEH$_2$YDR force field, compared to simulations by Akten et al. Lines are guides to the eye. Error bars within symbol size.

To see if the observed difference also plays a role at higher pressures, a comparison between the predicted adsorption by Darkrim et al. and the DEH$_2$YDR force field is made. Again, simulations were performed in the GCMC ensemble. The adsorption was simulated in the pressure range of 0 – 1500 bar. Results can be seen in figure 4.4 Upon inspection of this divergence of number of molecules adsorbed per unit cell at the system pressure of 875 bar, it is concluded that there is a difference of 40 molecules per unit cell.
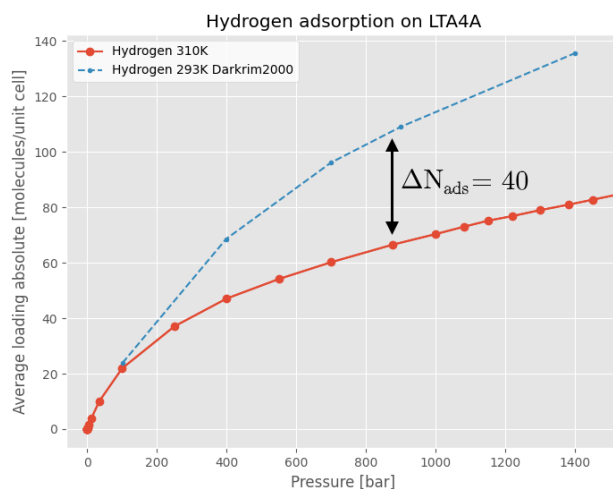
Figure 4.4: **Absolute loading.** GCMC simulations of adsorption of hydrogen on LTA4A at 310 K, using the DEH$_2$YDR force field, compared to experiments & simulations by Darkrim et al. at 293 K. Lines are guides to the eye. Error bars within symbol size.

Akten et al. also tested the influence of polarizability and note that the number of adsorbed hydrogen molecules is increased by 30% when polarization is taken into account. They argue that at high pressures, the omission of polarization effects can't be justified.

Computation of the chemical potential via the Peng–Robinson Equation of State could be the cause of this deviation. It is well established that this Equation of State can have poor performance in the high pressure regime [98]. Investigation of this influence is discussed in the last section of this chapter.

High pressure adsorption of hydrogen on various silicious zeolites at 300 K

Rahmati and Modarress investigated the high pressure adsorption of hydrogen on silicious zeolites ACO, ANA, ASV and MEP at pressures ranging from 0-10000 bar in the temperature range of 100-350 K [113]. From these, simulations at 1000 bar and 300 K were replicated since these are the closest to the system temperature and pressure used in this work. Results of these simulations can be seen in table 4.5.

Table 4.5: GCMC simulations of adsorption of hydrogen on various silicious zeolites at 300 K, using the DEH$_2$YDR force field, compared to simulations by Rahmati and Modarress

Structure Name	Pressure [bar]	Temperature [K]	Loading [mol/uc] DEH$_2$YDR	Loading [mol/uc] Rahmati2009	% diff	Source
ACO	1000	300	7	20	-66%	[113]
ASV	1000	300	4	24	-84%	[113]
MEP	1000	300	13	69	-81%	[113]
ANA	1000	300	12	69	-83%	[113]

To summarize, this leads to the conclusion that one has to be careful when interpreting the results for simulations of dehydration of hydrogen at high pressure. The GCMC simulations of binary adsorption of hydrogen and water on aluminosilicate zeolites will likely also underpredict the amount of hydrogen adsorbed by the zeolite framework. This issue might partially be circumvented by addressing the issue of predicting fugacity coefficients, which will be discussed in the last section of this chapter.

4.2. Water

In order to address the quality of the water model in the DEH$_2$HYDR force field, multiple experiments are conducted. First, the densities at atmospheric and at the elevated system pressure are calculated with Monte Carlo simulation in the NPT ensemble. Then, a GCMC simulation by Castillo et al. of low pressure adsorption of water on aluminosilicate zeolite LTA4A in a range of temperatures between 273 K and 374 K is replicated [98]. Finally, simulations by Desbiens et al. for low pressure adsorption of water on silicious zeolites are replicated.

NPT density

Results of NPT simulations of 512 water molecules at 310 K and pressures of 1 bar and 875 bar, using the DEH$_2$HYDR force field, are shown in table 4.6. As can be seen in appendix B under simulation inputs, changes in the volume of the system were attempted with a probability of 5%.

Table 4.6: Density calculations for water with the DEH2YDR force field in the NPT ensemble

Number of molecules [#]	Pressure [bar]	Temperature [K]	Density ρ [kg/m^3]	St. dev. σ_ρ
512	1	310	993.065	1.199
512	875	310	1032.828	2.517

These values are in good agreement with the experimental values at 310 K (993.42 kg/m^3) and the values obtained in the simulation study at elevated pressure by Rahbari et al.. The experimental values from REFPROP and values from their simulations with the Tip5p-Ew [108] force field are included. This can be seen in table 4.7.

Table 4.7: Density calculations for water in the NPT ensemble from Rahbari et al.

ρ [kg/m^3]			
Pressure [bar]	Temperature [K]	REFPROP	Tip5p-Ew [5]
800	323	1020.1	1025
1000	323	1027.4	1034

Low pressure adsorption of water on aluminosilicate zeolite LTA4A at 273–374 K

Simulations were performed in the GCMC ensemble. The zeolite framework and extra-framework cations were equilibrated without the presence of hydrogen for $5 \cdot 10^5$ cycles. The adsorption was simulated in the pressure range of $1 \cdot 10^{-2} – 5 \cdot 10^3$ Pa. All parameters used in the simulations of Castillo et al. were replicated in the DEH$_2$YDR force field. The results can be seen in figure 4.5.
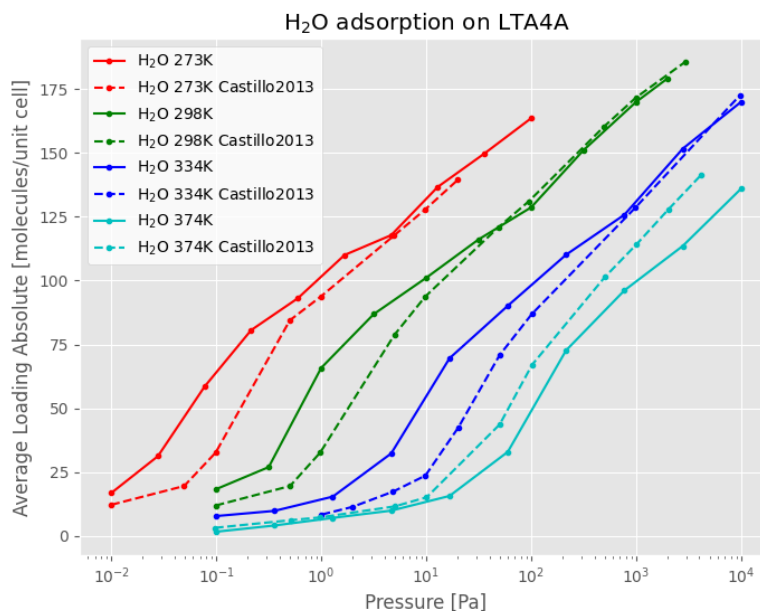
Figure 4.5: **Absolute loading.** GCMC simulations of adsorption of water on LTA4A at 273-374K, using the DEH$_2$YDR force field, compared to simulations by Castillo et al. Lines are guides to the eye. Error bars within symbol size.

The discrepancy with the simulations in this work can be caused by several factors:

- The atomic positions of the zeolite framework
- The equilibration of water adsorption simulations
- The equilibration of extra-framework cations
- The use of blocking pockets to exclude water from adsorbing inside sodalite type cages
- The application of tail corrections

These factors will be evaluated and compared to the base case adsorption plot of water adsorption on LTA4A at 374 K which can be seen in figure 4.6. Here, the framework characterisation from the IZA database has been used, no blocking pockets were implemented and no tail corrections were applied.

Framework atom positions

Castillo et al. compare simulation of adsorption of water on two different characterisation of the LTA4A framework, that of Fitch et al. and Olson for the hydrated and dehydrated zeolite structure respectively. This differs from the characterisations used in this work, that of the pure silicious structure as obtained from the IZA database [102] and, for verification purposes, that of Pluth and Smith for the dehydrated structure. These differences are likely to play a large role in the observed deviations [40].

The equilibration of water adsorption simulations

Ramachandran et al. report that for the case of calculations of water density or water adsorbed on zeolites, a unusually large number of equilibration steps is necessary. Castillo et al. elaborate on this argument with the point that pressures in the region that is between the inflection point and the saturation zone of the isotherm require extra equilibration. Their guidelines with regard to amount of equilibration cycles are abided.
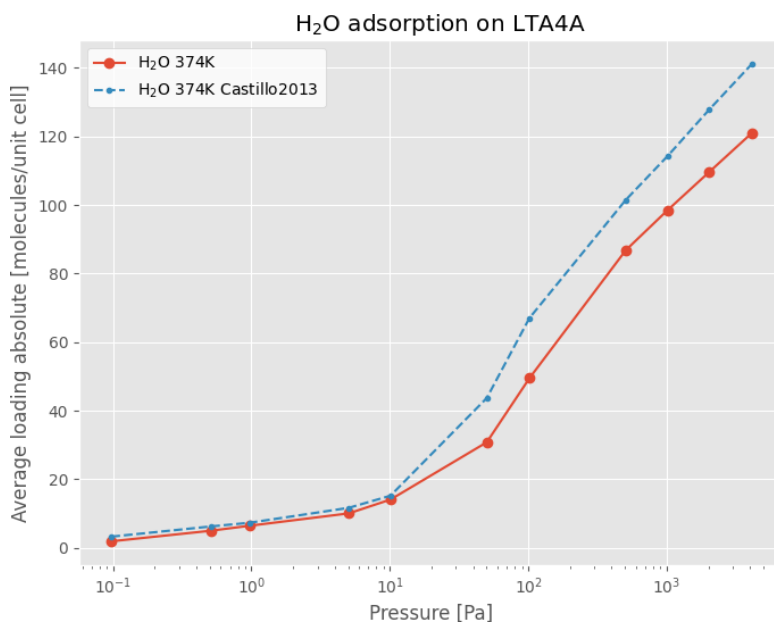
Figure 4.6: **Absolute loading. Best result, base case for comparison.** GCMC simulations of adsorption of water on LTA4A at 374K, using the DEH$_2$YDR force field, compared to simulations by Castillo et al. Lines are guides to the eye. Error bars within symbol size.

Equilibration of extra-framework cations

The influence of the equilibration of extra-framework cations can be seen in figure 4.7. In this simulation, sodium atoms of the type I and II are placed at their crystallographic equilibrium positions and no pre-equilibration of their location at 1000 K is performed. [98]. Inadequate equilibration of the sodium atoms results in a bad prediction of the adsorption behaviour.
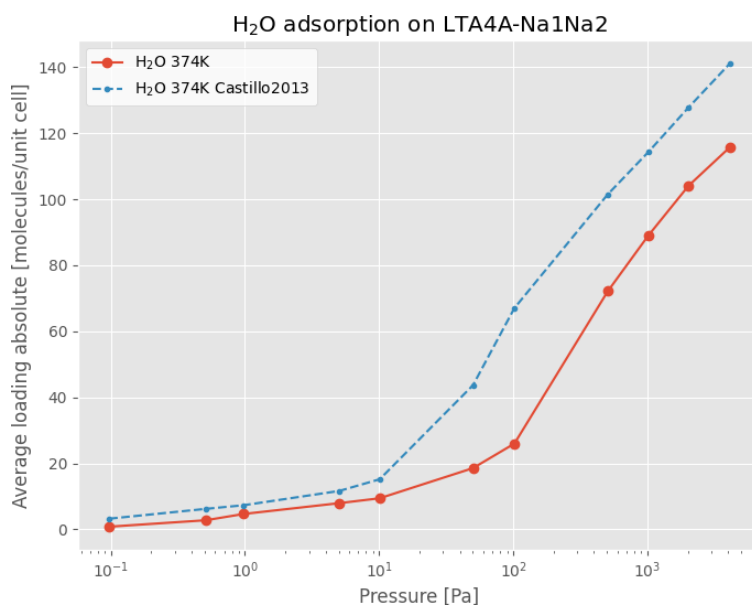
Figure 4.7: **Absolute loading. Result of inadequate extra-framework cation equilibration.** GCMC simulations of adsorption of water on LTA4A at 374K, using the DEH$_2$YDR force field, compared to simulations by Castillo et al. Lines are guides to the eye. Error bars within symbol size.

Blocking pockets excluding water from sodalite cages

The influence of the use of blocking pockets to exclude water from adsorbing inside sodalite type cages can be seen in figure 4.8. As expected it lowers the adsorption of the entire pressure range. As such it results in a relatively bad prediction of the adsorption behaviour.
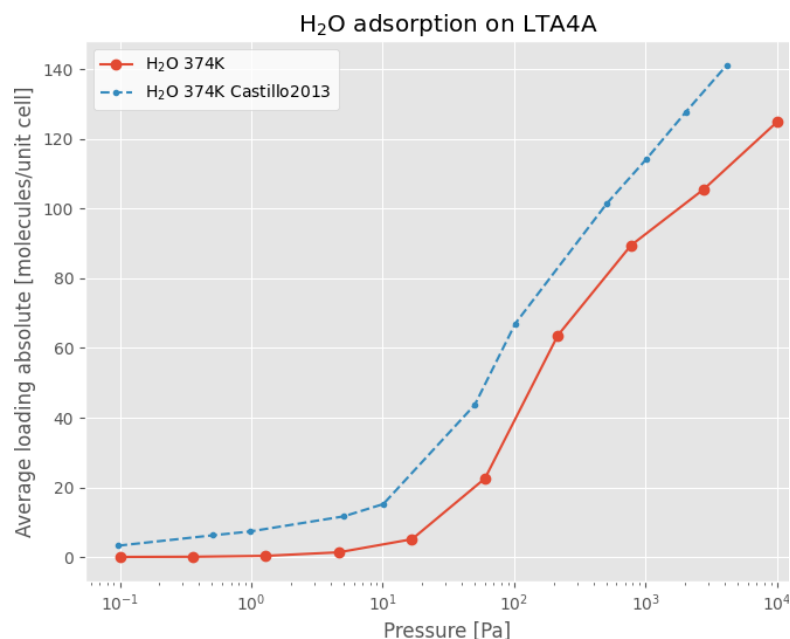
Figure 4.8: **Absolute loading. Result of excluding sodadite cages with blocking pockets (BP).** GCMC simulations of adsorption of water on LTA4A at 374K, using the DEH$_2$YDR force field, compared to simulations by Castillo et al. Lines are guides to the eye. Error bars within symbol size.

Tail corrections

The influence of implementing tail corrections can be seen in figure 4.9. It does not significantly influence the prediction capability of the adsorption behaviour.
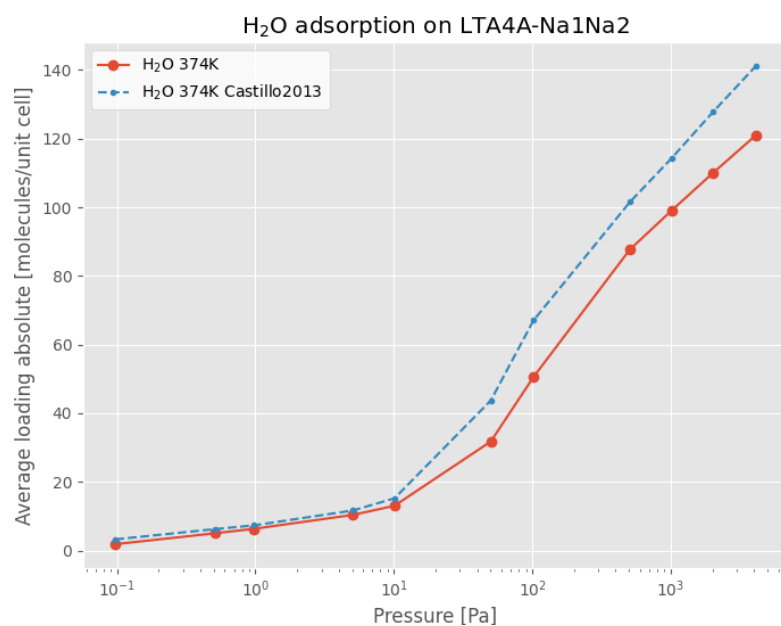
Figure 4.9: **Absolute loading. Result of implementing tail corrections.** GCMC simulations of adsorption of water on LTA4A at 374K, using the DEH$_2$YDR force field, compared to simulations by Castillo et al. Lines are guides to the eye. Error bars within symbol size.

Castillo et al. furthermore add that deviations observed at higher pressures can be attributed to the change in the water dipole moment, which is not taken into account in the DEH$_2$YDR force field, and warn that classical, non-polarizable water force fields are not transferable between different hydrophilic zeolite types.

Low pressure adsorption of water on silicious zeolite MFI

As discussed by Desbiens et al. and later by Lella et al., the experimental measurements of water adsorption on silicious zeolites is hindered by the fact that water adsorbs strongly on defects in the zeolite framework [40]. When modelling this adsorption on perfect zeolite structures in the low pressure regime, the absolute adsorption is extremely low. The order of magnitude is some 0.2 molecules per unit cell. This was verified by replicating simulations performed by Desbiens et al. The results are in good agreement, as can be seen in figure 4.10
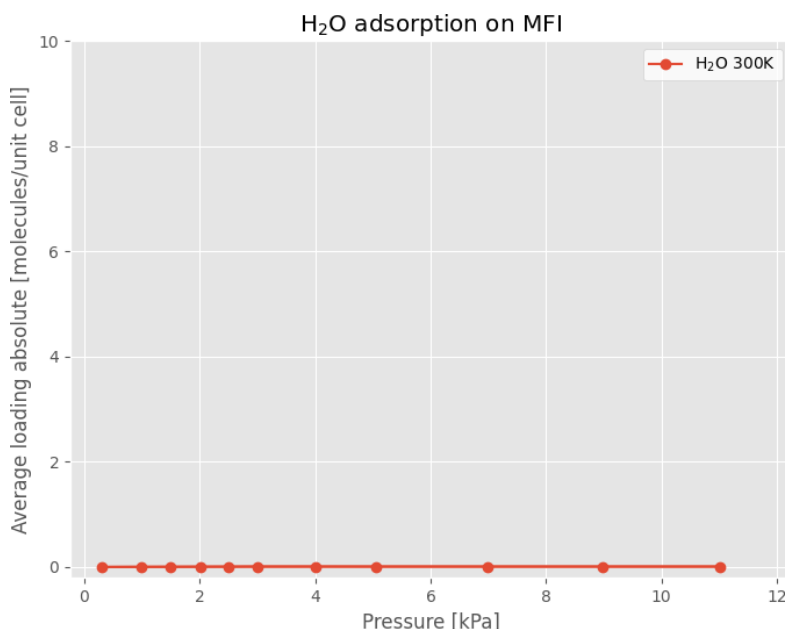
Figure 4.10: **Absolute loading near zero.** GCMC simulations of adsorption of water on MFI at 300K, using the DEH_2YDR force field, compared to simulations by Desbiens et al. Lines are guides to the eye. Error bars within symbol size.

High pressure adsorption of water on zeolites

The performance of predicting adsorption of pure water on zeolites at high pressures is not addressed in this work. Not much literature has been devoted to this topic, as such replication of (simulation) experiments is not feasible. Furthermore, it is hindered by the fact that pure water at elevated pressures undergoes a phase change to liquid, and as such the mechanisms of adsorption are hard to capture. Desbiens et al. describe condensation of water on zeolites at elevated pressures and conclude that saturated water vapour condensates on MFI at pressures of 750-1000 bar. Since water is present only in ppm amounts in the system investigated in this work, its partial pressure is not likely to reach the high pressure regime. The good agreements of water adsorption on zeolites in the low pressure regime is thus assumed a sufficient basis for calculation of binary adsorption at high pressures. Next, predictions of the binary adsorption of hydrogen and water on zeolites is addressed.

Binary adsorption of hydrogen and water on zeolites

To the best of the authors knowledge, the only experimental- or simulation work performed on systems involving hydrogen, water and zeolites was performed by Zhu et al. In their experiments, adsorption single-component isotherms of adsorption of hydrogen, water, CO and CO2 and their binary mixture permeations through a LTA4A membrane were measured experimentally. They conclude that the LTA4A zeolite shows a supreme selectivity (eq. 2.16) for water over hydrogen with a value of $S_{H_2O/H_2} = 5$ [117].

In general, by increasing temperature, the amount of water adsorbed on the zeolite decreases slightly. This will create space for the adsorption of hydrogen. Therefore, the selectivity is concluded to decrease with temperature. Furthermore they find a saturation capacity for water adsorption of 15.81 mol/kg which corresponds to 216 molecules/unit cell. In these experiments a total pressure of 1 atm was used and temperatures in the range of 300–400 K were tested.
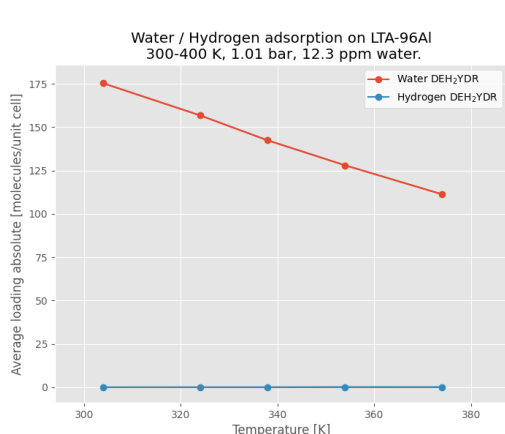
(a) **Absolute loading.** GCMC simulations of binary adsorption of hydrogen and water on LTA-96Al at 300-400K, using the DEH_2YDR force field. Lines are guides to the eye. Error bars within symbol size.
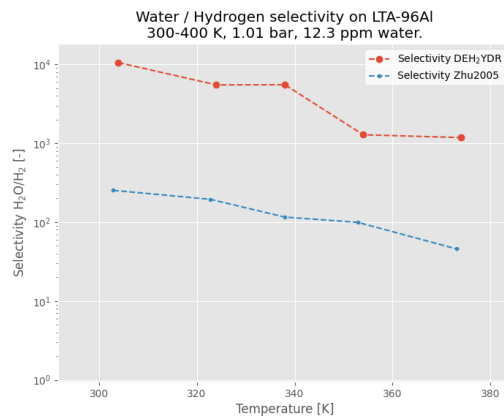
(b) **Selectivity** H_2O/H_2**.** GCMC simulations of binary adsorption of hydrogen and water on LTA-96Al at 300-400K, using the DEH_2YDR force field, compared to permeation experiments by Zhu et al. Lines are guides to the eye. Error bars within symbol size.

These findings are replicated with the DEH_2YDR force field. Simulations of single component water and binary component hydrogen/water were performed in the GCMC ensemble. The temperature, pressure and water mole fraction during these simulations were set to the system values of 310K, 875 bar and 12.3 ppm respectively. The zeolite framework and extra-framework cations were equilibrated without the presence of hydrogen for $5 \cdot 10^5$ cycles. The adsorption was simulated in the pressure range of $0.50 \cdot 10^{-3} - 1.25 \cdot 10^2$ kPa.

The results of these simulations can be seen in table 4.8. An extra row is added, where the selectivity of this framework at the system conditions is calculated.

Table 4.8: Selectivity of H_2O/H_2 on LTA4A at 300-400K compared to experimental results of Zhu et al.

Temperature [K]	P_{H_2O} [bar]	P_{tot} [bar]	mole frac H_2O [%]	mole frac H_2O [ppm]	Selectivity [-] Zhu2005	Selectivity DEH_2YDR	Factor diff.
304	0.0221	1	2.211%	221.1	253	10520	42
324	0.0221	1	2.211%	221.1	195	5489	28
338	0.0221	1	2.211%	221.1	116	5512	48
354	0.0221	1	2.211%	221.1	99	1280	13
374	0.0221	1	2.211%	221.1	46	1179	26
310	1.0763	875	0.123%	12.3	-	5.23	-

It is observed that at none of the specified temperatures the saturation loading of 216 molecules/unit cell is reached. Due to the perfect hydrophilicity of the framework, nearly no hydrogen is adsorbed during the simulations, this results is an extremely high predicted selectivity for water. These deviations with the experimental results, a factor of roughly 30, has to be taken into accounts when analyzing the results of simulation of binary hydrogen/water adsorption on aluminosilicate zeolites.

Next, the influence of accurately predicting fugacity coefficients is addressed.

4.3. Fugacity coefficients

The accuracy of Monte Carlo simulations in the Grand Canonical ensemble is directly related to the accuracy of predicting fugacity coefficients for the components, because the chemical potential specified in these simulations directly relates to this quantity. Therefore, the quality of two methods for obtaining fugacity coefficients are compared:

- Using the Peng–Robinson Equation of State (PR-EoS)
- Using simulations in the Continuous Fractional Component NPT (CFC-NPT) ensemble

The first method is the standard for simulations in the RASPA software environment, making use of the critical constants specified for each component as discussion in section 2.2.1. The second method is a more natural

choice for computing the fugacity coefficients for mixtures as the interactions specified by the force field are used as a direct input, therefore yielding an overall consistent approach.

Rahbari et al. note that the fugacity coefficients for hydrogen as obtained from the PR-EoS deviate from experimental data for pressures higher than 400 bar. They pioneered the calculation of fugacity coefficients for the hydrogen/water mixture at elevated pressures and note that the fugacity coefficients of pure hydrogen in the gas phase are best predicted using the Buch [60] and Marx [105] force fields. The Buch force field has a close resemblance to the parameterisation of the DEH_2YDR force field and as such will be included in the comparison. The results can be seen in table 4.9 and in figure 4.12.

Table 4.9: **Fugacity coefficient of hydrogen.** Calculated using CFCNPT for hydrogen water mixture at system conditions, compared to results of Rahbari et al.

Pressure [bar]	Fugacity coefficients for hydrogen [-] at T= 323 K as predicted by		
	Rahbari2019 Tip3p/Marx CFCNPT	PR-EOS	REFPROP
100	1.050	1.030	1.060
200	1.120	1.070	1.120
400	1.250	1.170	1.260
600	1.400	1.280	1.420
800	1.590	1.420	1.600
1000	1.790	1.570	1.800
	Fugacity coefficients for hydrogen [-] at T= 310 K as predicted by		
Pressure [bar]	DEH_2YDR CFCNPT	St. Dev.	
875	1.684	0.011383	
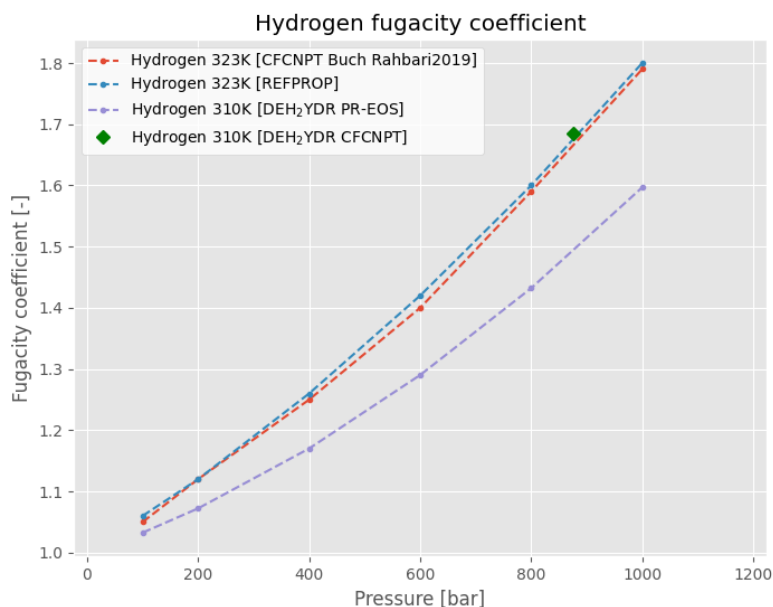
Figure 4.12: **Fugacity coefficient of hydrogen.** Calculated using CFCNPT for hydrogen water mixture at system conditions, compared to results of Rahbari et al.

This shows that the fugacity coefficient of hydrogen at the system conditions is underpredicted by 12% by the PR-EoS. Therefore, in the remainder of this work the result as obtained by simulation in the CFC-NPT ensemble will be used.

The fugacity coefficient for water in the mixture can be calculated by CFC-NPT calculation of a set of hydrogen molecules at the system conditions of 875 bar and 310 K with the addition of a single fractional component water molecule. The excess chemical potential for this water molecule can then be translated into a fugacity coefficient using the limit of infinite dilution as shown in section 2.2.1. The results can be seen in table 4.10 and in figure 4.13.

Table 4.10: **Fugacity coefficient of water.** Calculated using CFCNPT for hydrogen water mixture at system conditions, compared to results of Rahbari et al.

Pressure [bar]	Fugacity coefficients for water at infinite dilution [-] at T= 323 K as predicted by	
	Rahbari2019 Tip3p/Marx CFCNPT	PR-EOS
100	0.930	0.737919
300	1.144	0.482341
500	1.405	0.371852
800	1.900	0.301841
1000	2.295	0.283124
	Fugacity coefficients for water at infinite dilution [-] at T= 310 K as predicted by	
Pressure [bar]	DEH$_2$DR CFCNPT	stdev
875	1.460	0.017416
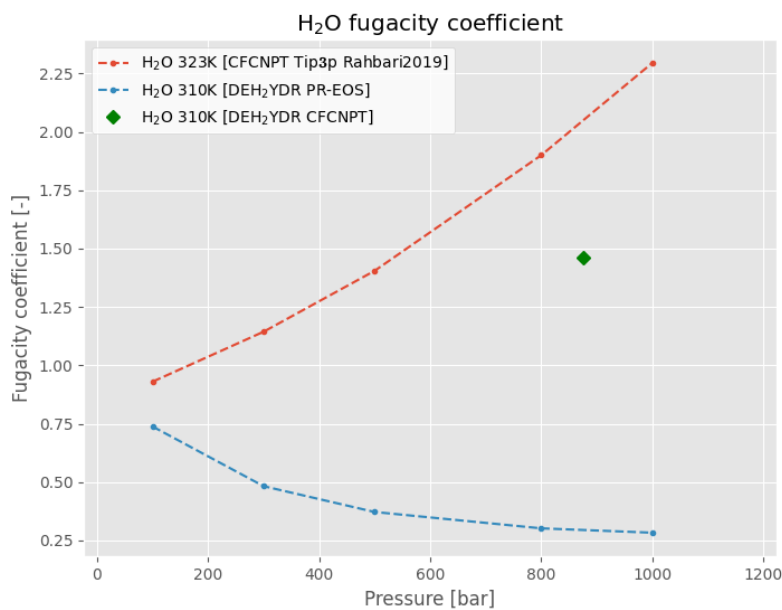
Figure 4.13: **Fugacity coefficient of water.** Calculated using CFCNPT for hydrogen water mixture at system conditions, compared to results of Rahbari et al.

This shows that the fugacity coefficient of water at the system conditions is underpredicted by almost 400% by the PR-EoS. Therefore, in the remainder of this work the result as obtained by simulation in the CFC-NPT ensemble will be used.

Prediction of adsorption of water and hydrogen on zeolites using the DEH$_2$YDR force field

To summarize the performance of predicting water adsorption on zeolites with the DEH$_2$DR force field, results are shown in table 4.11. It is noted that the GCMC simulations of binary adsorption of hydrogen and water on zeolites, using the DEH$_2$DR force field, will likely underpredict the amount of hydrogen adsorbed on the zeolite framework.

Table 4.11: Summary of the force field validation results

Guest(s)	Pressure	Zeolite classification	Adsorption prediction	Source
Hydrogen	Low	Hydrophillic	Good	S. Calero
Hydrogen	Low	Hydrophobic	Good	[91]
Hydrogen	High	Hydrophillic	Moderate	[63, 65]
Hydrogen	High	Hydrophobic	Moderate	[113]
Water	Low	Hydrophillic	Good	[98]
Water	Low	Hydrophobic	Good	[80]
Water	High	Hydrophillic	Not investigated	-
Water	High	Hydrophobic	Not investigated	-
Hydrogen & Water	Low	Hydrophillic	Moderate	[117]

The focus of the next chapter is the layout of a screening study of a set of industrially relevant zeolites.

5. Zeolite screening

In the course of this chapter, research objectives 2 and 3 will be addressed: Identifying screening criteria for determining the optimal zeolite for high pressure hydrogen dehydration and identifying key parameters for designing the optimal zeolite. The latter is achieved by a screening study of 6 zeolites of industrial relevance: The CHA, FAU, FER, LTA, MFI and MOR framework types. The details of this screening study will be presented, together with a detailed description of each framework type. Finally, research objective 4 will be addressed, identifying feasible routes to avoid computation of adsorption isotherms, here the application of the Ideal Adsorbed Solution Theory is presented.

5.1. Screening Criteria

To achieve maximum separation of water from the hydrogen mixture it is a requirement that water is strongly adsorbed on the zeolite whereas hydrogen is not. A quantitative measure of this criterion is given by the adsorption selectivity for water over hydrogen given by equation 5.1.

$$S_{H_2O/H_2} = \frac{N_{abs, \ H_2O}}{N_{abs, \ H_2}} \tag{5.1}$$

Where N_{H_2O} is the absolute amount of water molecules adsorbed on the zeolite framework and N_{H_2} is the absolute amount of hydrogen molecules adsorbed on the zeolite framework. A value of $S > 1$ thus indicates a preferable adsorption of water. This selectivity will be used as the screening criterion in this work, thereby rather straightforwardly fulfilling the second research objective. The next research objective is aimed at obtaining parameters that are strongly linked to the performance of the zeolite structure at selectively adsorbing water. These parameters can be of a physical, chemical or topological nature. Descriptors that will be discussed in this work include:

- Si/Al ratio
- Topological descriptors
- Temperature

Pressure is omitted from this list since it is not a variable that is allowed to change in the system investigated in this work. From the force field validation section, and the work of Zhu et al. we assume that an increase in temperature will lead to a decrease in selectivity. As such, only the system temperature of 310 K will be investigated.

Si/Al ratio

The adsorption of water on zeolites is known to be strongly linked to the hydrophilicity of the framework and thus to the Si/Al ratio [74]. Chen [118, 119] showed that there is a linear increase in the amount of water adsorbed the number of Al atoms in the zeolite framework, for a series of mordenites. Similarly, Olson et al. [120] demonstrated a similar relationship for HZSM5 type zeolites. There is thus a solid base for the hypothesis that the Si/Al ratio of the framework plays a large role in the selectivity of adsorption of hydrogen and water on zeolites.

Topological descriptors

To identify the dependency of selectivity on the topology of the investigated frameworks, topological descriptors are calculated using the Zeo++ software package [110], using Helium as a probe molecule. These one-dimensional descriptors include the accessible volume (AV), accessible surface area (ASA), diameter of the largest free- (MFS) and included spheres (MIS) of the pore space [23]. Their values for the zeolites investigated in this work are shown in table 5.1.

Structure Name	Structure	Space Group	Length A [Å]	Length B [Å]	Length C [Å]	Angle α [°]	Angle β [°]	Angle γ [°]	Simulation Box Size
CHA	trigonal	R -3 m (# 166)	13.675	13.675	14.767	90	90	120	2 2 2
FAU	cubic	F d -3 m (# 227)	24.345	24.345	24.345	90	90	90	1 1 1
LTA	cubic	P m -3 m (# 221)	11.919	11.919	11.919	90	90	90	3 3 3
MOR	orthorhombic	C m c m (# 63)	18.256	20.534	7.542	90	90	90	2 2 4
MFI	orthorhombic	P n m a (# 62)	20.09	19.738	13.142	90	90	90	2 2 2
FER	orthorhombic	I m m m (# 71)	19.018	14.303	7.541	90	90	90	2 2 4

Structure Name	Volume [Å^3]	AV [%]	HeVF [-]	ASA [Å^2/g]	MIS [Å]	MFS A [Å]	MFS B [Å]	MFS C [Å]	
CHA	2391.6	17.27	0.387787	1242.09	7.37	3.72	3.72	3.72	
FAU	14428.8	27.42	0.478338	1132.31	11.24	7.35	7.35	7.35	
LTA	1693.2	21.43	0.452335	1105.93	11.05	4.21	4.21	4.21	
MOR	2827.3	12.27	0.28918	759.828	6.7	1.57	2.95	6.45	
MFI	5211.3	9.81	0.250152	696.572	6.36	4.7	4.46	4.46	
FER	2051.3	10.01	0.273343	803.255	6.31	1.56	3.4	4.69	

Structure Name	Min ring size	Max ring size	Framew. dens. [T/1000Å3]
CHA	4	8	15.1
FAU	4	12	13.3
LTA	4	8	14.2
MOR	4	12	17
MFI	4	10	18.4
FER	5	10	17.6

Figure 5.1: Topological Descriptors for the zeolite frameworks investigated in this work.

The parameter space of one-dimensional descriptors of the zeolite structures in the from the IZA database are plotted in figures 5.2, 5.3 and 5.4. The CHA, FAU, FER, LTA, MFI and MOR framework types investigated in this work are highlighted.
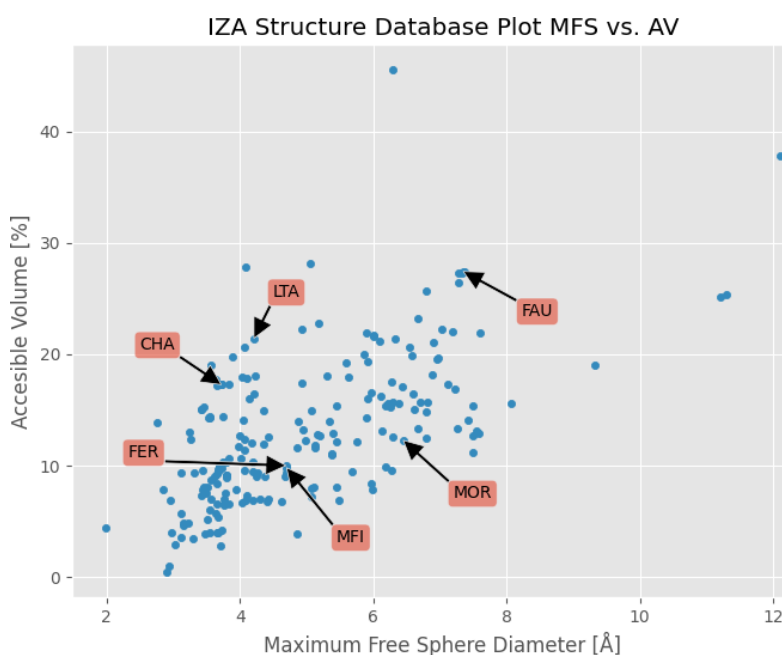
Figure 5.2: Accessible volume versus Maximum Free Sphere plot for all IZA zeolites.

IZA Structure Database Plot MIS vs. AV
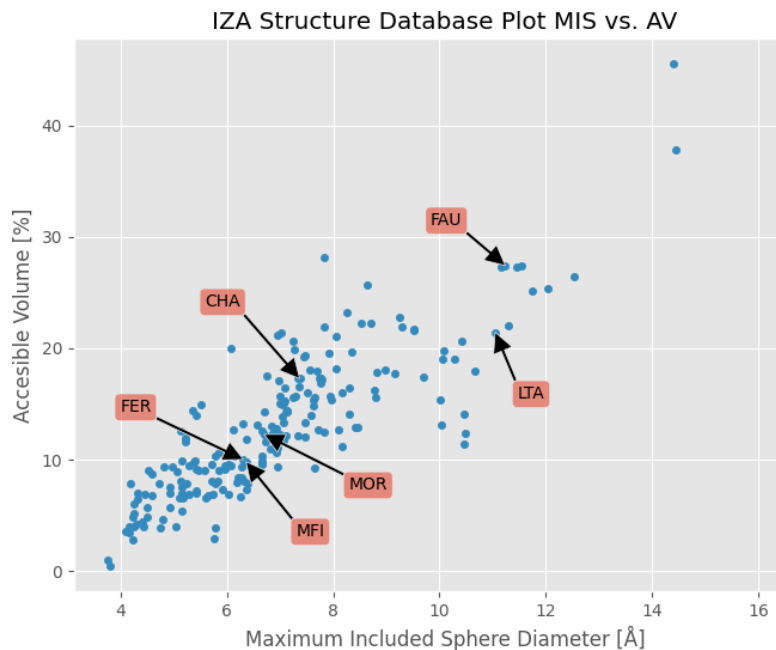
Figure 5.3: Accessible volume versus Maximum Included Sphere plot for all IZA zeolites.

IZA Structure Database Plot HeVF vs. ASA
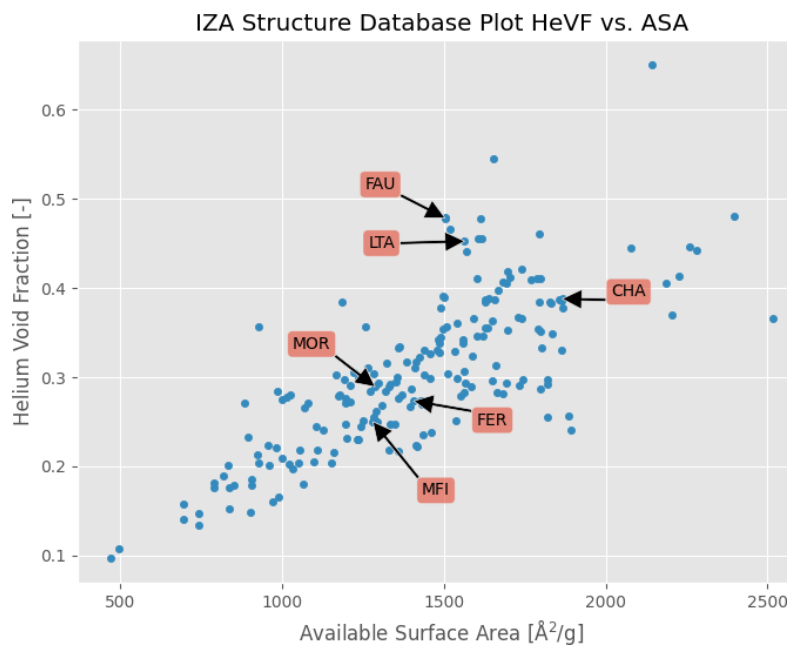
Figure 5.4: Helium void Fraction versus Accesible Surface Area plot for all IZA zeolites.

During all simulations, the effect of Blocking Pockets (BP) on the predicted adsorption is evaluated. The CHA, FAU, FER, LTA, MFI and MOR framework types are shortly introduced in the next sections. Building blocks that are used to describe zeolite topologies include channels and cages. Conventional naming of the type of cages and their characteristic dimension are listed in table 5.1.

Table 5.1: Common naming for cage types in zeolites

Cage type	Also called	Characteristic size
Supercage	α cage	13 Å
Sodalite cage	β cage	7 Å

5.2. Framework specifics

Chabazite (CHA)

Zeolites of the chabazite (CHA) type have a skewed unit cell where one of the angles is 120 degrees, containing 36 T-sites. These form a three-dimensional system of channels containing pores made from eight-membered rings of oxygen atoms. The channel structure is built up by hexagonal prisms that are connected by four-membered rings [121]. An orthographic representation along the 001-axis, together with a 3D representation are shown in figures 5.5a and 5.5b.
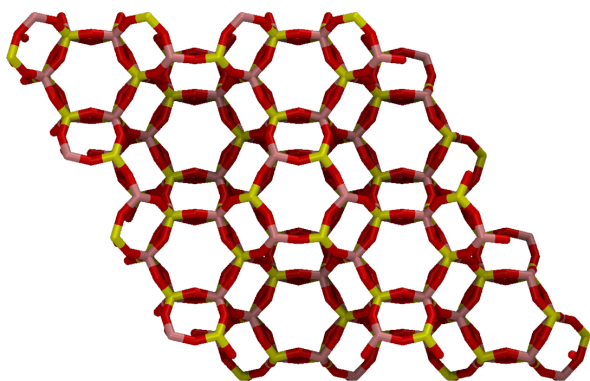
(a) Orthographic view of CHA along 001-axis.
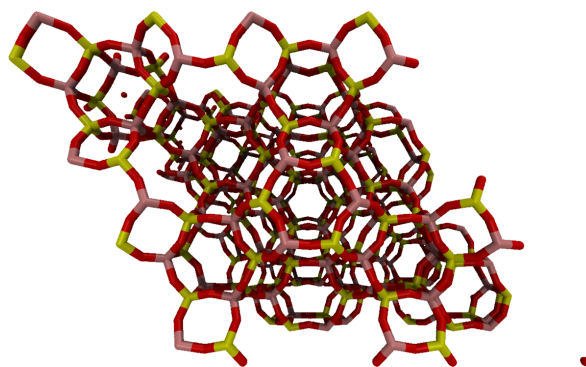
(b) 3D view of CHA

Of the structures investigated in this work CHA has the smallest window size and as such the smallest maximum free sphere diameter (MFS) whereas it has the largest available surface area (ASA).

Faujasite (FAU)

Zeolites of the faujasite (FAU) type have a unit cell with a length of 24.8536 Å in all directions that contains 192 T-sites. The structure contains hexagonal prisms and sodalite cages that connect to the 6-ring and 12-ring windows of the supercages [9]. An orthographic representation along the 001-axis, together with a 3D representation are shown in figures 5.6a and 5.6b.
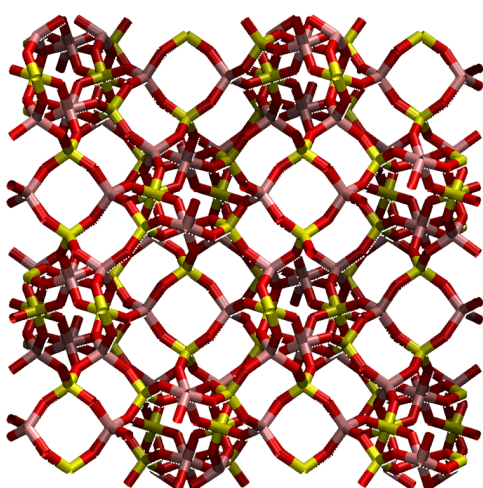
(a) Orthographic view of FAU along 001-axis.
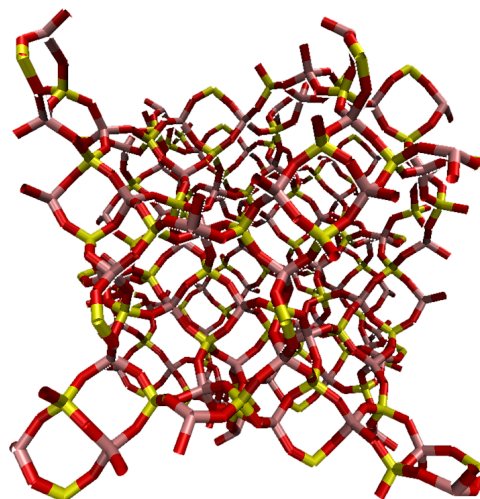
(b) 3D view of FAU

A noteworthy property of this type of zeolite is that it appears in nature with a minimum Si/Al ratio of 1.0 [101]. Among the structures investigated in this work FAU has the largest accessible volume (AV), maximum free sphere diameter (MFS) and maximum included sphere diameter (MIS).

Ferrierite (FAU)

Zeolites of the ferrierite (FER) type have a unit cell containing 36 T-sites, that consists of straight 10-rings that are stacked in the 001-direction and are interconnected by cages with 8-ring windows in the 110-plane. [85] An orthographic representation along the 001-axis, together with a 3D representation are shown in figures 5.7a and 5.7b.

(a) Orthographic view of FER along 001-axis.   (b) 3D view of FER
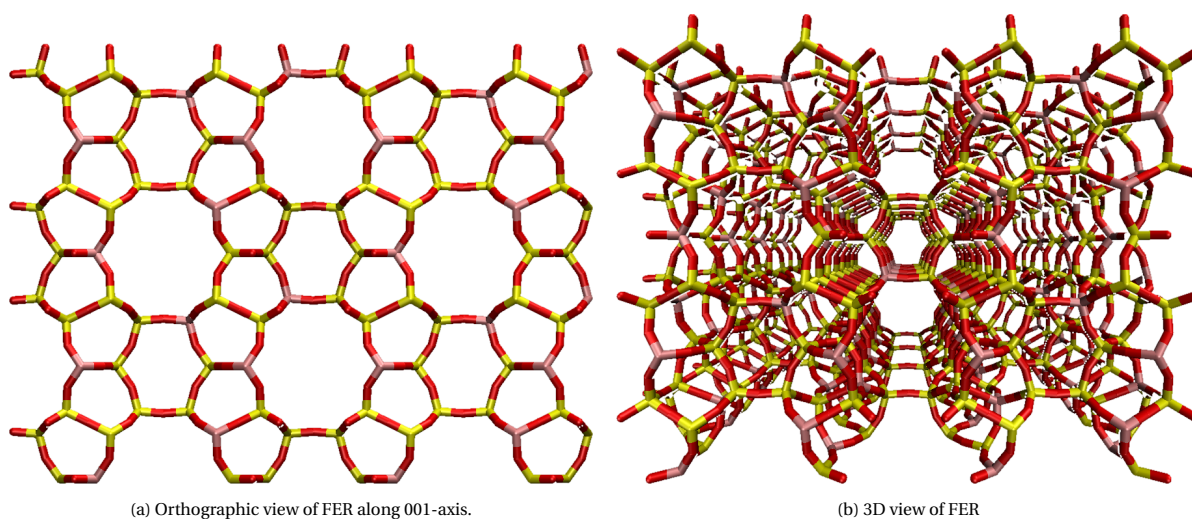
Among the structures investigated in this work FER has low accessible volume (AV), maximum free sphere diameter (MFS) and maximum included sphere diameter (MIS) indicating that the is not much void space and whilst having an average available surface area (ASA).

Zeolite Type A (LTA)

Zeolites of the Zeolite Type A (LTA) type have a unit cell containing 192 T-sites, that consists of supercages that are interconnected by 8-ring windows and sodalite cages [30]. An orthographic representation along the 001-axis, together with a 3D representation are shown in figures 5.8a and 5.8b.
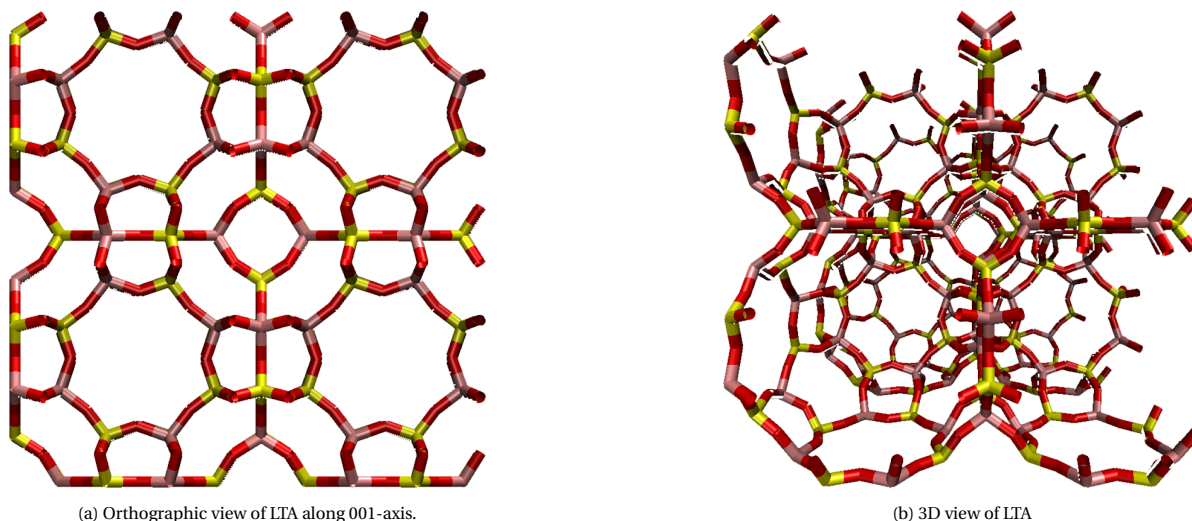
(a) Orthographic view of LTA along 001-axis.   (b) 3D view of LTA

A noteworthy property of this type of zeolite is that it appears in nature with a minimum Si/Al ratio of 1.0[101]. Among the structures investigated in this work LTA shows similarity to the FAU structure, but differs in the aspect that the has the accessible volume (AV) is slightly smaller and the maximum free sphere diameter (MFS) is significantly smaller.

MFI

Zeolites of the MFI type have a unit cell containing 96 T-sites, that consists of elliptical straight channels, which run in the 010-direction, zig-zag that run parallel to the 101-plane and their intersections. An orthographic representation along the 001-axis, together with a 3D representation are shown in figures 5.9a and 5.9b.
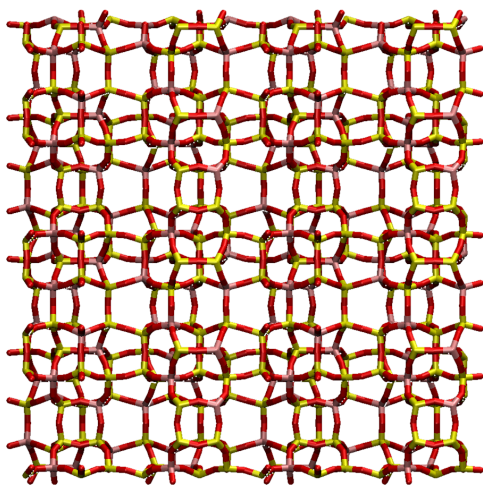
(a) Orthographic view of MFI along 001-axis.
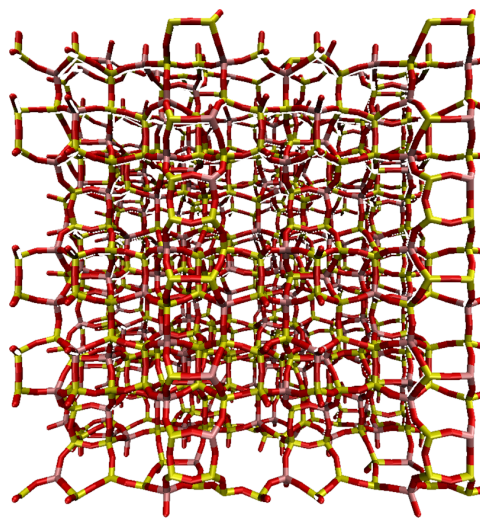
(b) 3D view of MFI

Among the structures investigated in this work this type of zeolite has the highest natural Si/Al ratio [122], as well as the lowest accessible volume (AV).

Mordenite (MOR)

Zeolites of the mordenite (MOR) type have a unit cell containing 48 T-sites, that consists of main channels in the 001-direction constructed from slightly elliptical 12-membered rings, connected to smaller side channels via a set of eight-membered rings [8]. An orthographic representation along the 001-axis, together with a 3D representation are shown in figures 5.9a and 5.9b.
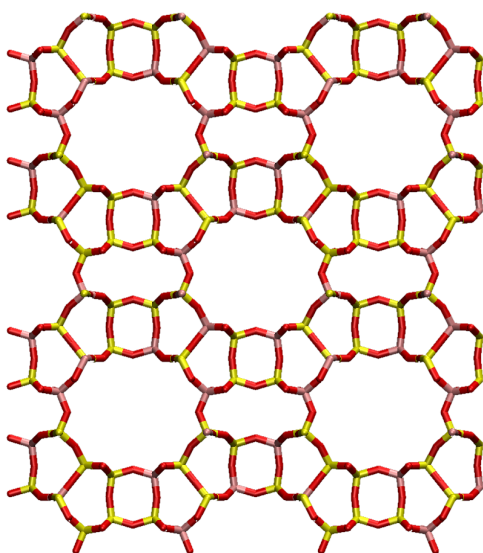
(a) Orthographic view of MOR along 001-axis.
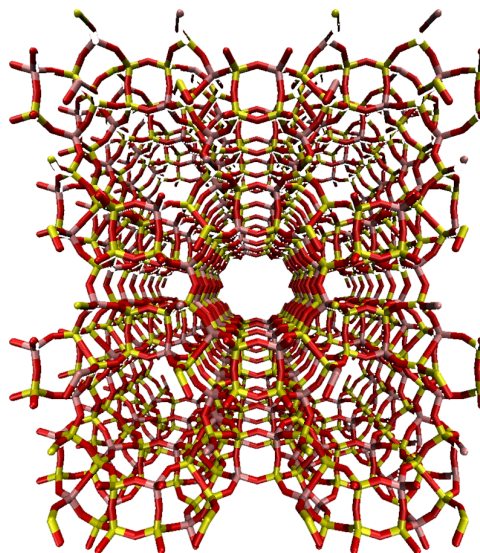
(b) 3D view of MOR

Among the structures investigated in this work this type of zeolite has a relatively low available surface area (ASA).

Using Ideal Adsorbed Solution Theory

To address research objective 4, identifying feasible routes to avoid computation of adsorption isotherms, the use of the Ideal Adsorbed Solution Theory (IAST) is investigated. In order to predict binary adsorption isotherms using IAST, single component isotherms are required. These can be calculated using GCMC simulations and fitted to a simplified adsorption model such as the Langmuir model, given by equation 2.27. Often, predicting a single point of a multicomponent adsorption isotherm and predicting it for a single-component isotherm have roughly the same computational cost. [22] Therefore, it is desired to predict the single component isotherms using quantities that are cheaper to compute.

In the case of the Langmuir model, the Henry coefficient (K_H) can be predicted using Widom's test particle insertion method[48]. The maximum loading (q_{max}) can be estimated by assuming that the zeolite pore structure at the system conditions of 875 bar and 310 K will always be saturated. It will consequently be a function that can be estimated using the following parameters:

1. The free pore volume V_{Free}, given by equation 5.2
2. The density of the adsorbent at the system conditions, calculated with simulation in the NPT ensemble:

$$\rho_{ads}(310\,K,\,875\,bar)$$

3. The fraction of the kinetic radii of Helium and the adsorbent:

$$F_{kin} = \frac{\sigma_{He}}{\sigma_{ads}}$$

$$V_{Free} = HeVF \cdot V_{unitcell} - N_{Na} \cdot V_{Na} \tag{5.2}$$

Here, HeVF is the Helium void fraction of the zeolite framework [-], $V_{unitcell}$ is the volume of the unit cell [Å^3], N_{Na} the number of extra-framework cations and V_{Na} is the volume occupied by a single extra-framework cation.

The estimation of the saturation loading for component i is then given by equation 5.3.

$$q_{max,\,i} = V_{\text{free}} \cdot \rho_i \cdot F_{\text{kin},i} \tag{5.3}$$

An algorithm for predicting binary adsorption using this strategy is given below:

- Calculate density of component 1 at system conditions in NPT ensemble (once)
- Calculate density of component 2 at system conditions in NPT ensemble (once)
- Calculate Helium void fraction (HeVF) of zeolite framework (once)

1. Calculate Henry coefficient for component 1 at specific pressure
2. Calculate Henry coefficient for component 2 at specific pressure
3. Estimate q_{max} for component 1 for specific N_{Na} using equation 5.3.
4. Estimate q_{max} for component 2 for specific N_{Na} using equation 5.3.
5. Perform IAST calculation using pyIAST software package [123] yielding binary adsorption isotherm

5.3. Screening Procedure

The screening procedure consists of performing GCMC simulations of binary adsorption of hydrogen and water on the zeolites at the system temperature (T=310 K), pressure (P=875 bar) and mole fractions ($f_{H_2O} = 12.3 \cdot 10^{-6}$). For each zeolite framework, multiple Si/Al ratios will be simulated. These frameworks are created from the silicious structures as obtained from the IZA database [102], by random substitution of Si atoms by Al atoms. During this process, it is enforces that Löwensteins rule is obeyed by the framework. In the hydrophilic limit, this algorithm aims to find the structure with the highest amount of Al atoms by using a brute force search. The minimum possible Si/Al ratio obtained by this algorithm for the framework types investigated in this work are listed in table 5.2, together with the minimum Si/Al ratios found in literature. Although some of the Si/Al ratios used in this work are not experimentally feasible yet, there is nothing that obstructs simulations of these limits.

Table 5.2: Lower Si/Al ratio limits for the investigated frameworks

Framework name	Number of Si atoms [#]	Number of Al atoms [#]	min Si/Al ratio theoretical [-]	min Si/Al ratio from literature [-]
CHA-144Al	144	144	1	2.4 [124]
FAU-96Al	96	96	1	1.0 [101]
FER-160Al	160	62	2.6	3.0 [101]
LTA-96Al	96	96	1	1.0 [101]
MFI-256Al	256	128	2	9.3 [122]
MOR-256Al	256	128	2	5.0 [125]

The screening procedure consists of the following steps, for each framework type:

1. Creation of the aluminosilicate zeolite frameworks with specified Si/Al ratio from the silicious IZA structure
2. Equilibration of extra-framework Na atoms without presence of hydrogen and water at $T = 1000K$ for $5 \cdot 10^5$ cycles to ensure equilibrium positions
3. Performing simulations
   (a) GCMC simulations of binary adsorption of hydrogen and water on the aluminosilicate zeolite framework at the system temperature ($T = 310K$) and mole fractions ($f_{H_2O} = 12.3 \cdot 10^{-6}$) and with varying pressures ($P = 0$–$1000bar$)
   (b) GCMC simulations of single component adsorption of hydrogen or water on the aluminosilicate zeolite framework at the system temperature ($T = 310K$) and mole fractions ($f_{H_2O} = 12.3 \cdot 10^{-6}$) and with varying pressures ($P = 0$–$1000bar$)
   (c) GCMC simulation of binary adsorption of hydrogen and water on the aluminosilicate zeolite framework at the system temperature ($T = 310K$), pressure ($P = 875bar$) and mole fractions ($f_{H_2O} = 12.3 \cdot 10^{-6}$)
4. Processing results
   (a) Fitting adsorption isotherms to results of single component GCMC simulations for predicting binary adsorption isotherms with Ideal Adsorbed Solution Theory (IAST), as will be discussed in the last section of this chapter.
   (b) Calculate adsorption selectivity for binary adsorption simulations, defined by equation 2.16.
5. Analyse results and trends in selectivity versus descriptors

Possible shortcomings and extensions of this analysis are discussed in section 6. The next chapter will highlight the results of the screening study that was introduced.

6. Results & Discussion

Ideal Adsorbed Solution Theory

The performance of the Ideal Adsorbed Solution Theory (IAST) on predicting binary adsorption of hydrogen and water at the system temperature (T=310 K), pressure (P=875 bar) and mole fraction ($f_{H_2O} = 12.3 \cdot 10^{-6}$) on zeolite LTA was tested at two Si/Al ratios, zeolite MFI was tested at one Si/Al ratio. The specifics of these GCMC simulations are summarized in table 6.1.

Table 6.1: List of simulation conditions that are used to assess performance of IAST.

Framework	Si/Al ratio [-]	Temperature [K]	Pressure [bar]	Mole fraction H_2O [ppm]
LTA-96Al	1.0	310	0 - 1000	12.3
LTA-50Al	2.8	310	0 - 1000	12.3
MFI-30AL	2.2	310	0 - 1000	12.3

The IAST calculations in this section were performed by fitting the K_H and q_{max} parameters to the single component isotherms, this would not be the case if this method was to be used to achieve research objective 4, identifying feasible routes to avoid computation of adsorption isotherms. In that case, the value of q_{max} would be predicted using equation 5.3, and k_H by means of Widom insertion. Even using the fitted values, the predictions of IAST are quite poor as is illustrated below.

Figure 6.1a shows results for the IAST calculations on framework LTA-96Al, also known as LTA4A. These contain Langmuir adsorption isotherms calculated with the fitted values for K_H and q_{max}, as well as the estimated values obtained by Widom's test particle insertion method and by using equation 5.3. As can be seen in figure 6.1b, the prediction of the binary adsorption is very poor, especially for the water.

(a) **Absolute loading.** GCMC simulations of **single-component** adsorption of hydrogen/water on LTA-96Al at 310K, using the DEH$_2$YDR force field. Error bars within symbol size. Dashed lines represent Langmuir isotherm constructed by calculated values of k_H and q_{max}. Solid lines represent **fitted Langmuir isotherms**.

(b) **Absolute loading.** GCMC simulations of **binary adsorption** of hydrogen and on LTA-96Al at 310K, using the DEH$_2$YDR force field. Error bars within symbol size. Solid lines represent **mixture isotherms as calculated with IAST**.

Figure 6.2b shows results for the IAST calculations on framework LTA-50Al. This framework contains less Al atoms and thus also less extra-framework cations. As can be seen the prediction of the binary adsorption is better than for LTA-96Al. In this case however, the prediction of q_{max} for water by equation 5.3 is quite poor, as is indicated by the dashed line. and therefore the prediction of the binary adsorption is reasonable.
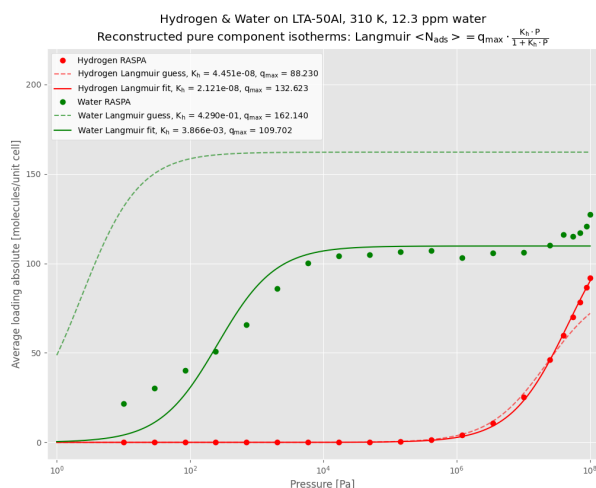
(a) **Absolute loading.** GCMC simulations of **single-component** adsorption of hydrogen/water on LTA-50Al at 310K, using the DEH$_2$YDR force field. Error bars within symbol size. Dashed lines represent Langmuir isotherm constructed by calculated values of k_H and q_{max}. Solid lines represent **fitted Langmuir isotherms**.
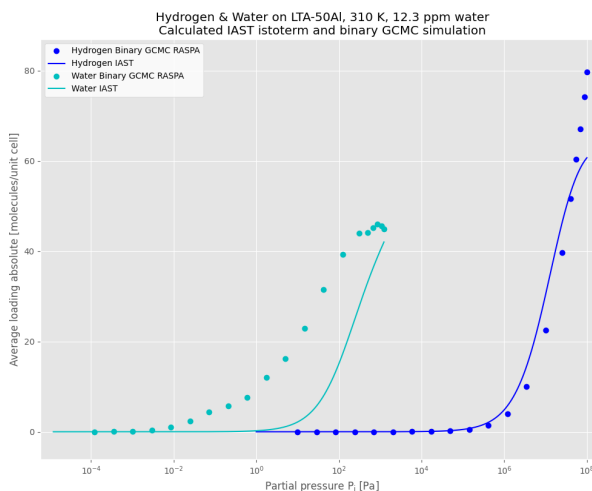
(b) **Absolute loading.** GCMC simulations of **binary adsorption** of hydrogen and on LTA-50Al at 310K, using the DEH$_2$YDR force field. Error bars within symbol size. Solid lines represent **mixture isotherms as calculated with IAST**.

Finally, figure 6.3b shows results for the IAST calculations on framework MFI-30Al. Once more, the prediction of the binary adsorption is quite poor, as well as the prediction of q_{max} for water.
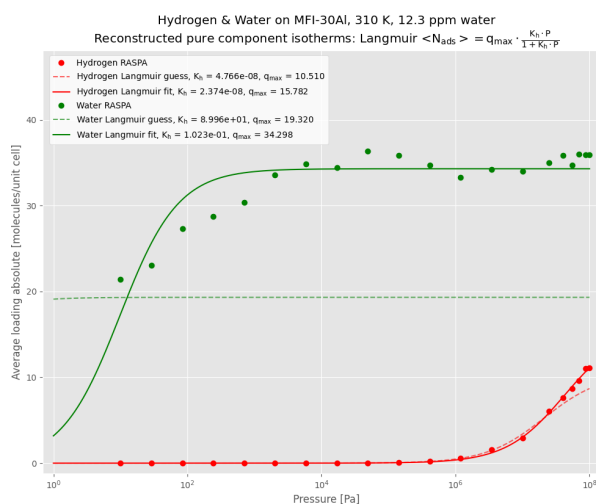
(a) **Absolute loading.** GCMC simulations of **single-component** adsorption of hydrogen/water on MFI-30Al at 310K, using the DEH$_2$YDR force field. Error bars within symbol size. Dashed lines represent Langmuir isotherm constructed by calculated values of k_H and q_{max}. Solid lines represent **fitted Langmuir isotherms**.
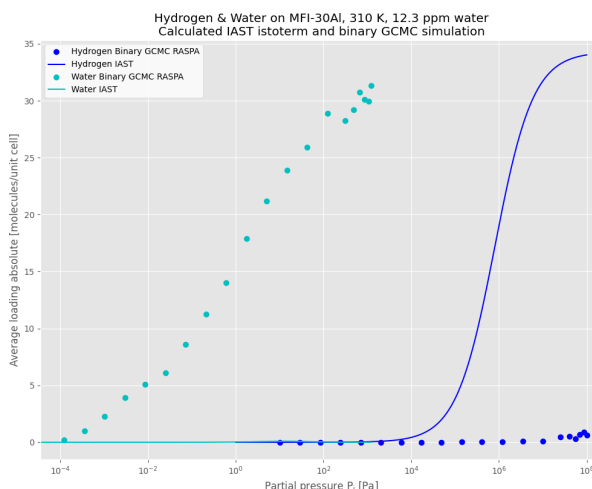
(b) **Absolute loading.** GCMC simulations of **binary adsorption** of hydrogen and on MFI-30Al at 310K, using the DEH$_2$YDR force field. Error bars within symbol size. Solid lines represent **mixture isotherms as calculated with IAST**.

To investigate why the predictions of IAST for the system investigated in this work are poor, the assumption regarding IAST that were addressed in section 2.3 are revisited:

1. Adsorbate molecules in the mixture have equal access to the entire surface area of the adsorbent
2. The adsorbent is homogeneous
3. The adsorbed phase is an ideal solution in which interactions between molecules are equivalent in strength.

With regards to the third assumption we evaluate the Lennard–Jones interaction potentials of the guest molecules, these are given in table 6.2 and illustrated in figure 6.4. The table displays the percentual difference of the Lennard–Jones interaction strengths with regard to the lowest off all interaction pairs, the H2–H2 interaction.

Table 6.2: Relative interaction strength of 12-6 Lennard-Jones potentials in the DEH$_2$YDR force field.

Interaction pair	Type of interaction	p_0/k_B [K]	% diff
wO - wO	12-6 Lennard-Jones	89.5160	144%
wO - H2	12-6 Lennard-Jones	57.3428	56%
wO - Na	12-6 Lennard-Jones	75.0000	104%
H2 - H2	12-6 Lennard-Jones	36.7330	0%
H2 - Na	12-6 Lennard-Jones	220.0000	500%
Na - Na	12-6 Lennard-Jones	251.7800	585%
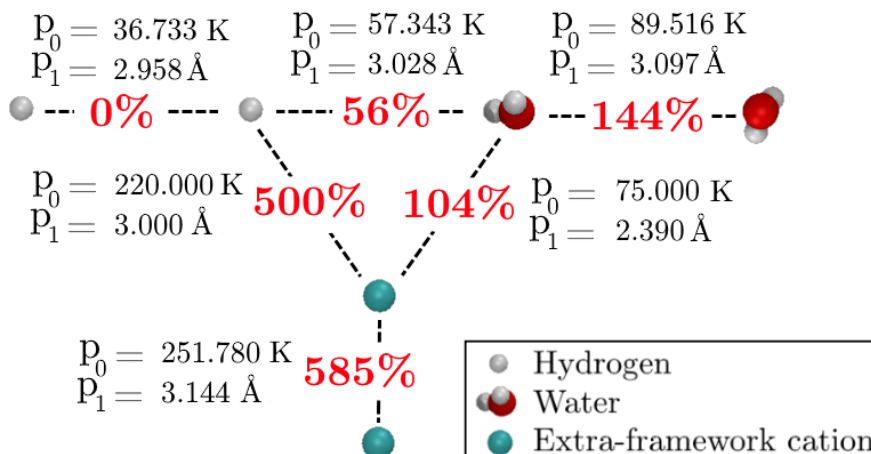
Figure 6.4: Relative interaction strength of 12-6 Lennard-Jones potentials in the DEH$_2$YDR force field.

The interaction strengths of the extra-framework cations reach up to 500% of the strength of the H2–H2 interactions. Additionally, as more Al atoms are introduced into the framework, the Coulombic interactions also increase tremendously. As reported by Vlugt et. al [41], the interactions of the extra-framework cations and the zeolite framework are very strong. As such, the adsorbed phase can not be assumed to be an ideal solution.

This result was also observed by Akten et al. during binary simulations of H_2/CO_2 and H_2/N_2 mixtures on zeolite LTA4A. They conclude that the IAST predictions do not perform well at describing the variation in adsorption selectivity with pressure [65].

Practical implementation of the algorithm formulated in section 5 is hindered by the fact that the Henry coefficient for water in aluminosilicate zeolites with the presence of mobile extra-framework cations are hard to predict. Desbiens et al. observe large fluctuations of this quantity, making it hard to get representative statistics. In this work, several attempts were made to circumvent this problem: By immobilizing the cations after their equilibration, by attempting to get estimates of K_H by omitting the presence of the cations and by disabling electrostatics during the simulations. None of these methods yielded values of K_H within reasonable accuracy of the Langmuir fit.

The models used to fit the single component isotherms were varied using combinations of all adsorption models available in the pyIAST package. Of these isotherms, the Langmuir model yielded the lowest R^2 value for both hydrogen and water, even though upon inspection the hydrogen isotherm does not reach a saturation loading within the specified pressure regime.

The single component water isotherm does display Langmuir behaviour but is concluded that q_{max} is not dependent only on free volume, but rather on the Si/Al ratio of the framework. This observation will be discussed in the next section.

More complex alternatives to IAST are available [126–128], although they still can't cope entirely with competitive adsorption that arises from a large difference in adsorption due to polarity [129–131].

Zeolite Screening

Binary adsorption of hydrogen and water at the system temperature (T=310 K), pressure (P=875 bar) and mole fraction ($f_{H_2O} = 12.3 \cdot 10^{-6}$) on 6 zeolite framework types was simulated using the GCMC ensemble. In this process, for each framework type, 10 Si/Al ratios ranging from the lower theoretical limit (see table 5.2) to ∞ were created. The selectivity of water over hydrogen is calculated.

For all simulations, the influence of blocking pockets was evaluated. It is well known that 6-membered rings that host hydrated extra-framework cations are impermeable by hydrogen [132]. Water on the other hand, can displace the cations and enter the cages. At the high pressures investigated in this work, blocking pockets did not have a significant effect of the predicted adsorption.

A plot of absolute loading versus Si/Al ratio is given in figure 6.5. Even though it shows the adsorption on the FAU type zeolite framework, a pattern emerges that is characteristic for the simulations in all six zeolite types: A near linear decrease of adsorbed hydrogen, and a near linear increase of adsorbed water.
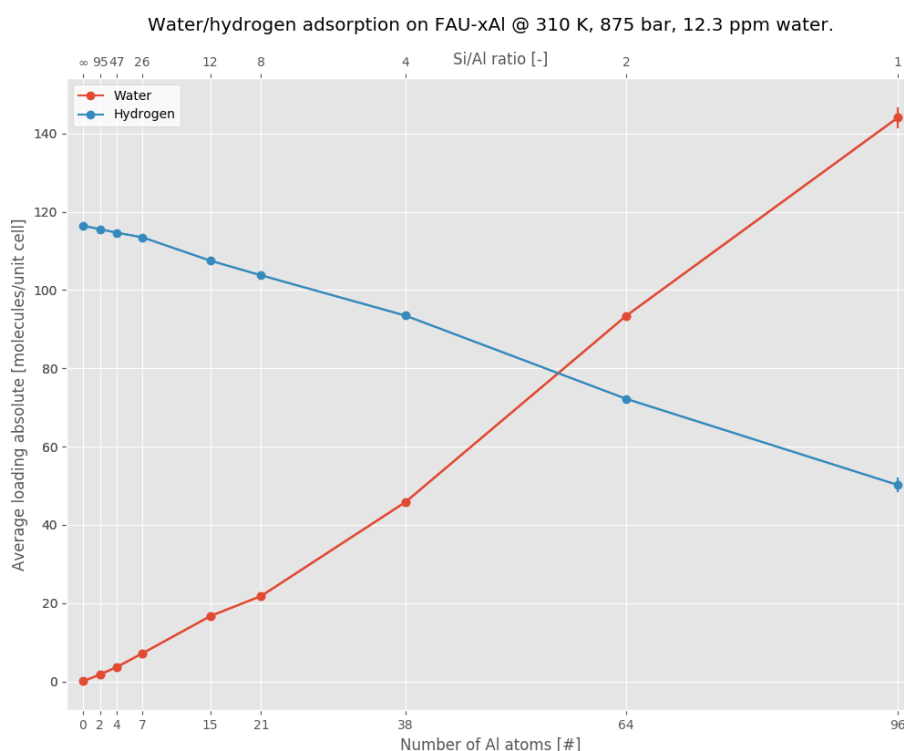
Figure 6.5: **Absolute loading.** GCMC simulations of **binary adsorption** of hydrogen and water on FAU with **varying Si/Al ratio** at 310 K, using the DEH$_2$YDR force field. Lines are guides to the eye. Error bars within symbol size.

A selectivity versus Si/Al curve also shows a near linear increase with the increase in number of framework Al atoms and extra-framework cations, and as such a decrease in Si/Al ratio. This can be seen in figure 6.6.

The increase in selectivity with decreasing Si/Al ratio is not equivalent for all frameworks, this is an indication that the topology of the framework also plays are role in the binary adsorption mechanism. To investigate this trend, the selectivity for all frameworks is plotted in figure 6.7.

To unveil how the selectivity in the specific frameworks depends on the topological descriptors, a Pearson correlation analysis is performed. It gives a measure of the linear correlation between the selectivity and a certain descriptor. A value of 1 corresponds to a perfectly linear positive correlation, 0 corresponds to no correlation, and -1 corresponds to a perfectly linear negative correlation. The Pearson correlation scores are listed in table table 6.3.

This indicates that the performance of the aluminosilicate zeolite frameworks as selective adsorption of water over hydrogen is linked to descriptors that can be classified in two distinct categories: chemical composition
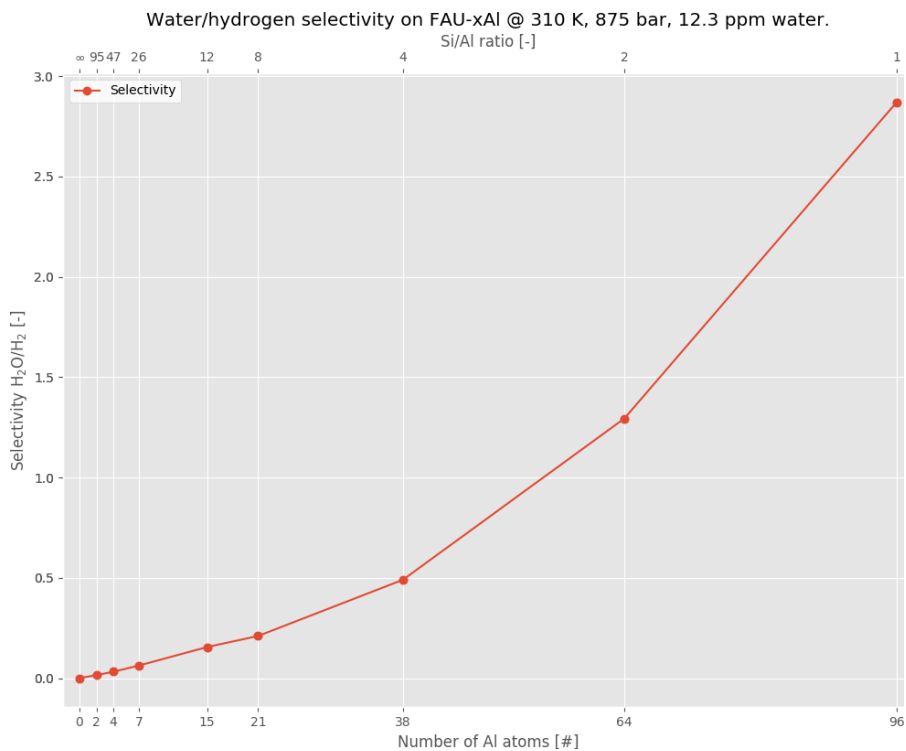
Figure 6.6: **Adsorption selectivity** H_2O/H_2**.** GCMC simulations of **binary adsorption** of hydrogen and water on FAU with **varying Si/Al ratio** at 310 K, using the DEH$_2$YDR force field. Lines are guides to the eye.
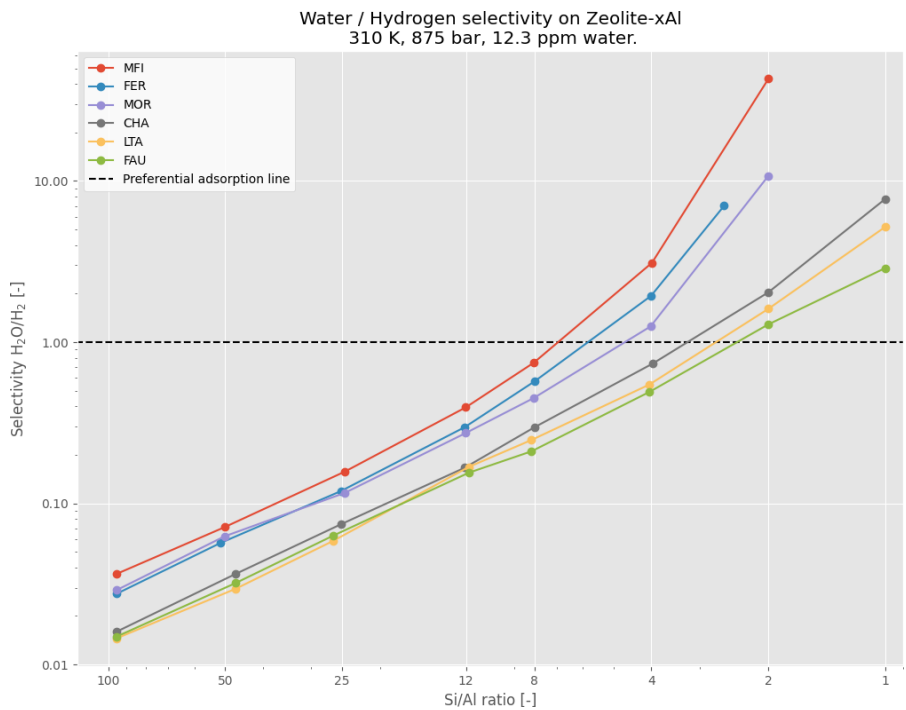
Figure 6.7: **Adsorption selectivity** H_2O/H_2**.** GCMC simulations of **binary adsorption** of hydrogen and water for **all frameworks** with **varying Si/Al ratio** at 310 K, using the DEH$_2$YDR force field. Lines are guides to the eye.

Table 6.3: Pearson correlations for descriptors on predicting selectivity of water over hydrogen, ranked by performance.

Descriptor	Pearson R
Si/Al ratio [-]	-0.24
Framework density [T/1000Å^3]	0.22
Helium Void Fraction [-]	-0.21
Accesible Surface Area [Å^2/g]	-0.20
Accesible Volume [%]	-0.19
Maximum Included Sphere Diameter [Å]	-0.17
Maximum Free Sphere Diameter dir C [Å]	-0.08
Maximum Free Sphere Diameter dir B [Å]	-0.05
Min ring size [#]	-0.04
Max ring size [#]	0.00
Maximum Free Sphere Diameter dir A [Å]	0.00

and void space.

Chemical composition
- Si/Al ratio, lower values give higher selectivity
- Framework T-site density, higher values give higher selectivity

Olson et al. review a number of papers that observe a linear increase in the amount of water adsorbed with increasing aluminum content. The water absorption is concluded to reach essentially zero at zero aluminum. This is closely related to the T-site density of a framework, as the water molecules have the strongest interactions with the Al atoms and the associated extra-framework cations.

Void Space
- Helium Void Fraction
- Accessible Surface Area
- Accessible Volume
- Maximum Included Sphere Diameter

For all of these (closely interlinked) descriptors, a lower value gives a higher selectivity.

Shirono et al. formulated an adsorption mechanism for water in the FAU type zeolites by means of Molecular Dynamics simulations. It consists of three steps: [103]

1. Adsorption around the extra-framework cations
2. Adsorption of a single layer on the zeolite surface
3. Filling of the remaining pore space in the supercages

It is hypothesized that, since the water interacts most strongly with the surface of the zeolite, hydrogen is effectively only able to adsorb when large void spaces are present in the zeolite, of which the centres are relatively far away from the surface of the zeolite. If these void spaces can be minimized, water will not have to compete with hydrogen in step 3 of this adsorption mechanism.

Bougeard and Smirnov conclude that zeolite structures containing significant void space, such as supercages, host two types of water molecules. The first type is coordinated to the extra-framework cations, and is found to be relatively immobile. The second type is not coordinated to the extra-framework cations and behaves more like liquid water. In zeolites with more confined pore spaces only water of the first type is found [86].

From the radial distribution functions (RDF) obtained during the GCMC simulations, the coordination number of water and hydrogen surrounding the extra-framework cations can be investigated. Figure 6.8a shows these RDF's for water–cation (wO–Na) and hydrogen–cation (H2–Na) distances during simulation of adsorption on a FER type framework with respectively 6 and 160 Al atoms. This shows that when there is relatively few extra-framework cations, many water molecules will coordinate around it, leaving no room for hydrogen. This corresponds to the first type of water as coined by Bougeard and Smirnov. When the number of Al atoms, and thus the number of extra-framework cations is increased, the coordination number of water drops

significantly and there is room for hydrogen to coordinate. This refers to the case where there is water of the second type present. In this limit, as long as the extra-framework cations and coordinated molecules fill the void space of the zeolite there will be a favourable selectivity.

(a) **RDF plot** for water–cation **(wO–Na)** and hydrogen–cation **(H2–Na)** with calculated **coordination numbers** for **binary adsorption on FER-6Al**.

(b) **RDF plot** for water–cation **(wO–Na)** and hydrogen–cation **(H2–Na)** with calculated **coordination numbers** for **binary adsorption on FER-166Al**.
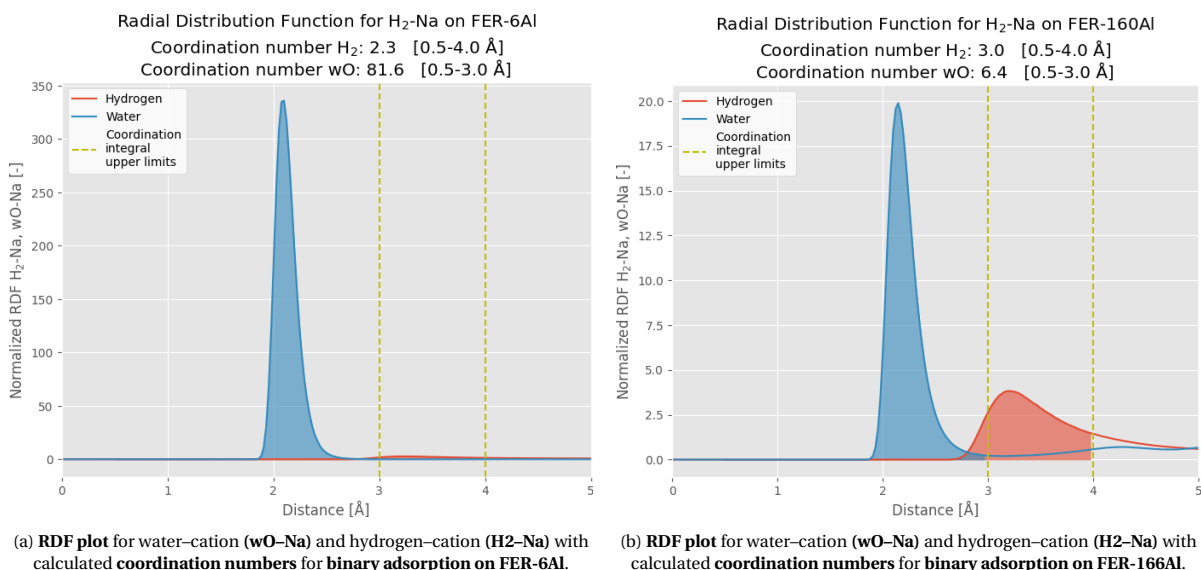
Figure 6.9 shows a log-log plot of the coordination numbers of hydrogen and the water oxygen molecule (wO) around the extra-framework cations versus the Si/Al ratio of the various zeolite frameworks.
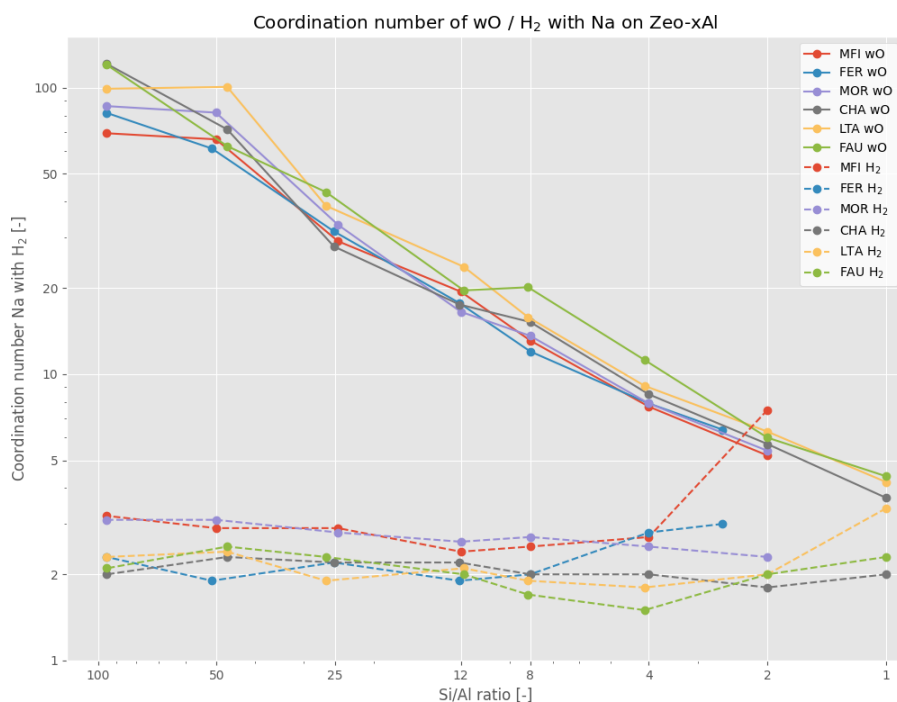
Figure 6.9: **log-log plot of coordination numbers for wO-Na & H2-Na.** GCMC simulations of **binary adsorption** of hydrogen and water **for all frameworks** with **varying Si/Al ratio** at 310 K, using the DEH$_2$YDR force field. Lines are guides to the eye.

The effect of the presence of significant void spaces is investigated by generating density plots of the most probable locations of the guest molecules. During each GCMC simulation, samples of all atomic positions were taken. These were averaged over each spatial dimension to generate a density probability plot.

Figures 6.10, 6.11 and 6.12 show the density probability for binary adsorption of hydrogen and water on MFI

with Si/Al ratio's ∞, 25.0 and 2.0. At Si/Al = ∞, only hydrogen is adsorbed. At Si/Al = 25.0 water adsorbs on the surface of the zeolite. In this case, the void space of the channels is still mainly occupied by hydrogen. At Si/Al = 2.0, water is adsorbed almost exclusively.
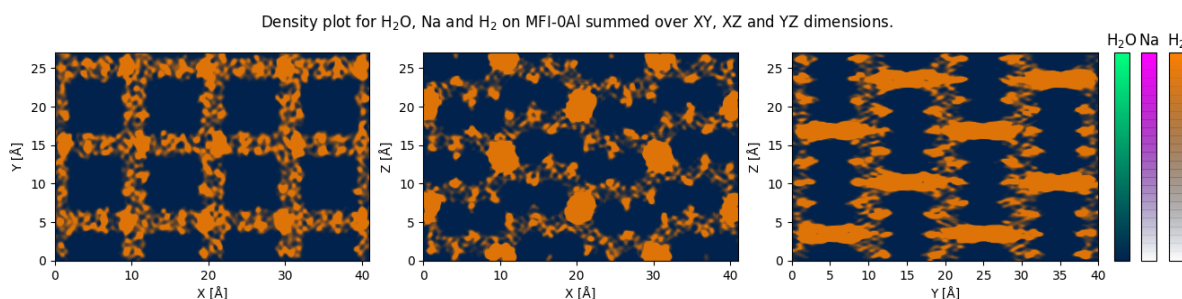
Figure 6.10: Density probability for GCMC simulation of binary adsorption of hydrogen and water on MFI-0Al.
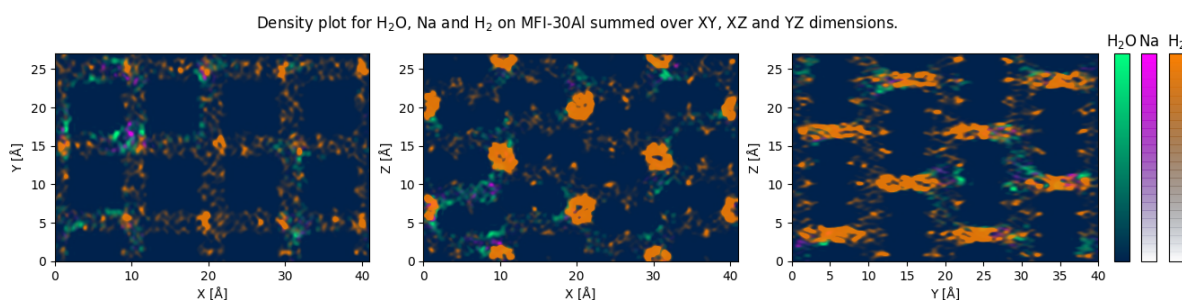
Figure 6.11: Density probability for GCMC simulation of binary adsorption of hydrogen and water on MFI-30Al.
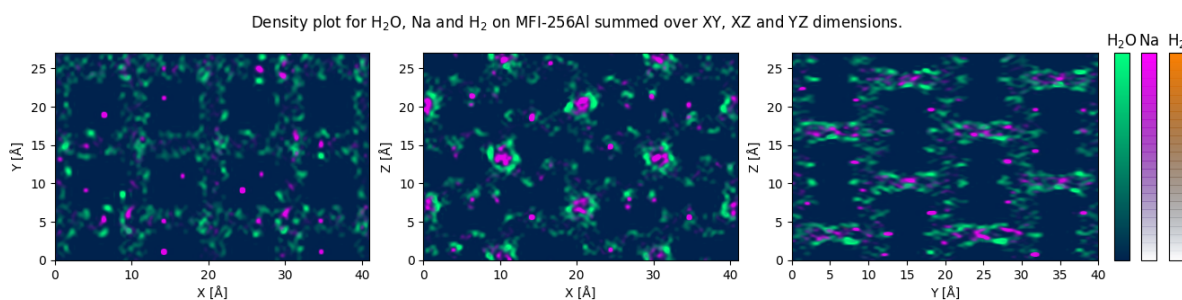
Figure 6.12: Density probability for GCMC simulation of binary adsorption of hydrogen and water on MFI-256Al.

Figures 6.13, 6.14 and 6.15 show the density probability for binary adsorption of hydrogen and water on LTA with Si/Al ratio's inf, 2.0 and 1.0. At Si/Al = inf, only hydrogen is adsorbed. At Si/Al = 2.0 water adsorbs on the surface of the zeolite and hydrogen adsorbs near hydrophobic defects and inside the supercage. At Si/Al = 1.0, water adsorbs on the surface of the zeolite and hydrogen is only likely to be present in the centre of the supercages.

Density plot for H$_2$O, Na and H$_2$ on LTA-0Al summed over XY, XZ and YZ dimensions.
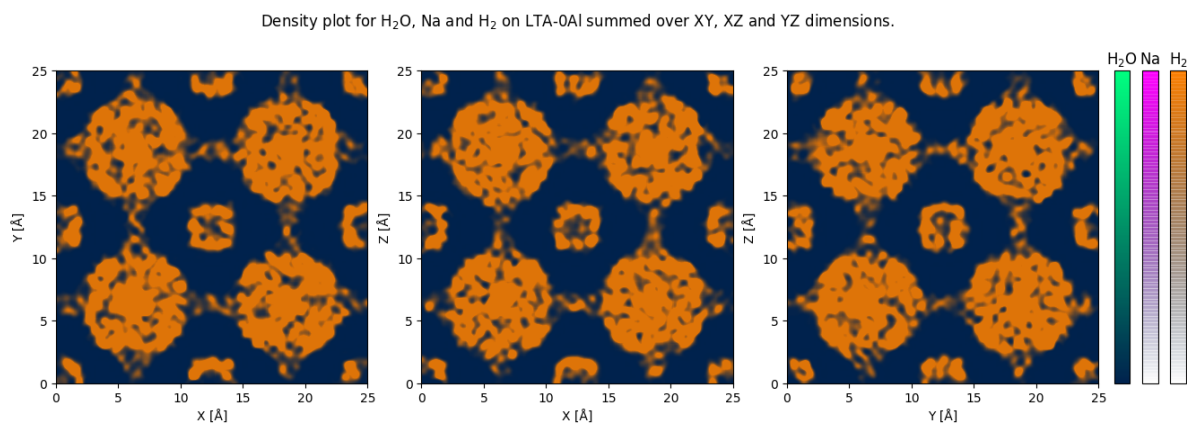
Figure 6.13: Density probability for GCMC simulation of binary adsorption of hydrogen and water on LTA-0Al.

Density plot for H$_2$O, Na and H$_2$ on LTA-64Al summed over XY, XZ and YZ dimensions.
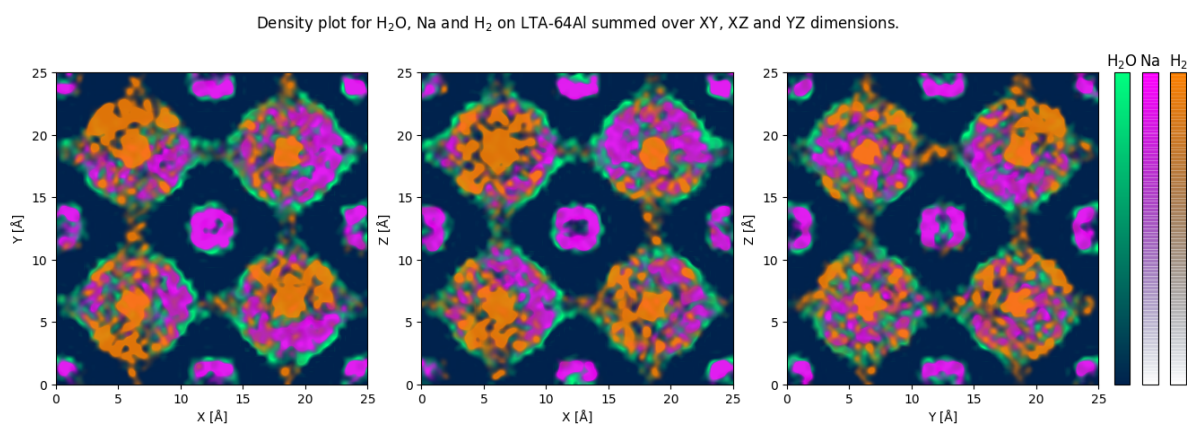
Figure 6.14: Density probability for GCMC simulation of binary adsorption of hydrogen and water on LTA-64Al.

Density plot for H$_2$O, Na and H$_2$ on LTA-96Al summed over XY, XZ and YZ dimensions.
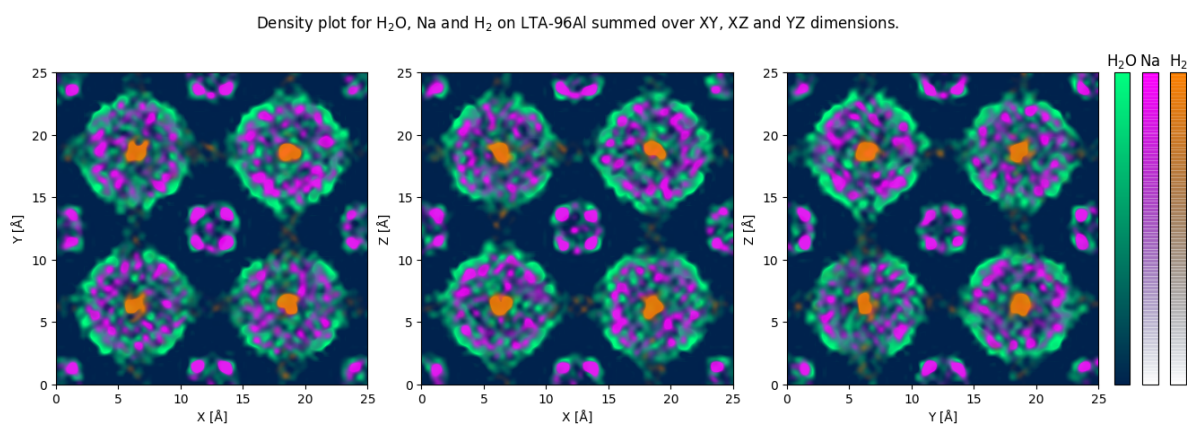
Figure 6.15: Density probability for GCMC simulation of binary adsorption of hydrogen and water on LTA-96.

To summarize, in this section the third research objective is addressed: Identifying key parameters for designing the optimal zeolite. It is hypothesized that the optimal zeolite framework for high pressure hydrogen dehydration can be found by investigating aluminosilicate zeolite framework types that have a low Si/Al ratio and a low amount of void space.

In this work, several assumptions were made to enable the modelling of high pressure hydrogen dehydration using zeolites. Some of these assumptions will have to be validated by additional research. These are discussed in the next section.

Discussion

Since the scale of this screening study is limited, it is not possible to fully leverage the statistical methods that were discussed in the introduction. Before embarking on a journey to scale up the analysis and calculate selectivities for all (hypothetical) zeolites, it is important to address some uncertainties and challenges that were encountered.

The 1D descriptors that were used in this work have often shown to carry insufficient information on the topology of zeolite frameworks to account for a full predictive capability of the molecular mechanisms at play. Krishnapriyan et al. note that in the case of high pressure adsorption, the entire void space of the zeolite is usually occupied and therefore the 1D descriptors are able to correlate to the global behaviour. During the training of their predictive models, these 1D descriptors became the most important to the model.

For many zeolites there are multiple possibilities with regards to their exact framework structure at low Si/Al ratios. The use of a brute force silicious framework generator that takes the silicious structure as an input will have to be compensated by extensive cross validation of these possible structures, and the and the associated equilibration of extra-framework cations. Furthermore, taking the atomic positions of the silicious structures is disadvantageous considering the sensibility of the simulations to these parameters [40].

The stability of zeolites at high temperatures is known to be good, as can be seen by large-scale implementation of these materials in high temperature in catalysis. Heard et al. recently concluded that understanding of zeolite framework behaviour at lower temperatures is not yet sufficiently developed [96]. The process of hydrolysis occurs when zeolites are put in contact with liquid water. This can lead to fast, reversible bond breaking of framework T-sites and oxygen atoms, which can result in a change in framework structure. In term, this can also affect the positions and mobility of extra-frame work cations [86].

Given the literature that the force field in this work was based on, it must be stressed that a considerable shortcoming of the current analysis is the omission of polarization effects. Even at the moderate pressures considered by Castillo et al. the polarizability of water in simulations of adsorption on hydrophilic zeolites lead to a 20% difference in predicted adsorption [98]. Similarly, it was demonstrated by Akten et al. that the predicted number of adsorbed hydrogen molecules is increased by 30% when polarization is taken into account [65].

As a final remark, Castillo et al. have stated that their force field is in general not transferable between different zeolite types. This is a significant disadvantage to the efforts of this work, and imposes the need to perform additional experimental- and theoretical validation of the DEH$_2$YDR force field.

7. Conclusion & Outlook

For application in high pressure hydrogen dehydration, it is concluded that hydrophilic zeolites show promising results at selectively adsorbing water. This selectivity is almost linearly correlated to the amount of Al atoms in the zeolite framework, and the corresponding extra-framework cations. Furthermore, it is observed that topologies which feature a low amount of void space outperform those where significant void spaces are present. This can be attributed to the fact that the interactions of the zeolite with water are stronger than those with hydrogen in the limit of a low Si/Al ratio of the zeolite framework. It is theorised that water adsorbs preferentially at the surface of the zeolite, and competitive adsorption by hydrogen can only take place in sufficiently large void spaces.

The difference in polarity of water and hydrogen is found to limit applicability of the Ideal Adsorbed Solution Theory (IAST) as a means of avoiding computation of adsorption isotherms. The accuracy of predicting binary adsorption isotherms using IAST with parameters that were fitted to single component isotherms is very poor. In a practical setting, these parameters would not be fitted. Rather, the Henry coefficient (k_H) would be calculated using, for instance, the Widom test particle insertion method. However, it's predictive capability for the Henry coefficient of water also seems to suffer from the strong Coulombic interactions of water with the zeolite. The saturation capacity q_{max} for the individual components was not solely dependent on the free void space of the zeolite, but also linked to the framework Si/Al ratio.

Key factor in the modeling of this chemical environment was the development of a force field. It has proven to be hard to parameterize the force field to produce accurate results in the limits of both low and high pressure as well as both hydrophilic and hydrophobic zeolite frameworks simultaneously. The DEH$_2$YDR force field has shown to accurately predict adsorption for water and hydrogen at moderate pressures, whereas at high pressures the adsorption of hydrogen might be under-predicted. Furthermore, it is found that, at high pressures, accurate calculation of the fugacity coefficients the hydrogen/water mixture is crucial.

In terms of enhancing the performance of the force field, it is suggested that the inclusion of polarizability is investigated. On top of that, further research could be aimed at the influence of random Al distribution on the predicted adsorption, diffusion behaviour of the cations by means of Molecular Dynamics simulations, the parameterization of different extra-cation species and finally the transferability to hydrophilic zeolites other than LTA4A. The transferability, and the performance of the force field in general could also be verified experimentally.

A possible future implementation of these findings could be in a high throughput screening study. To search for the most suitable zeolite material for efficient high pressure hydrogen dehydration, the computation of selectivity through Grand Canonical Monte Carlo Simulations can be combined with advanced topology based learning algorithms, such as the one recently proposed by Krishnapriyan et al.. This might unveil new details on the mechanisms that govern this high pressure adsorption process.

Bibliography

[1] World energy outlook. International Energy Agency, 2019. URL https://www.iea.org/reports/world-energy-outlook-2019. Accessed on 24/03/2020.

[2] The future of hydrogen. International Energy Agency, 2019. URL https://www.iea.org/reports/the-future-of-hydrogen. Accessed on 24/03/2020.

[3] Iso standard 14687:2019 "hydrogen fuel quality product specification". International Organization for Standardization, 2019. URL https://www.iso.org/standard/69539.html.

[4] Y. Ligen, H. Vrubel, and H. Girault. Energy efficient hydrogen drying and purification for fuel cell vehicles. *International Journal of Hydrogen Energy*, 45(18):10639–10647, 2020. ISSN 0360-3199. doi:10.1016/j.ijhydene.2020.02.035.

[5] A. Rahbari, J. Brenkman, R. Hens, M. Ramdin, L. J. P. V. D. Broeke, R. Schoon, R. Henkes, O. A. Moultos, and T. J. H. Vlugt. Solubility of water in hydrogen at high pressures: A molecular simulation study. *Journal of Chemical & Engineering Data*, 64(9):4103–4115, 2019. ISSN 0021-9568. doi:10.1021/acs.jced.9b00513.

[6] Hyet hydrogen bv. URL https://hyet.nl/hydrogen. Accessed on 24/03/2020.

[7] J. Brenkman, T. Vlugt, R. Schoon, R. Henkes, M. Ramdin, R. Rahbari, and D. Vermaas. High pressure hydrogen dehydration using ionic liquids. Master's thesis, TU Delft, 2019. URL http://resolver.tudelft.nl/uuid:c2d9d36a-62e7-4e02-8c83-7e84f06b3016.

[8] G. Maurin, R. G. Bell, S. Devautour, F. Henn, and J. C. Giuntini. Modeling the effect of hydration in zeolite na+-mordenite. *The Journal of Physical Chemistry B*, 108(12):3739–3745, 2004. ISSN 1520-6106. doi:10.1021/jp034151a.

[9] C. Abrioux, B. Coasne, G. Maurin, F. Henn, A. Boutin, A. D. Lella, C. Nieto-Draghi, and A. H. Fuchs. A molecular simulation study of the distribution of cation in zeolites. *Adsorption*, 14(4-5):743–754, 2008. ISSN 0929-5607. doi:10.1007/s10450-008-9123-z.

[10] M. W. Deem, R. Pophale, P. A. Cheeseman, and D. J. Earl. Computational discovery of new zeolite-like materials. *The Journal of Physical Chemistry C*, 113(51):21353–21360, 2009. ISSN 1932-7447. doi:10.1021/jp906984z.

[11] R. L. Martin, B. Smit, and M. Haranczyk. Addressing challenges of identifying geometrically diverse sets of crystalline porous materials. *Journal of Chemical Information and Modeling*, 52(2):308–318, 2012. ISSN 1549-9596. doi:10.1021/ci200386x. URL https://infoscience.epfl.ch/record/200672/files/Martin-2012-AddressingChallenge.pdf.

[12] B. A. Helfrecht, R. Semino, G. Pireddu, S. M. Auerbach, and M. Ceriotti. A new kind of atlas of zeolite building blocks. *The Journal of Chemical Physics*, 151(15):154112, 2019. ISSN 0021-9606. doi:10.1063/1.5119751.

[13] D. J. Earl and M. W. Deem. Toward a database of hypothetical zeolite structures. *Industrial & Engineering Chemistry Research*, 45(16):5449–5454, 2006. ISSN 0888-5885. doi:10.1021/ie0510728.

[14] L.-C. Lin, A. H. Berger, R. L. Martin, J. Kim, J. A. Swisher, K. Jariwala, C. H. Rycroft, A. S. Bhown, M. W. Deem, M. Haranczyk, and B. Smit. In silico screening of carbon-capture materials. *Nature Materials*, 11(7):633–641, 2012. ISSN 1476-1122. doi:10.1038/nmat3336. URL https://infoscience.epfl.ch/record/200777/files/lin121_nmat3336-s1.pdf.

[15] A. W. Thornton, D. A. Winkler, M. S. Liu, M. Haranczyk, and D. F. Kennedy. Towards computational design of zeolite catalysts for co2 reduction. *RSC Advances*, 5(55):44361–44370, 2015. ISSN 2046-2069. doi:10.1039/c5ra06214d.

[16] M. L. Green, C. L. Choi, J. R. Hattrick-Simpers, A. M. Joshi, I. Takeuchi, S. C. Barron, E. Campo, T. Chiang, S. Empedocles, J. M. Gregoire, A. G. Kusne, J. Martin, A. Mehta, K. Persson, Z. Trautt, J. V. Duren, and A. Zakutayev. Fulfilling the promise of the materials genome initiative with high-throughput experimental methodologies. *Applied Physics Reviews*, 4(1):011105, 2017. ISSN 1931-9401. doi:10.1063/1.4977487. URL https://authors.library.caltech.edu/78308/1/1%252E4977487.pdf.

[17] M. Fernandez, P. G. Boyd, T. D. Daff, M. Z. Aghaji, and T. K. Woo. Rapid and accurate machine learning recognition of high performing metal organic frameworks for co2 capture. *The Journal of Physical Chemistry Letters*, 5(17):3056–3060, 2014. ISSN 1948-7185. doi:10.1021/jz501331m.

[18] A. W. Thornton, C. M. Simon, J. Kim, O. Kwon, K. S. Deeg, K. Konstas, S. J. Pas, M. R. Hill, D. A. Winkler, M. Haranczyk, and B. Smit. Materials genome in action: Identifying the performance limits of physical hydrogen storage. *Chemistry of Materials*, 29(7):2844–2854, 2017. ISSN 0897-4756. doi:10.1021/acs.chemmater.6b04933. URL https://doi.org/10.1021/acs.chemmater.6b04933.

[19] C. M. Simon, R. Mercado, S. K. Schnell, B. Smit, and M. Haranczyk. What are the best materials to separate a xenon/krypton mixture? *Chemistry of Materials*, 27(12):4459–4475, 2015. ISSN 0897-4756. doi:10.1021/acs.chemmater.5b01475. URL https://ntnuopen.ntnu.no/ntnu-xmlui/bitstream/11250/2465205/1/paper_xe_kr.pdf.

[20] H. Dureckova, M. Krykunov, M. Z. Aghaji, and T. K. Woo. Robust machine learning models for predicting high co2 working capacity and co2/h2 selectivity of gas adsorption in metal organic frameworks for precombustion carbon capture. *The Journal of Physical Chemistry C*, 123(7):4133–4139, 2019. ISSN 1932-7447. doi:10.1021/acs.jpcc.8b10644.

[21] G. E. Dahl, N. Jaitly, and R. Salakhutdinov. Multi-task neural networks for qsar predictions. *arXiv preprint arXiv:1406.1231*, 2014.

[22] K. S. Walton and D. S. Sholl. Predicting multicomponent adsorption: 50 years of the ideal adsorbed solution theory. *AIChE Journal*, 61(9):2757–2762, 2015. ISSN 0001-1541. doi:10.1002/aic.14878.

[23] I. G. García, M. Bernabei, and M. Haranczyk. Toward automated tools for characterization of molecular porosity. *Journal of Chemical Theory and Computation*, 15(1):787–798, 2019. ISSN 1549-9618. doi:10.1021/acs.jctc.8b00764.

[24] F.-X. Coudert and A. H. Fuchs. Computational characterization and prediction of metal–organic framework properties. *Coordination Chemistry Reviews*, 307:211–236, 2016. ISSN 0010-8545. doi:10.1016/j.ccr.2015.08.001. URL http://arxiv.org/pdf/1506.08219.

[25] T. F. Willems, C. H. Rycroft, M. Kazi, J. C. Meza, and M. Haranczyk. Algorithms and tools for high-throughput geometry-based analysis of crystalline porous materials. *Microporous and Mesoporous Materials*, 149(1):134–141, 2012. ISSN 1387-1811. doi:10.1016/j.micromeso.2011.08.020.

[26] M. Fernandez, N. R. Trefiak, and T. K. Woo. Atomic property weighted radial distribution functions descriptors of metal–organic frameworks for the prediction of gas uptake capacity. *The Journal of Physical Chemistry C*, 117(27):14095–14105, 2013. ISSN 1932-7447. doi:10.1021/jp404287t.

[27] Y. Lee, S. D. Barthel, P. Dłotko, S. M. Moosavi, K. Hess, and B. Smit. High-throughput screening approach for nanoporous materials genome using topological data analysis: Application to zeolites. *Journal of Chemical Theory and Computation*, 14(8):4427–4437, 2018. ISSN 1549-9618. doi:10.1021/acs.jctc.8b00253. URL https://cronfa.swan.ac.uk/Record/cronfa44307/Download/0044307-18092018132126.pdf.

[28] X. Zhang, J. Cui, K. Zhang, J. Wu, and Y. Lee. Machine learning prediction on properties of nanoporous materials utilizing pore geometry barcodes. *Journal of Chemical Information and Modeling*, 59 (11):4636–4644, 2019. doi:10.1021/acs.jcim.9b00623. URL https://doi.org/10.1021/acs.jcim.9b00623. PMID: 31661958.

[29] A. S. Krishnapriyan, M. Haranczyk, and D. Morozov. Topological descriptors help predict guest adsorption in nanoporous materials. *arXiv*, pages arXiv–2001, 2020.

[30] F.-X. Coudert, F. Cailliez, R. Vuilleumier, A. H. Fuchs, and A. Boutin. Water nanodroplets confined in zeolite pores. *Faraday Discussions*, 141:377–398, 2009. ISSN 1359-6640. doi:10.1039/b804992k. URL https://hal.archives-ouvertes.fr/hal-02116837/document.

[31] W. Zhou. Microscopic study of crystal defects enriches our knowledge of materials chemistry. *Journal of Materials Chemistry*, 18(44):5321, 2008. ISSN 0959-9428. doi:10.1039/b808158a.

[32] N. Almora-Barrios, A. R. Ruiz-Salvador, A. Gómez, M. Mistry, and D. W. Lewis. Understanding si/al distributions in al-rich zeolites: the role of water in determining the structure of goosecreekite. *Chemical Communications*, (6):531–532, 2001. ISSN 1359-7345. doi:10.1039/b009623g.

[33] A. Kiselev, A. Lopatkin, and A. Shulga. Molecular statistical calculation of gas adsorption by silicalite. *Zeolites*, 5(4):261–267, 1985. ISSN 0144-2449. doi:10.1016/0144-2449(85)90098-3.

[34] B. Smit. Simulating the adsorption isotherms of methane, ethane, and propane in the zeolite silicalite. *The Journal of Physical Chemistry*, 99(15):5597–5603, 1995. ISSN 0022-3654. doi:10.1021/j100015a050.

[35] T. Vlugt, J. Eerden, and M. Dijkstra. Introduction to molecular simulation and statistical thermodynamics, 01 2008.

[36] J. Castillo, S. Calero, J. Gross, and T. Vlugt. *Molecular simulations in microporous materials, Adsorption and separation.* PhD thesis, TU Delft, 2010. URL http://resolver.tudelft.nl/uuid:6b2bdf4b-1990-496d-9d38-ce8264fdf03c.

[37] N. B. Wilding and M. Schoen. Absence of simulation evidence for critical depletion in slit pores. *Physical review. E, Statistical physics, plasmas, fluids, and related interdisciplinary topics*, 60(1):1081–1083, 1999. ISSN 1063-651X. doi:10.1103/physreve.60.1081.

[38] M. G. Martin, A. P. Thompson, and T. M. Nenoff. Effect of pressure, membrane thickness, and placement of control volumes on the flux of methane through thin silicalite membranes: A dual control volume grand canonical molecular dynamics study. *The Journal of Chemical Physics*, 114(16):7174–7181, 2001. ISSN 0021-9606. doi:10.1063/1.1360256.

[39] A. Y. Toukmaji and J. A. Board. Ewald summation techniques in perspective: a survey. *Computer Physics Communications*, 95(2-3):73–92, 1996. ISSN 0010-4655. doi:10.1016/0010-4655(96)00016-1.

[40] J. Castillo, D. Dubbeldam, T. Vlugt, B. Smit, and S. Calero. Evaluation of various water models for simulation of adsorption in hydrophobic zeolites. *Molecular Simulation*, 35(12-13):1067–1076, 2009. ISSN 0892-7022. doi:10.1080/08927020902865923. URL https://hal.archives-ouvertes.fr/hal-00530449/document.

[41] T. J. H. Vlugt, E. García-Pérez, D. Dubbeldam, S. Ban, and S. Calero. Computing the heat of adsorption using molecular simulations: The effect of strong coulombic interactions. *Journal of Chemical Theory and Computation*, 4(7):1107–1118, 2008. ISSN 1549-9618. doi:10.1021/ct700342k.

[42] D. Frenkel and B. Smit. Understanding molecular simulation, 2002.

[43] J. Gao, D. Habibollazadeh, and L. Shao. A polarizable intermolecular potential function for simulation of liquid alcohols. *The Journal of Physical Chemistry*, 99(44):16460–16467, 1995. ISSN 0022-3654. doi:10.1021/j100044a039.

[44] D. J. Adams, E. M. Adams, and G. J. Hills. The computer simulation of polar liquids. *Molecular Physics*, 38(2):387–400, 1979.

[45] M. Neumann and O. Steinhauser. On the calculation of the dielectric constant using the ewald-kornfeld tensor. *Chemical Physics Letters*, 95(4-5):417–422, 1983. ISSN 0009-2614. doi:10.1016/0009-2614(83)80585-5.

[46] B. Widom. Some topics in the theory of fluids. *The Journal of Chemical Physics*, 39(11):2808–2812, 1963. ISSN 0021-9606. doi:10.1063/1.1734110.

[47] O. Talu and A. L. Myers. Molecular simulation of adsorption: Gibbs dividing surface and comparison with experiment. *AIChE Journal*, 47(5):1160–1168, 2001. ISSN 0001-1541. doi:10.1002/aic.690470521.

[48] T. J. H. Vlugt. Efficiency of parallel cbmc simulations. *Molecular Simulation*, 23(1):63–78, 1999. ISSN 0892-7022. doi:10.1080/08927029908022112.

[49] R. Pini. Interpretation of net and excess adsorption isotherms in microporous adsorbents. *Microporous and Mesoporous Materials*, 187:40–52, 2014. ISSN 1387-1811. doi:10.1016/j.micromeso.2013.12.005.

[50] D.-Y. Peng and D. B. Robinson. A new two-constant equation of state. *Industrial & Engineering Chemistry Fundamentals*, 15(1):59–64, 1976. doi:10.1021/i160057a011. URL https://doi.org/10.1021/i160057a011.

[51] P. Sindzingre, G. Ciccotti, C. Massobrio, and D. Frenkel. Partial enthalpies and related quantities in mixtures from computer simulation. *Chemical Physics Letters*, 136(1):35–41, 1987. ISSN 0009-2614. doi:10.1016/0009-2614(87)87294-9.

[52] A. Rahbari, R. Hens, I. K. Nikolaidis, A. Poursaeidesfahani, M. Ramdin, I. G. Economou, O. A. Moultos, D. Dubbeldam, and T. J. H. Vlugt. Computation of partial molar properties using continuous fractional component monte carlo. *Molecular Physics*, 116(21-22):3331–3344, 2018. ISSN 0026-8976. doi:10.1080/00268976.2018.1451663. URL https://www.tandfonline.com/doi/pdf/10.1080/00268976.2018.1451663?needAccess=true.

[53] W. Shi and E. J. Maginn. Continuous fractional component monte carlo:- an adaptive biasing method for open system atomistic simulations. *Journal of Chemical Theory and Computation*, 3(4):1451–1463, 2007. ISSN 1549-9618. doi:10.1021/ct7000039.

[54] A. L. Myers and J. M. Prausnitz. Thermodynamics of mixed-gas adsorption. *AIChE Journal*, 11(1): 121–127, 1965. ISSN 0001-1541. doi:10.1002/aic.690110125.

[55] P. Bai, M. Tsapatsis, and J. I. Siepmann. Multicomponent adsorption of alcohols onto silicalite-1 from aqueous solution: Isotherms, structural analysis, and assessment of ideal adsorbed solution theory. *Langmuir*, 28(44):15566–15576, 2012. ISSN 0743-7463. doi:10.1021/la303247c.

[56] O. Talu. Net adsorption of gas/vapor mixtures in microporous solids. *The Journal of Physical Chemistry C*, 117(25):13059–13071, 2013. ISSN 1932-7447. doi:10.1021/jp4021382. URL http://pubs.acs.org/doi/abs/10.1021/jp4021382.

[57] D. Dubbeldam, S. Calero, D. E. Ellis, and R. Q. Snurr. Raspa: molecular simulation software for adsorption and diffusion in flexible nanoporous materials. *Molecular Simulation*, 42(2):81–101, 2016. ISSN 0892-7022. doi:10.1080/08927022.2015.1010082. URL https://pure.uva.nl/ws/files/2770778/174040_527070.pdf.

[58] R. Hens, A. Rahbari, S. CaroOrtiz, N. Dawass, M. Erdös, A. Poursaeidesfahani, H. Salehi, A. Celebi, M. Ramdin, O. Moultos, D. Dubbeldam, , and T. Vlugt. Brickcfcmc: open source software for monte carlo simulations of phase and reaction equilibria using the continuous fractional component method. *Paper submitted*, 2020.

[59] I. F. Silvera. The solid molecular hydrogens in the condensed phase: Fundamentals and static properties. *Reviews of Modern Physics*, 52(2):393–452, 1980. ISSN 0034-6861. doi:10.1103/revmodphys.52.393.

[60] V. Buch. Path integral simulations of mixedpara-d2andortho-d2clusters: The orientational effects. *The Journal of Chemical Physics*, 100(10):7610–7629, 1994. ISSN 0021-9606. doi:10.1063/1.466854.

[61] F. Darkrim and D. Levesque. Monte carlo simulations of hydrogen adsorption in single-walled carbon nanotubes. *The Journal of Chemical Physics*, 109(12):4981–4984, 1998. ISSN 0021-9606. doi:10.1063/1.477109.

[62] C.-R. Anderson, D. F. Coker, J. Eckert, and A. L. R. Bug. Computational study of molecular hydrogen in zeolite na-a. i. potential energy surfaces and thermodynamic separation factors for ortho and para hydrogen. *The Journal of Chemical Physics*, 111(16):7599–7613, 1999. ISSN 0021-9606. doi:10.1063/1.480104. URL https://works.swarthmore.edu/cgi/viewcontent.cgi?article=1177&context=fac-physics.

[63] F. Darkrim, A. Aoufi, P. Malbrunot, and D. Levesque. Hydrogen adsorption in the naa zeolite: A comparison between numerical simulations and experiments. *The Journal of Chemical Physics*, 112 (13):5991–5999, 2000. ISSN 0021-9606. doi:10.1063/1.481201.

[64] R. F. Cracknell. Molecular simulation of hydrogen adsorption in graphitic nanofibres. *Physical Chemistry Chemical Physics*, 3(11):2091–2097, 2001. ISSN 1463-9076. doi:10.1039/b100144m.

[65] E. D. Akten, R. Siriwardane, and D. S. Sholl. Monte carlo simulation of single- and binary-component adsorption of co2, n2, and h2in zeolite na-4a. *Energy & Fuels*, 17(4):977–983, 2003. ISSN 0887-0624. doi:10.1021/ef0300038.

[66] H. Langmi, A. Walton, M. Al-Mamouri, S. Johnson, D. Book, J. Speight, P. Edwards, I. Gameson, P. Anderson, and I. Harris. Hydrogen adsorption in zeolites a, x, y and rho. *Journal of Alloys and Compounds*, 356-357:710–715, 2003. ISSN 0925-8388. doi:10.1016/s0925-8388(03)00368-2.

[67] S. H. Jhung, J. W. Yoon, H.-K. Kim, and J.-S. Chang. Low temperature adsorption of hydrogen on nanoporous materials. *Bulletin of the Korean Chemical Society*, 26(7):1075–1078.

[68] X. Solans-Monfort, V. Branchadell, M. Sodupe, C. M. Zicovich-Wilson, E. Gribov, G. Spoto, C. Busco, and P. Ugliengo. Can cu+-exchanged zeolites store molecular hydrogen? an ab-initio periodic study compared with low-temperature ftir. *The Journal of Physical Chemistry B*, 108(24):8278–8286, 2004. ISSN 1520-6106. doi:10.1021/jp0486651.

[69] Q. Yang and C. Zhong. Molecular simulation of carbon dioxide/methane/hydrogen mixture adsorption in metal-organic frameworks. *The Journal of Physical Chemistry B*, 110(36):17776–17783, 2006. ISSN 1520-6106. doi:10.1021/jp062723w.

[70] M. K. Song and K. T. No. Molecular simulation of hydrogen adsorption in organic zeolite. *Catalysis Today*, 120(3-4):374–382, 2007. ISSN 0920-5861. doi:10.1016/j.cattod.2006.09.011.

[71] J. L. Belof, A. C. Stern, and B. Space. An accurate and transferable intermolecular diatomic hydrogen potential for condensed phase simulation. *Journal of Chemical Theory and Computation*, 4(8):1332–1337, 2008. ISSN 1549-9618. doi:10.1021/ct800155q.

[72] P. Bai, M. Tsapatsis, and J. I. Siepmann. Trappe-zeo: Transferable potentials for phase equilibria force field for all-silica zeolites. *The Journal of Physical Chemistry C*, 117(46):24375–24387, 2013. ISSN 1932-7447. doi:10.1021/jp4074224.

[73] J. Camp, V. Stavila, M. D. Allendorf, D. Prendergast, and M. Haranczyk. Critical factors in computational characterization of hydrogen storage in metal–organic frameworks. *The Journal of Physical Chemistry C*, 122(33):18957–18967, 2018. ISSN 1932-7447. doi:10.1021/acs.jpcc.8b04021.

[74] D. Olson, W. Haag, and W. Borghard. Use of water as a probe of zeolitic properties: interaction of water with hzsm-5. *Microporous and Mesoporous Materials*, 35-36:435–446, 2000. ISSN 1387-1811. doi:10.1016/s1387-1811(99)00240-1.

[75] M. LiSal, J. Kolafa, and I. Nezbeda. An examination of the five-site potential (tip5p) for water. *The Journal of Chemical Physics*, 117(19):8892–8897, 2002. ISSN 0021-9606. doi:10.1063/1.1514572.

[76] E. Beerdsen, B. Smit, and S. Calero. The influence of non-framework sodium cations on the adsorption of alkanes in mfi- and mor-type zeolites. *The Journal of Physical Chemistry B*, 106(41):10659–10667, 2002. ISSN 1520-6106. doi:10.1021/jp026257w. URL https://infoscience.epfl.ch/record/200689/files/Beerdsen-2002-Theinfluenceofnon.pdf.

[77] E. Beerdsen, D. Dubbeldam, B. Smit, T. J. H. Vlugt, and S. Calero. Simulating the effect of nonframework cations on the adsorption of alkanes in mfi-type zeolites. *The Journal of Physical Chemistry B*, 107(44): 12088–12096, 2003. ISSN 1520-6106. doi:10.1021/jp035229q. URL https://infoscience.epfl.ch/record/200687/files/3439648772ber031.pdf.

[78] S. Calero, D. Dubbeldam, R. Krishna, B. Smit, T. J. H. Vlugt, J. F. M. Denayer, J. A. Martens, and T. L. M. Maesen. Understanding the role of sodium during adsorption: a force field for alkanes in sodium-exchanged faujasites. *Journal of the American Chemical Society*, 126(36):11377–11386, 2004. ISSN 0002-7863. doi:10.1021/ja0476056. URL https://infoscience.epfl.ch/record/200664/files/3905192448cal041.pdf.

[79] D. Dubbeldam, S. Calero, T. J. H. Vlugt, R. Krishna, T. L. M. Maesen, and B. Smit. United atom force field for alkanes in nanoporous materials. *The Journal of Physical Chemistry B*, 108(33):12301–12313, 2004. ISSN 1520-6106. doi:10.1021/jp0376727. URL https://dspace.library.uu.nl/bitstream/1874/16710/1/2003-007.pdf.

[80] N. Desbiens, A. Boutin, and I. Demachy. Water condensation in hydrophobic silicalite-1 zeolite: a molecular simulation study. *The Journal of Physical Chemistry B*, 109(50):24071–24076, 2005. ISSN 1520-6106. doi:10.1021/jp054168o.

[81] N. Desbiens, I. Demachy, A. H. Fuchs, H. Kirsch-Rodeschini, M. Soulard, and J. Patarin. Water condensation in hydrophobic nanopores. *Angewandte Chemie International Edition*, 44(33): 5310–5313, 2005. ISSN 1433-7851. doi:10.1002/anie.200501250.

[82] C. E. Ramachandran, S. Chempath, L. J. Broadbelt, and R. Q. Snurr. Water adsorption in hydrophobic nanopores: Monte carlo simulations of water in silicalite. *Microporous and Mesoporous Materials*, 90 (1-3):293–298, 2006. ISSN 1387-1811. doi:10.1016/j.micromeso.2005.10.021.

[83] A. D. Lella, N. Desbiens, A. Boutin, I. Demachy, P. Ungerer, J.-P. Bellat, and A. H. Fuchs. Molecular simulation studies of water physisorption in zeolites. *Physical Chemistry Chemical Physics*, 8(46):5396, 2006. ISSN 1463-9076. doi:10.1039/b610621h.

[84] E. García-Pérez, D. Dubbeldam, B. Liu, B. Smit, and S. Calero. A computational method to characterize framework aluminum in aluminosilicates. *Angewandte Chemie International Edition*, 46(1-2):276–278, 2007. ISSN 1433-7851. doi:10.1002/anie.200603136.

[85] B. Liu, E. García-Pérez, D. Dubbeldam, B. Smit, and S. Calero. Understanding aluminum location and non-framework ions effects on alkane adsorption in aluminosilicates:- a molecular simulation study. *The Journal of Physical Chemistry C*, 111(28):10419–10426, 2007. ISSN 1932-7447. doi:10.1021/jp0683521.

[86] D. Bougeard and K. S. Smirnov. Modelling studies of water in crystalline nanoporous aluminosilicates. *Physical Chemistry Chemical Physics*, 9(2):226–245, 2007. ISSN 1463-9076. doi:10.1039/b614463m.

[87] B. Liu, B. Smit, F. Rey, S. Valencia, and S. Calero. A new united atom force field for adsorption of alkenes in zeolites. *The Journal of Physical Chemistry C*, 112(7):2492–2498, 2008. ISSN 1932-7447. doi:10.1021/jp075809d. URL https://infoscience.epfl.ch/record/200710/files/2442544640liu072.pdf.

[88] S. Neumeier, T. Echterhof, R. Bolling, H. Pfeifer, and U. Simon. Zeolite based trace humidity sensor for high temperature applications in hydrogen atmosphere. *Sensors and Actuators B Chemical*, 134(1): 171–174, 2008. ISSN 0925-4005. doi:10.1016/j.snb.2008.04.022.

[89] J. Kuhn, J. M. Castillo-Sanchez, J. Gascon, S. Calero, D. Dubbeldam, T. J. H. Vlugt, F. Kapteijn, and J. Gross. Adsorption and diffusion of water, methanol, and ethanol in all-silica dd3r: Experiments and simulation. *The Journal of Physical Chemistry C*, 113(32):14290–14301, 2009. ISSN 1932-7447. doi:10.1021/jp901869d.

[90] C. Vega and J. L. F. Abascal. Simulating water with rigid non-polarizable models: a general perspective. *Physical Chemistry Chemical Physics*, 13(44):19663, 2011. ISSN 1463-9076. doi:10.1039/c1cp22168j.

[91] K. S. Deeg, J. J. Gutiérrez-Sevillano, R. Bueno-Pérez, J. B. Parra, C. O. Ania, M. Doblaré, and S. Calero. Insights on the molecular mechanisms of hydrogen adsorption in zeolites. *The Journal of Physical Chemistry C*, 117(27):14374–14380, 2013. ISSN 1932-7447. doi:10.1021/jp4037233.

[92] S. Calero and P. Gómez-Álvarez. Effect of the confinement and presence of cations on hydrogen bonding of water in lta-type zeolite. *The Journal of Physical Chemistry C*, 118(17):9056–9065, 2014. ISSN 1932-7447. doi:10.1021/jp5014847.

[93] A. Martin-Calvo, J. J. Gutiérrez-Sevillano, J. B. Parra, C. O. Ania, and S. Calero. Transferable force fields for adsorption of small gases in zeolites. *Physical Chemistry Chemical Physics*, 17(37):24048–24055, 2015. ISSN 1463-9076. doi:10.1039/c5cp03749b. URL https://digital.csic.es/bitstream/10261/126482/1/Tranferable_force_Martin_Calvo.pdf.

[94] J. Perez-Carbajo, D. Dubbeldam, S. Calero, and P. J. Merkling. Diffusion patterns in zeolite mfi: The cation effect. *The Journal of Physical Chemistry C*, 122(51):29274–29284, 2018. ISSN 1932-7447. doi:10.1021/acs.jpcc.8b08963.

[95] N. Xue, A. Vjunov, S. Schallmoser, J. L. Fulton, M. Sanchez-Sanchez, J. Z. Hu, D. Mei, and J. A. Lercher. Hydrolysis of zeolite framework aluminum and its impact on acid catalyzed alkane reactions. *Journal of Catalysis*, 365:359–366, 2018. ISSN 0021-9517. doi:10.1016/j.jcat.2018.07.015.

[96] C. J. Heard, L. Grajciar, C. M. Rice, S. M. Pugh, P. Nachtigall, S. E. Ashbrook, and R. E. Morris. Fast room temperature lability of aluminosilicate zeolites. *Nature Communications*, 10(1), 2019. ISSN 2041-1723. doi:10.1038/s41467-019-12752-y.

[97] I. N. Tsimpanogiannis, O. A. Moultos, L. F. M. Franco, M. B. D. M. Spera, M. Erdős, and I. G. Economou. Self-diffusion coefficient of bulk and confined water: a critical review of classical molecular simulation studies. *Molecular Simulation*, 45(4-5):425–453, 2019. ISSN 0892-7022. doi:10.1080/08927022.2018.1511903. URL https://repository.tudelft.nl/islandora/object/uuid%3A65e6bb86-b5df-4d81-a8d8-1a187a01b2f4/datastream/OBJ/download.

[98] J. M. Castillo, J. Silvestre-Albero, F. Rodriguez-Reinoso, T. J. H. Vlugt, and S. Calero. Water adsorption in hydrophilic zeolites: experiment and simulation. *Physical Chemistry Chemical Physics*, 15(40):17374, 2013. ISSN 1463-9076. doi:10.1039/c3cp52910j. URL http://rua.ua.es/dspace/bitstream/10045/39543/3/2013_Castillo_etal_PCCP.pdf.

[99] A. Garcia-Sanchez, C. O. Ania, J. B. Parra, D. Dubbeldam, T. J. H. Vlugt, R. Krishna, and S. Calero. Transferable force field for carbon dioxide adsorption in zeolites. *The Journal of Physical Chemistry C*, 113(20):8814–8820, 2009. ISSN 1932-7447. doi:10.1021/jp810871f.

[100] D. A. Faux. Molecular dynamics studies of sodium diffusion in hydrated na+ zeolite-4a. *The Journal of Physical Chemistry B*, 102(52):10658–10662, 1998. ISSN 1520-6106. doi:10.1021/jp981801f.

[101] K. Muraoka, W. Chaikittisilp, and T. Okubo. Energy analysis of aluminosilicate zeolites with comprehensive ranges of framework topologies, chemical compositions, and aluminum distributions. *Journal of the American Chemical Society*, 138(19):6184–6193, 2016. ISSN 0002-7863. doi:10.1021/jacs.6b01341. URL https://doi.org/10.1021/jacs.6b01341.

[102] C. Baerlocher and L. B. McCusker. Multi-task neural networks for qsar predictions. 2011. URL http://www.iza-structure.org/databases/.

[103] K. Shirono, A. Endo, and H. Daiguji. Molecular dynamics study of hydrated faujasite-type zeolites. *The Journal of Physical Chemistry B*, 109(8):3446–3453, 2005. ISSN 1520-6106. doi:10.1021/jp047293t.

[104] S. Goryainov, R. Secco, Y. Huang, and H. Liu. Pressure dependence of ionic conductivity of hydrated and dehydrated zeolites a. *Physica B Condensed Matter*, 390(1-2):356–365, 2007. ISSN 0921-4526. doi:10.1016/j.physb.2006.08.037.

[105] D. Marx and P. Nielaba. Path-integral monte carlo techniques for rotational motion in two dimensions: Quenched, annealed, and no-spin quantum-statistical averages. *Physical Review A*, 45(12):8968–8971, 1992. ISSN 1050-2947. doi:10.1103/physreva.45.8968.

[106] M. Chaplin. Water structure and science repository. URL http://www1.lsbu.ac.uk/water/water_models.html.

[107] B. Guillot. A reappraisal of what we have learnt during three decades of computer simulations on water. *Journal of molecular liquids*, 101(1-3):219–260, 2002.

[108] S. W. Rick. A reoptimization of the five-site water potential (tip5p) for use with ewald sums. *The Journal of Chemical Physics*, 120(13):6085–6093, 2004. ISSN 0021-9606. doi:10.1063/1.1652434. URL https://scholarworks.uno.edu/cgi/viewcontent.cgi?article=1007&context=chem_facpubs.

[109] Y. Mao and Y. Zhang. Thermal conductivity, shear viscosity and specific heat of rigid water models. *Chemical Physics Letters*, 542:37–41, 2012. ISSN 0009-2614. doi:10.1016/j.cplett.2012.05.044.

[110] M. Haranczyk, C. Rycroft, R. Martin, and T. Willems. Zeo++: High-throughput analysis of crystalline porous materials, v0. 2.2. *Lawrence Berkeley National Laboratoy, Berkeley*, 2012.

[111] A. Michels, W. D. Graaff, and C. T. Seldam. Virial coefficients of hydrogen and deuterium at temperatures between -175°c and +150°c. conclusions from the second virial coefficient with regards to the intermolecular potential. *Physica*, 26(6):393–408, 1960. ISSN 0031-8914. doi:10.1016/0031-8914(60)90029-x.

[112] F. Darkrim, J. Vermesse, P. Malbrunot, and D. Levesque. Monte carlo simulations of nitrogen and hydrogen physisorption at high pressures and room temperature. comparison with experiments. *The Journal of Chemical Physics*, 110(8):4020–4027, 1999. ISSN 0021-9606. doi:10.1063/1.478283.

[113] M. Rahmati and H. Modarress. Grand canonical monte carlo simulation of isotherm for hydrogen adsorption on nanoporous siliceous zeolites at room temperature. *Applied Surface Science*, 255(9): 4773–4778, 2009. ISSN 0169-4332. doi:10.1016/j.apsusc.2008.11.072.

[114] A. N. Fitch, H. Jobic, and A. Renouprez. Localization of benzene in sodium-y-zeolite by powder neutron diffraction. *The Journal of Physical Chemistry*, 90(7):1311–1318, 1986. doi:10.1021/j100398a021. URL https://doi.org/10.1021/j100398a021.

[115] D. H. Olson. The crystal structure of dehydrated nax. *Zeolites*, 15(5):439–443, 1995. ISSN 0144-2449. doi:10.1016/0144-2449(95)00029-6.

[116] J. J. Pluth and J. V. Smith. Accurate redetermination of crystal structure of dehydrated zeolite a. absence of near zero coordination of sodium. refinement of silicon,aluminum-ordered superstructure. *Journal of the American Chemical Society*, 102(14):4704–4708, 1980. doi:10.1021/ja00534a024. URL https://doi.org/10.1021/ja00534a024.

[117] W. Zhu, L. Gora, A. V. D. Berg, F. Kapteijn, J. Jansen, and J. Moulijn. Water vapour separation from permanent gases by a zeolite-4a membrane. *Journal of Membrane Science*, 253(1-2):57–66, 2005. ISSN 0376-7388. doi:10.1016/j.memsci.2004.12.039.

[118] N. Chen. Selective sorption of less polar molecules with crystalline zeolites of high silica/alumina ratio, May 8 1973. US Patent 3,732,326.

[119] N. Chen. Hydrophobic properties of zeolites. *The Journal of Physical Chemistry*, 80(1):60–64, 1976.

[120] D. Olson, W. Haag, and R. Lago. Structure-selectivity relationship in xylene isomerization. *Journal of Catalysis*, 61:390–398, 1980.

[121] L. J. Smith, H. Eckert, and A. K. Cheetham. Site preferences in the mixed cation zeolite, li,na-chabazite: a combined solid-state nmr and neutron diffraction study. *Journal of the American Chemical Society*, 122(8):1700–1708, 2000. ISSN 0002-7863. doi:10.1021/ja992882b.

[122] K. Itabashi, Y. Kamimura, K. Iyoki, A. Shimojima, and T. Okubo. A working hypothesis for broadening framework types of zeolites in seed-assisted synthesis without organic structure-directing agent. *Journal of the American Chemical Society*, 134(28):11542–11549, 2012. ISSN 0002-7863. doi:10.1021/ja3022335.

[123] C. M. Simon, B. Smit, and M. Haranczyk. pyiast: Ideal adsorbed solution theory (iast) python package. *Computer Physics Communications*, 200:364–380, 2016. ISSN 0010-4655. doi:10.1016/j.cpc.2015.11.016. URL https://manuscript.elsevier.com/S0010465515004403/pdf/S0010465515004403.pdf.

[124] D. E. Akporiaye, I. M. Dahl, H. B. Mostad, and R. Wendelbo. Aluminum distribution in chabazite: an experimental and computational study. *The Journal of Physical Chemistry*, 100(10):4148–4153, 1996. ISSN 0022-3654. doi:10.1021/jp952189k.

[125] G. Maurin, P. Senet, S. Devautour, F. Henn, J. Giuntini, and V. V. Doren. Monte carlo simulations of dielectric relaxation in na-mordenites. *Computational Materials Science*, 22(1-2):106–111, 2001. ISSN 0927-0256. doi:10.1016/s0927-0256(01)00175-6.

[126] E. Costa, J. L. Sotelo, G. Calleja, and C. Marrón. Adsorption of binary and ternary hydrocarbon gas mixtures on activated carbon: Experimental determination and theoretical prediction of the ternary equilibrium data. *AIChE Journal*, 27(1):5–12, 1981. ISSN 0001-1541. doi:10.1002/aic.690270103.

[127] L. Hamon, N. Heymans, P. L. Llewellyn, V. Guillerm, A. Ghoufi, S. Vaesen, G. Maurin, C. Serre, G. D. Weireld, and G. D. Pirngruber. Separation of co2–ch4 mixtures in the mesoporous mil-100(cr) mof: experimental and modelling approaches. *Dalton Transactions*, 41(14):4052, 2012. ISSN 1477-9226. doi:10.1039/c2dt12102f.

[128] A. D. Wiersum, J.-S. Chang, C. Serre, and P. L. Llewellyn. An adsorbent performance indicator as a first step evaluation of novel sorbents for gas separations: Application to metal–organic frameworks. *Langmuir*, 29(10):3301–3309, 2013. ISSN 0743-7463. doi:10.1021/la3044329.

[129] Q. Yang, C. Xue, C. Zhong, and J.-F. Chen. Molecular simulation of separation of co2 from flue gases in cu-btc metal-organic framework. *AIChE Journal*, 53(11):2832–2840, 2007. ISSN 0001-1541. doi:10.1002/aic.11298.

[130] Y.-S. Bae, K. L. Mulfort, H. Frost, P. Ryan, S. Punnathanam, L. J. Broadbelt, J. T. Hupp, and R. Q. Snurr. Separation of co2from ch4using mixed-ligand metal-organic frameworks. *Langmuir*, 24(16): 8592–8598, 2008. ISSN 0743-7463. doi:10.1021/la800555x.

[131] A. N. Dickey, A. Özgür Yazaydın, R. R. Willis, and R. Q. Snurr. Screening co2/n2selectivity in metal-organic frameworks using monte carlo simulations and ideal adsorbed solution theory. *The Canadian Journal of Chemical Engineering*, 90(4):825–832, 2012. ISSN 0008-4034. doi:10.1002/cjce.20700.

[132] J. Weitkamp. Zeolites as media for hydrogen storage*1. *International Journal of Hydrogen Energy*, 20 (12):967–970, 1995. ISSN 0360-3199. doi:10.1016/0360-3199(95)00058-l.

Abbreviations

Abbreviation	Expanded
AP-RDF	Atomic Property Weighted Radial Distribution Functions
ASA	Accessible Surface Area [Topological Descriptor]
AV	Accessible Volume [Topological Descriptor]
BP	Blocking Pockets
CFC	Continuous Fractional Component
CFCNPT	Continuous Fractional Component Monte Carlo in The NPT Ensmble
EHC	Electrochemical Hydrogen Compressor
FH	Feynman–Hibbs Quantum Effective Potential
GCMC	Grand Canonical Monte Carlo
HEVF	Helium Void Fraction
HTS	High Hroughput Screening
IAST	Ideal Adsorbed Solution Theory
ISO	International Organization For Standardization
IZA	International Zeolite Association
LJ	12-6 Lennard-Jones Potential
MC	Monte Carlo
MFS	Maximum Free Sphere Diameter [Topological Descriptor]
MIS	Maximum Included Sphere Diameter [Topological Descriptor]
NPT	Isobaric-Isothermal Ensemble
PEM	Proton-Exchange Membrane
PPM	Parts Per Million
PR-EOS	Peng-Robinson Equation Of State
QSPR	Quantitative Structure-Property Relationships
RDF	Radial Distribution Function

List of Figures

List of Tables

A. DEH$_2$YDR force field parameters

Table A.1: Pairwise 12-6 Lennard-Jones interaction parameters of the DEH$_2$YDR force field.

Interaction pair	Type of interaction	p_0/k_B [K]	p_1 [Å]	Mixing rule	Source
wO - wO	12-6 Lennard-Jones	89.5160	3.0970	-	[98, 108]
wO - H2	12-6 Lennard-Jones	57.3428	3.0275	Lorentz-Berthelot	-
wO - O	12-6 Lennard-Jones	13.7100	3.3765	-	[98]
wO - Oa	12-6 Lennard-Jones	13.7100	3.3765	-	[98]
wO - Na	12-6 Lennard-Jones	75.0000	2.3900	-	[98]
H2 - H2	12-6 Lennard-Jones	36.7330	2.9580	-	S. Calero, [91]
H2 - Si	12-6 Lennard-Jones	28.2560	1.8540	-	S. Calero, [91]
H2 - Al	12-6 Lennard-Jones	26.5120	1.9870	-	S. Calero, [91]
H2 - O	12-6 Lennard-Jones	66.0550	2.8900	-	S. Calero, [91]
H2 - Oa	12-6 Lennard-Jones	66.0550	2.8900	-	S. Calero, [91]
H2 - Na	12-6 Lennard-Jones	220.0000	3.0000	-	S. Calero, [91]
O - Na	12-6 Lennard-Jones	33.0000	3.2000	-	[98]
Oa - Na	12-6 Lennard-Jones	23.0000	3.4000	-	S. Calero, [91]
Na - Na	12-6 Lennard-Jones	251.7800	3.1440	-	[98]

Table A.2: Point charges used for electrostatics in the DEHY$_2$DR force field

Pseudo atom identifier	Type of interaction	point charge [e]	Source
Si	Coulombic	0.78598	[91, 98, 99]
Al	Coulombic	0.48598	[91, 98, 99]
O	Coulombic	-0.39299	[91, 98, 99]
Oa	Coulombic	-0.41384	[91, 98, 99]
Na	Coulombic	0.38340	[98]
H2	Coulombic	0.00000	S. Calero, [91]
wO	Coulombic	0.00000	[98, 108]
wH	Coulombic	0.24100	[98, 108]
wL	Coulombic	-0.24100	[98, 108]

Table A.3: Critical constants used in the DEHY$_2$DR force field

Molecule	Temperature [T]	Pressure [Pa]	Acentric factor [-]
Hydrogen	33.14	1296400	-0.219
Water	647.14	22064000	0.344292084

B. Simulation inputs

Example of BRICK simulation input file [1/2](topology.in) for CFCNPT simulation of hydrogen/water mixture at sytem conditions:

```
Molecule          # Box 1
H2                  512
H2O_TIP5P–Ew         0
##############################################################
1 Fractional Group(s)
Type, Box, NinFrac, MoleculeTypes and Name
NVT    1    1        H2O_TIP5P–Ew frac_H2O
##############################################################
0 Reaction(s)
##############################################################
Box    Length      dVolume
 1    34.014        156.25
_____
                  Box 1
MolType        dtrans   drotate
H2              0.50     90.0
H2O_TIP5P–Ew    0.50     90.0
_____
               Box 1
Fractional   dlambda   N_LambdaBins    LambdaSwitch
   1          0.2         100              1.0
##############################################################
0 MolType Pair(s)
_____
Cluster Radius = 0.0
```

Example of BRICK simulation input file [2/2(settings.in) for CFCNPT simulation of hydrogen/water mixture at sytem conditions:

```
Nbox     Temperature  Pressure    Reduced Units?
 1           310          875 bar          .false.
_____
Nproduction     Nequilibrate    Ninitialize
   5E5              5E4             1E2
_____
Nconfiguration     Ndata        Naverage        Nrdf
   1E3              1E3            1E2            0E0
_____
Linit     Lweight    Lseed      Seed
.true.    .false.    .false.    1669196305
_____
Lrdf_molecule Lrdf_atom    Linsertions     LWolfPlot
   .false.       .false.      .false.         .false.
_____
 LWL    Fmod  Fred  Flatc
.true.   0.1   4.0    0.2

###################################################

–––– Translation Moves ––––
Normal      Pair       Cluster
  35          0           0

––––––– Rotation Moves –––––––
Normal      Pair       Cluster
  30          0           0
```

```
————— Volume  Moves —————
Normal    Cluster
  1          0


——– Intramolecular  Moves ——–
Bending    Torsion
  0          0


————— Lambda  Moves —————
Normal    GCMC
  17          0


————— CFC Hybrid  Moves —————
NVT/NPT    GE        RXMC
  17          0         0


——– Hybrid Move  Switches ——–
NVT/NPT    GE        RXMC
0.0 1.0    0.0 0.0    0.0 0.0
```

Example of RASPA simulation input for NPT simulation of water:

```
SimulationType                   MonteCarlo
NumberOfCycles                   500000
NumberOfEquilibrationCycles      50000
PrintEvery                       1000
RestartFile                      no


Forcefield                       Local


Box 0
BoxLengths 30 30 30
ExternalTemperature 310.0
ExternalPressure 8.75e7


VolumeChangeProbability          0.05


Component 0 MoleculeName              Tip5p
            StartingBead              0
            TranslationProbability    1.0
            RotationProbability       1.0
            ReinsertionProbability    1.0
            CreateNumberOfMolecules   512
```

Example of RASPA simulation input for equilibration of extra-framework cations in the absence of other guest molecules:

```
SimulationType                   MonteCarlo
NumberOfCycles                   500000
NumberOfEquilibrationCycles      0
RestartFile                      no
PrintEvery                       5000


Forcefield                       Local


Framework 0
FrameworkName MOR–256Al
RemoveAtomNumberCodeFromLabel yes
ModifyOxgensConnectedToAluminium yes
UnitCells 1 1 1
ExternalTemperature 1000
Component 0 MoleculeName                  sodium
            MoleculeDefinition            TraPPE
            TranslationProbability        1.0
            RandomTranslationProbability  1.0
            ExtraFrameworkMolecule        yes
            CreateNumberOfMolecules       256
```

Example of RASPA simulation input for GCMC simulation of binary adsorption of water and hydrogen on a zeolite framework, with the presence of extra-framework cations:

```
SimulationType                    MonteCarlo
NumberOfCycles                    500000
NumberOfEquilibrationCycles       50000
RestartFile                       yes
PrintEvery                        1000
ComputeRDF                        yes
WriteRDFEvery                     1000
Movies                            yes
WriteMoviesEvery                  5000


Forcefield                        Local

Framework 0
FrameworkName MOR-256Al
RemoveAtomNumberCodeFromLabel yes
ModifyOxgensConnectedToAluminium yes
UnitCells 1 1 1
HeliumVoidFraction 0.28918
ExternalTemperature 310.0
ExternalPressure 8.75e7

Component 0  MoleculeName                    sodium
             MoleculeDefinition              TraPPE
             TranslationProbability          1.0
             RandomTranslationProbability    1.0
             ExtraFrameworkMolecule          yes
             CreateNumberOfMolecules         0

Component 1  MoleculeName                    hydrogen
             BlockPockets                    no
             MolFraction                     0.9999877
             FugacityCoefficient             1.68361
             TranslationProbability          0.5
             RotationProbability             0.5
             ReinsertionProbability          0.5
             SwapProbability                 1.0
             CreateNumberOfMolecules         0

Component 2  MoleculeName                    Tip5p
             BlockPockets                    no
             MolFraction                     12.3e-6
             FugacityCoefficient             1.45975
             RotationProbability             0.15
             TranslationProbability          0.15
             RegrowProbability               0.1
             SwapProbability                 0.6
             CreateNumberOfMolecules         0
```